Identifying Prospective Inhibitors against Ldt$_{Mt5}$ from *Mycobacterium tuberculosis* as a Potential Drug Target

VICTOR. T. SABE

217080874

UNIVERSITY OF ™
KWAZULU - NATAL

INYUVESI
YAKWAZULU-NATALI

2018

Identifying Prospective Inhibitors against Ldt$_{Mt5}$ from *Mycobacterium tuberculosis* as a Potential Drug Target

VICTOR. T. SABE

217080874

2018

A thesis submitted to the School of Pharmacy and Pharmacology, Faculty of Health Science, University of KwaZulu-Natal, Westville, for the degree of Master of Medical Science.

This is the thesis in which the chapters are written as a set of discrete research publications, with an overall introduction and final summary. Typically, these chapters will have been published in internationally recognized, peer-reviewed journals.

This is to certify that the content of this thesis is the original research work of Mr. Victor Tinashe Sabe.

As the candidate's supervisor, I have approved this thesis for submission.

Supervisor: Signed: --------------------- Name: **Prof. H.G. Kruger**   Date:

Co-Supervisor: Signed: ---------------- Name: **Dr. B. Honarparvar**   Date:

Co-Supervisor: Signed: ---------------- Name: **Dr. G.E.M. Maguire**   Date:

ABSTRACT

Tuberculosis (TB) caused by the bacterium, *Mycobacterium tuberculosis* (*M.tb*) has resulted in an unprecedented number of deaths over centuries. L,D-transpeptidase enzymes are known to play a crucial role in the biosynthesis of the cell wall, which confers resistance to most antibiotics. These enzymes catalyze the 3→3 peptidoglycan cross-links of the *M.tb* cell wall. Specific *β*-lactam antibiotics (carbapenems) have been reported to inhibit cell wall polymerization of *M.tb* and they inactivate L,D-transpeptidases through acylation. L,D-transpeptidase 5 (Ldt$_{Mt5}$) is a unique paralog and a vital protein in maintaining integrity of the cell wall specifically in peptidoglycan metabolism therefore making it an important protein target. Carbapenems inhibit Ldt$_{Mt2}$, but do not show reasonable inhibitory activities against Ldt$_{Mt5}$. We therefore sought to perform virtual screening in order to acquire potential inhibitors against Ldt$_{Mt5}$ and to investigate the affinity and to calculate the binding free energies between Ldt$_{Mt5}$ and potential inhibitors. Furthermore, we sought to investigate the nature of the transition state involved in the catalytic reaction mechanism; to determine the activation free energies of the mechanism using ONIOM through the thermodynamics and energetics of the reaction path and lastly to express, purify and perform inhibition studies on Ldt$_{Mt5}$.

A total of 12766 compounds were computationally screened from the ZINC database to identify potential leads against Ldt$_{Mt5}$. Docking was performed using two different software programs. Molecular dynamics (MD) simulations were subsequently performed on compounds obtained through virtual screening. Density functional theory (DFT) calculations were then carried out to understand the catalytic mechanism of Ldt$_{Mt5}$ with respect to *β*-lactam derivatives using a hybrid ONIOM quantum mechanics/molecular mechanics (QM/MM) method. Ldt$_{Mt5}$ complexes with six selected *β*-lactam compounds were evaluated. Finally, a lyophilised pET28a-Ldt$_{Mt5}$ was used to transform *E. coli* strain BL21 (DE3) and SDS-PAGE was used to verify the purity, molecular weight and protein profile determination. Finally, an *in vitro* binding thermodynamics analysis using isothermal titration calorimetry (ITC) was later on performed on a single compound (the strongest binder) from the final set, in a bid to further validate the calculated binding energy values.

A number of compounds from four different antimicrobial classes (n = 98) were obtained from the virtual screening and those with docking scores ranging from -7.2 to -9.9 kcal mol^{-1} were considered for MD analysis (n = 37). A final set of 10 compounds which exhibited the greatest affinity, from four antibiotic classes was selected and Molecular Mechanics/Generalized Born

Surface Area (MM-GBSA) binding free energies (ΔG_{bind}) from the set were characterised. The calculated binding free energies ranged from -30.68 to -48.52 kcal mol^{-1}. The β-lactam class of compounds demonstrated the highest ΔG_{bind} and also the gretaest number of potential inhibitors. The DFT activation energies ($\Delta G^{\#}$) obtained for the acylation of Ldt$_{Mt5}$ by the six selected β-lactams were calculated as 13.67, 20.90, 22.88, 24.29, 27.86 and 28.26 kcal mol^{-1}. The $\Delta G^{\#}$ results from the 6-membered ring transition state (TS) revealed that all selected six β-lactams were thermodynamically more favourable than previously calculated activation energy values for imipenem and meropenem complexed with Ldt$_{Mt5}$. The results are also comparable to those observed for Ldt$_{Mt2}$, however for compound 1 the values are considerably lower than those obtained for meropenem and imipenem in complex with Ldt$_{Mt2}$, thus suggesting in theory that compound 1 is a more potent inhibitor of Ldt$_{Mt5}$. We also report the successful expression and and purification of Ldt$_{Mt5}$, however the molecule selected for the *in vitro* inhibition study gave a poor result. On further review, we concluded that the main cause of this outcome was due to the relatively low insolubility of the compound.

The outcome of this study provides insight into the design of potential novel leads for Ldt$_{Mt5}$. Our screening obtained ten novel compounds from four different antimicrobial classes. We suggest that further *in vitro* binding thermodynamics analysis of the novel compounds from the four classes, including the carbapenems be performed to evaluate inhibition of these compounds on Ldt$_{Mt5}$. If the experimental observations suggest binding affinity to the protein, catalytic mechanistic studies can be undertaken. These results will also be used to verify or modify our computational model.

DECLARATION: PLAGIARISM

I, Victor Tinashe Sabe, declare that

The research reported in this thesis, except otherwise indicated, is my original research.

This thesis has not been submitted for any degree or examination at any other university.

This thesis does not contain other person's data, pictures, graphs or other information, unless specifically acknowledged as being sourced from other persons.

This thesis does not contain other persons' writing, unless specifically acknowledged as being sourced from other researchers. Where other written sources have quoted, then:

Their words have been rewritten but the general information attributed to them has been referenced.

Where their exact words have been used, then their writing have been placed in italics and inside quotation marks and referenced.

This thesis does not contain text, graphics or tables copied and pasted from the Internet, unless specifically acknowledged, and the source being detailed in the thesis and in the References sections.

A detailed contribution to publications that form part and/or include research presented in this thesis is stated (include publications submitted, accepted, in press and published).

Signed:_____

TABLE OF CONTENTS

LIST OF PUBLICATIONS

Identification of potent L,D-transpeptidase 5 inhibitors for Mycobacterium tuberculosis as potential anti-TB leads: Virtual Screening and Molecular Dynamics Simulations (**submitted to the Journal of Molecular Modelling**)
Author Contributions:

Victor T. Sabe: Principal investigator in the design of this project and first author responsible for writing and preparation of this manuscript.

Gideon F. Tolufashe and Collins U. Ibeji: Provided technical assistance on the project.

Sibusiso Maseko: Performed experimental work.

Thavendran Govender and *Gyanu Lamichhane*: Provided technical and experimental assistance in the overall project.

Hendrik G. Kruger: Supervisor.

Bahareh Honarparvar and Glenn E. M. Maguire: Co-supervisors.

Investigating the Reaction Mechanism of L,D-transpeptidase 5 by β-lactams using ONIOM Method. (**submitted to the Journal of Molecular Graphics and Modelling**)
Author Contributions:

Victor T. Sabe: Principal investigator in the contextualisation and design of the project.

Gideon F. Tolufashe: Responsible for writing and preparation of the manuscript.

Collins U. Ibeji and Monsurat M. Lawal: Provided technical assistance to the project.

Hendrik G. Kruger: Supervisor.

Bahareh Honarparvar and Glenn E. M. Maguire: Co-supervisors.

DEDICATION

To Gloria and Moses

ACKNOWLEDGEMENTS

LIST OF ABBREVIATIONS

2D	2-Dimensional
3D	3-Dimensional
AG	Arabinogalactan
Alr	Alanine racemase
AMBER	Assisted Model Building with Energy Refinement
CADD	Computer-Aided Drug Design
CF	Cell-Free
CHARMM	Chemistry at Harvard Macromolecular Mechanics
DCCM	Dynamic Cross-Correlation Matrix
Ddl	D-alanine:D-alanine ligase
DFT	Density Functional Theory
DFTB/MM	Density Functional Tight Binding Molecular Mechanics
DMSO	Dimethyl sulfoxide
DNA	Deoxyribonucleic acid
DTT	Dithiothreitol
E. coli	*Escherichia coli*
ESP	Molecular electrostatic potential
FMO	Frontier Molecular Orbital
$\Delta G^{\#}$	Activation free energy
ΔG	Gibbs free energy of binding
ΔG_{bind}	Binding free energy
GAFF	General AMBER Force Field
GB	Generalized Born solvation model
GlcNAc	*N*-acetyl glucosamine
GROMOS	GROningen Molecular Simulation
ΔH	Binding enthalpy
HIV	Human Immunodeficiency Virus
HOMO	Highest Occupied Molecular Orbitals
HPLC	High Performance Liquid Chromatography

HTVS	High Throughput Virtual Screening
IC_{50}	Half maximal inhibitory concentration
ICM	Internal Coordinate Mechanics
IRC	Intrinsic Reaction Coordinates
ITC	Isothermal Titration Calorimetry
K*b*	Binding constant
K*D*	Dissociation constant
K*i*	Inhibition constant
LAM	Lipoarabinomannan
LB	Luria-Bertani
LDT or Ldt	L,D-transpeptidase
Ldt_{Mt2}	L,D-transpeptidase 2 from *Mycobacterium tuberculosis*
Ldt_{Mt5}	L,D-transpeptidase 5 from *Mycobacterium tuberculosis*
LM	Lipomannan
LUMO	Lowest Unoccupied Molecular Orbitals
mAGP	mycolyl-Arabinogalactan-Peptidoglycan
MD	Molecular Dynamics
MDR	Multi-Drug Resistant
MFEP	Minimum Free Energy Path
MM	Molecular Mechanics
MM-GBSA	Molecular Mechanics Generalized Born Surface Area
MM-PBSA	Molecular Mechanics Generalized Poisson-Boltzmann Surface Area
M.tb	*Mycobacterium tuberculosis* or *M. tuberculosis*
Mur	Muramic acid
MurNAc	*N*-acetyl muramic acid
NADPH	Nicotinamide Adenine Dinucleotide Phosphate
NAMD	Nanoscale Molecular Dynamics
NBO	Natural Bond Orbital
ONIOM	our Own N-layer Integrated molecular Orbital molecular Mechanics
OPLS3	Optimized Potential for Liquid Simulations 3

PDB	Penicillin Binding Protein
PDB	Protein Data Bank
PDIM	Phthioceroldimycocerates
PG	Peptidoglycan
PIM	Phosphatidylinositol Mannoside
PME	Partial Mesh Ewald
PMSF	Phenylmethylsulfonyl fluoride
QM	Quantum Mechanics
QM/MM	hybrid Quantum Mechanics/Molecular Mechanic
RMSD	Root-Mean-Square Deviation
RMSF	Root-Mean Square Fluctuation
RNI	Reactive Nitrogen radical
ROI	Reactive Oxygen Intermediate
ΔS	Binding entropy
SBVS	Structure-Based Virtual Screening
SDS	Sodium Dodecyl Sulphate
SDS-PAGE	Sodium Dodecyl Sulphate Polyacrylamide Gel Electrophoresis
$-T\Delta S$	Entropy
TB	Tuberculosis
TDA	Thermal Denaturation Assay
TNF	Tumour Necrosis Factor
TS	Transition State
UDP	Uridine Diphosphate
VS	Virtual Screening
XDR	Extensively-Drug Resistant

LIST OF FIGURES

Chapter 1

Chapter 2

Chapter 3

Chapter 4

LIST OF TABLES
Chapter 2

Chapter 1

Introduction

1.0 Background

1.1 Global Tuberculosis burden

Tuberculosis (TB) on the global scale of infectious diseases has the highest mortality rate to date, resulting in 1.8 million deaths per year[1]. With such human carnage, tuberculosis was declared a global emergency in 1993[3]. The current global incidence of the disease as of year 2016 stands at 10.4 million[4]. This was facilitated by multi-drug resistant (MDR) and extensively drug resistant (XDR) *Mycobacterium tuberculosis* (*M.tb*) strains, which render the available antibacterial drug regimens compromised[5-7]. Drug-resistant TB is responsible for a yearly mortality of 250 000 and multi drug-resistant TB patients require a complicated multidrug treatment. Only 52 % of MDR-TB patients are successfully treated globally and only a finite number of second-line medicines are available. It is also estimated that in 50 % of MDR TB patients worldwide, there is second-line drug resistance and the treatment of XDR TB is successful in only one third of the patients[1, 8]. This resistance does not only encumber the capacity to treat bacterial infections but has extensive socio-economic implications. Such a situation creates an urgent need to develop antimicrobial drugs suitable to counteract the ever-evolving bacterium *M.tb*[8].

Tuberculosis and HIV-1 epidemics are closely related in South Africa[9, 10]. It has been identified that almost all patients with XDR tuberculosis are HIV-positive[9, 11]. This deadly synergy brings about a fatal outcome, with high mortality rates in co-infected patients[9]. It was also revealed through phylogenetic analysis that in spite of stringent treatment adherence, there was a stepwise evolution of drug resistance, thus suggesting that the existing TB drug regimens are inadequate to curb the spread of drug-resistant TB within this HIV co-infected population[12]. Data from several studies strongly suggests the need to strengthen the existing interventions in order to prevent the spread of this likely incurable disease and public health scourge[9, 11-14]. To improve the probability of finding new effective drugs against MDR and XDR TB, whole cell and targeted drug design approaches were therefore suggested by Kana *et al.*[15], as a multi-disciplinary approach is bound to yield better results. The whole cell approach provides novel and chemically validated targets, useful for target-based optimization of compounds. The

targeted drug design approach can be utilised to improve the efficiency of the drug discovery process for TB, by reducing attrition in processes of hit isolation and optimization[15].

L,D-transpeptidases (LDTs) are essential for peptidoglycan biosynthesis in *M.tb* and targeting them is likely to be effective in controlling the bacterium. Recent findings revealed that carbapenems fail to inactivate Ldt$_{Mt5}$[16], a unique protein responsible for maintaining the integrity of the cell wall therefore making it an important *M.tb* target[17]. Despite several theoretical studies on Ldt$_{Mt2}$[18-23], and a few experimental studies on Ldt$_{Mt5}$[16, 17], to the best of our knowledge there has been no computational study on the structure and function of Ldt$_{Mt5}$ as well as identifying potential inhibitors effective against Ldt$_{Mt5}$. A need to perform virtual screening of various inhibitors against Ldt$_{Mt5}$ therefore exists. Furthermore, this study will seek to investigate the interactions and binding free energy between Ldt$_{Mt5}$ and potential inhibitors using molecular dynamics (MD) simulations, to evaluate the mechanistic reaction between *β*-lactams and Ldt$_{Mt5}$ and the *in vitro* validation of the screened inhibitors.

1.1.1 Infection life cycle of *Mycobacterium tuberculosis*

Tuberculosis can be transmitted from an infected person as a colloid through coughing[24]. An initial infection triggers the production of chemokines and cytokines which direct the migration of phagocytes to the infected areas such as lungs[25, 26]. This movement works to the advantage of the mycobacterium in that it resides in these phagocytic cells and it has developed several mechanisms to exploit the expansive cellular niche[24]. The host's professional phagocytic cells include dendritic cells, macrophages, monocytes and neutrophils[26]. The *M.tb* survival mechanisms include resistance to reactive oxygen intermediates (ROIs), such as hydrogen peroxide[27] and hydroxyl radicals[28]; nitric oxide and reactive nitrogen radicals (RNI) tolerance[29, 30]; inhibition of phagosome maturation[31]; translocation of the mycobacterium to the cytosol to avoid phagolysosomal degradation[32]; apoptosis inhibition[33] and mycobacterium-induced macrophage necrosis[34]. A critical balance or equilibrium is subsequently reached between the host's immune system and mycobacterium adaptation resulting in a process called latency. Latent TB can develop into active TB which is characterized by coughing and increased production of sputum. The activation of TB is mainly attributed to a compromised or defective immune system. Two mechanisms of reactivation have been established in the human host: the defect and depletion of CD4$^+$ T cells[35] and the neutralization of tumour necrosis factor (TNF)[36].

1.1.2 Mycobacteria cell wall

The mycobacterial cell wall (envelope) is a complex structural feature, distinct from other prokaryotes[37]. It is essential for the well-being of the organism and it serves in the control of the movement of substances in and out of the cell. In principle it consists of three main components i.e. capsule, cell wall and membrane[38].

1.1.2.1 The structural cell wall of *Mycobacterium tuberculosis*

The cell envelope possesses structures which are not found in animal cells, but unique to mycobacteria thereby making it a lucrative target for selective inhibition[38]. Antibiotic and chemotherapeutic agent resistance of *M.tb* has been attributed to the relatively unyielding bacterial and cellular impermeability of the cell wall. The primary structure of the cell wall is commonly referred to as the mycolyl-arabinogalactan-peptidoglycan (mAGP) complex[37] or the 'core' can be described as a dynamic and asymmetric lipid bilayer[39]. It has soluble and insoluble fractions. The soluble lipid upper layer above the mycolic acids is made up of free lipids which comprise of cord factor, sulpholipids and phthioceroldimycocerates (PDIM)[40]. It is composed of an assortment free long chain and short α-chain lipids[40]. There are 70-90 carbon-containing lipids known as mycolic acids within that region[41, 42]. These lipids are occasionally interrupted by proteins known as phosphatidylinositol mannosides (PIMs) and two types of lipids, lipoarabinomannan (LAM) and lipomannan (LM)[40]. The lower section is composed of peptidoglycan (PG), covalently attached to arabinogalactan (AG) which is connected to the mycolic acids[40, 42] (**Figure 1**). This is the highly insoluble and impermeable lipid region which confers resistance to immunological, antibiotic and chemical stress.
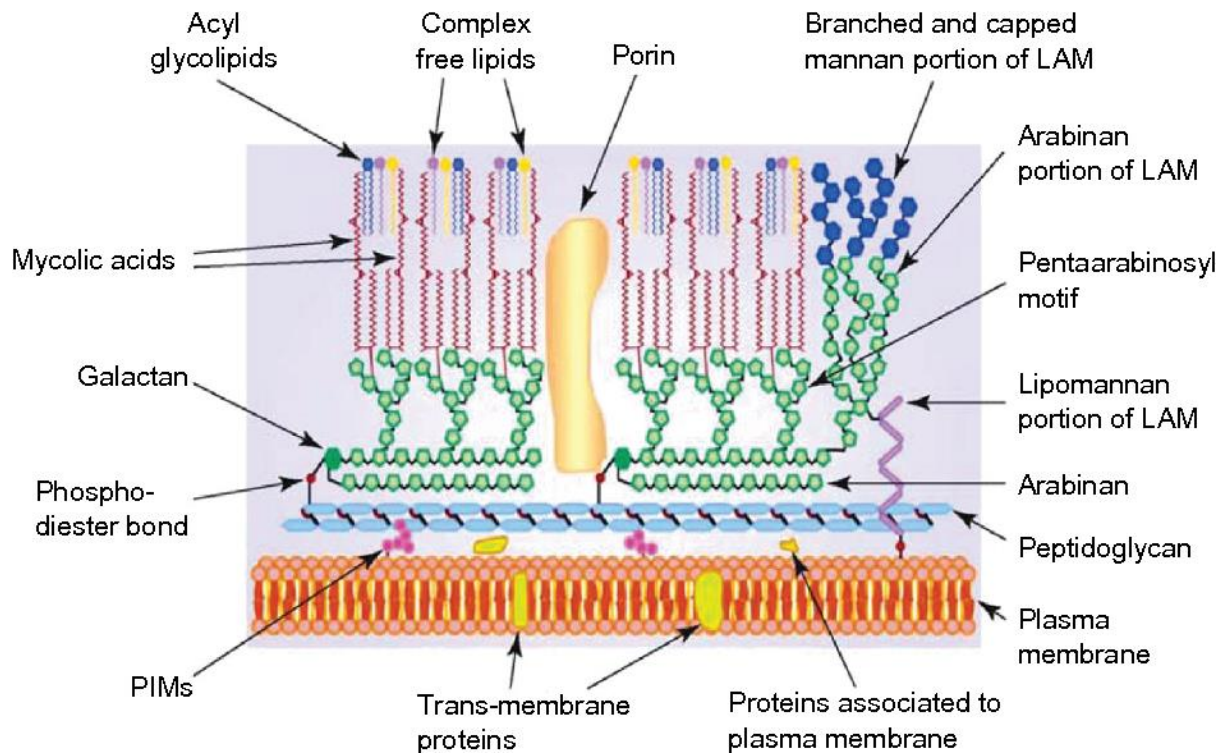
Figure 1. The cell wall of *Mycobacterium tuberculosis* exhibiting its various structural components (Image use permission granted by © SAGE Publications Copyright © 2013[43])

The peptidoglycan or murein layer is a mesh-like rigid structure which offers a structural scaffold to the cell to withstanding osmotic pressure and maintaining cellular integrity[37]. It is composed of repeating *N*-acetyl glucosamine (GlcNAc) and *N*-acetyl muramic acid (MurNAc) residues linked by *β* (1→4) glycosidic bonds. *N*-acetylmuramic acid residues are a combination of *N*-acetyl and *N*-glycolyl groups, in which *N*-acetyl would be oxidised to MurNGly, which is an *N*-gylcolyl function[44]. The reason for the structural modification and oxidation is not clear, however, it is speculated that they provide the additional strength to the mesh through hydrogen bonds[45, 46]. The side chains (four or five amino acid peptides long) made up of L-alaninyl-D-isoglutaminyl-meso-diaminopimelyl-D-alanine are crosslinked with peptides of adjacent glycan linkages.

1.1.2.2 Peptidoglycan layer of *Mycobacterium tuberculosis*

Peptidoglycan biosynthesis starts in the cytoplasm since soluble amino acids and nucleotide activated sugars are required to initiate the process[37]. UDP-GlcNAc is the starter molecule which is synthesized in a four-stage process involving three enzymes. D-fructose-6-phosphate is first converted to D-glucosamine-1-phosphate which is converted to D-glucosamine-6-phosphate, then catalysed to form UDP-GlcNAc. The enzymes involved are GlmS an aminotransferase, GlmM a mutase and GlmU respectively[47]. GlmU performs both acetylation

and uridylation[48]. The carboxy-terminal domain of GluU catalyses the acylation of D-glucosamine-6-phosphate and uridylation of N-acetylglucosamine-1-phosphate is carried out on the amino-terminal domain[49]. The UDP-GlcNAc is further converted to UDP-MurNAc in two stages catalysed by the enzymes MurA, an enolpyruvyl transferase and MurB, a reductase. The process in which MurA catalyses the movement of enolpyruvate from phosphoenoylpyruvate to position-3 of N-acetylglucosamine portion of UDP-GlcNAc thereby releasing inorganic phosphate[50]. MurB catalyses the production of UDP-MurNAc utilising NADPH thus transforming the enolpyruvate into D-lactoyl[37]. Muramic acid ligase enzymes MurC, MurD, MurE and MurF sequentially catalyse the synthesis of either UDP-N-acetylmuramyl pentapeptide from UDP-MurNAc or UDP-N-glycolylmuramylpentapeptide from UDPMurNGlyc[37]. These enzymes are functionally intracellular ATP-dependent. Within the peptidoglycan pathway, amino acid residues are added by the ligase enzymes to form UDP-MurNAc and UDP-MurNGlyc intermediates. L-alanine and D-glutamate are added by MurC and MurD respectively, while meso-DAP, and D-alanyl-D-alanine, are added by MurE and MurF[51]. Common within the Mur ligases is the addition of a carboxyl group to the uridine diphosphate substrate via phosphorylation by adenosine triphosphate, to produce adenosine diphosphate. An amino acid or dipeptide attack on the UDP-substrate phospho-intermediate ensues, resulting in adjunction via amino-acylation of the uridine diphosphate precursor thereby expelling inorganic phosphate[52, 53]. *M. tuberculosis* MurC ligates both L-alanine and L-glycine to UDPMurNAc[54]. **Figure 2** provides a schematic summary of the process of peptidoglycan biosynthesis.
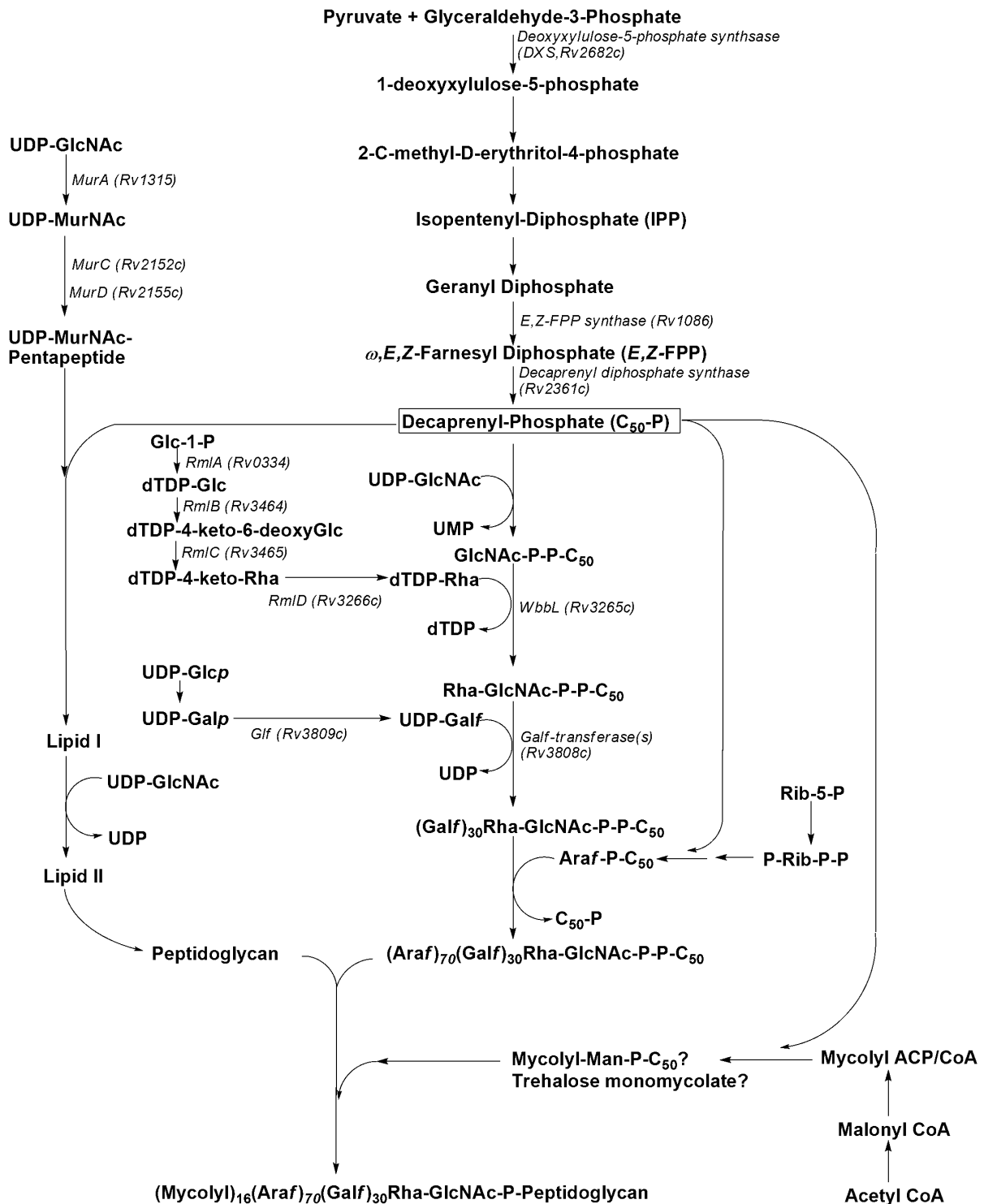
Figure 2. Biosynthesis of mycolic acid-arabinogalactan-peptidoglycan complex (MAPc) belonging to M.tb, according to contemporary knowledge of MAPc structure and the activities of known proteins (italicised) expressed by *M.tb*. There are many enzymes associated with the mycolic acids synthesis, however some are not listed (Image adopted and redrawn from Crick *et al*.[2])

Alr and Ddl are other enzymes crucial in the cytoplasmic assembly of PG by providing racemase and ligase activity, respectively[55]. Polyprenyl phosphates are critical in the biosynthesis of the cell envelop, by making a lipid anchor which permits the synthesis of the

cell wall to happen whilst firmly attached onto a cytoplasmic membrane[34]. MurX is an enzyme which relays phospho-MurNAc-pentapeptide to decaprenol phosphate lipid which is a long carbon chain unique to mycobacteria, to form lipid I from Park's nucleotide. MurG, a glycosyltransferase uses UDP-GlcNAc making a β (1→4) glycosidic bond on GlcNAc and MurNAc or MurNGlyc sugar belonging to lipid I to form lipid II thus concluding the cytoplasmic pathway of PG biosynthesis[34]. The plasma membrane and the periplasmic space are the sites where the other reaction involved in PG biosynthesis take place. In mycobacterial cells, lipid II makes a demarcation between the cytoplasm and periplasmic space[37]. Translocation of lipid II across the plasma membrane is carried out by two proteins namely MurJ and FtsW. Lipid II is a substrate for two penicillin-binding proteins, PonA1 and PonA2 which perform transglycolase and transpeptidase reactions[56, 57]. Both proteins are crucial in the maintenance of cell integrity and viability in mycobacteria. Studies have shown that PonA1 is important in the modulation of peptidoglycan hydrolysis through its interaction with the RipA-RpfB complex, while PonA2 being a vital protein for dormancy in *M.tb*[58].

1.1.2.3 Transpeptidases and mycobacterial cell wall biosynthesis
In many bacterial species peptidoglycan cross-linking is mainly carried out by D,D-transpeptidases which are also known as classical penicillin binding proteins (PDBs). However the activity of these enzymes can be bypassed by another family of transpeptidase enzymes called L,D-transpeptidases[59, 60]. Contrary to other bacteria, *M.tb* peptidoglycan cross-linking is predominantly performed by the L,D-transpeptidases. The D,D and L,D-transpeptidases are peptidoglycan polymerases which are structurally different, whereby they contain different active-site nucleophiles, the former having serine and the latter, cysteine[59, 61]. D,D-transpeptidases catalyse the formation of 4→3 peptidoglycan cross-links while L,D-transpeptidases form 3→3 crosslinks. In bacterial peptidoglycan crosslinking, a pair of stem peptides from adjoining glycan chains function as acyl donor and acceptor[60]. D,D-transpeptidases have a pentapeptide donor stem on which they split a D-Ala^4–D-Ala^5 (D,D) bond and a carbonyl of D-Ala^4 is connected to an amine on the third residue of the acceptor thereby form 4→3 cross-links[60, 61]. The L,D-transpeptidases possess a tetrapeptide donor stem and they cleave the L-Lys^3–D-Ala^4 (L,D) peptide bond from the acyl donor linking it to same acceptor (the carbonyl of D-Ala^4) to generate the 3→3 cross-links[60, 61]. Among all known bacteria *M.tb* is the only one expressing a high (80 %) percentage of 3→3 cross-links[62]. There is a difference in the peptidoglycan of actively replicating and dormant *M.tb*. The 4→3 trans-

peptide bonds mainly occur in the active *M.tb* while the non-replicating *M.tb* contains significantly more 3→3 linkages[37].

1.1.2.4 Inhibition of L,D Transpeptidase enzymes

L,D-transpeptidase enzymes are non-classical transpeptidases which are inhibited by a class of *β*-lactams, known as carbapenems, especially meropenem. The cysteine active residues of LDTs react forming thioester bonds with the *β*-lactam ring. Carbapenems in collaboration with clavulanic acid were shown to be effective against XDR strains of *M.tb*[63]. Clavulanate is a chemical compound which inhibits broad-spectrum BlaC *β*-lactamase irreversibly[64]. L,D-transpeptidases are essential proteins for peptidoglycan biosynthesis in *M.tb* and targeting them is likely to effectively control *M.tb*. *Mycobacterium tuberculosis* produces five paralogs of the enzyme (Ldt$_{Mt1}$ to Ldt$_{Mt5}$)[21] and the cause of such a redundancy is not yet understood. The most dominant and widely studied L,D-transpeptidase enzyme is Ldt$_{Mt2}$. Recent findings, however revealed that carbapenems fail to inactivate the paralog Ldt$_{Mt5}$. Cordillot *et al*. investigated peptidoglycan inhibition by *β*-lactams, and all five *M.tb* LDT paralogs were characterized according to acylation and peptidoglycan dimer formation by carbapenems[16]. It was discovered that the carbapenems failed to inactivate Ldt$_{Mt5}$ and the enzyme remained active in the peptidoglycan cross-linking assay. The study concluded that the antibacterial activity of carbapenems infer that Ldt$_{Mt5}$ is unique and it is not capable to compensate for the activity of other LDTs[16]. An experimental study conducted by Basta *et al*. determined the first crystal structures of the apo-form and Meropenem-bound Ldt$_{Mt5}$ and it was shown that the active site of Ldt$_{Mt5}$ possessed a structurally unique catalytic site which had a proline-rich C-terminal subdomain. Furthermore, it was discovered that *M.tb* lacking a functional copy of Ldt$_{Mt5}$ was vulnerable to denaturation by certain carbapenems, osmotic shock and crystal violet[17]. This strongly suggests that Ldt$_{Mt5}$ is not a mere functionally redundant paralog, but it is a unique and vital protein in maintaining integrity of the cell wall specifically in peptidoglycan metabolism therefore making it an important protein target[17].

1.1.2.5 Computational studies on L,D Transpeptidase enzymes

A number of computational studies have previously been performed on L,D-transpeptidases[18-23, 65, 66]. The reaction mechanism of (Ldt$_{Mt2}$) from *M.tb* with its natural substrate was evaluated through hybrid quantum mechanics/molecular mechanic (QM/MM) simulations and umbrella sampling[20]. The binding energies from the QM/MM MD simulations and the free energy profile associated with the catalytic mechanism of Ldt$_{Mt2}$[20] were in line with the isothermal

titration calorimetry (ITC) experimental binding energy trend and they revealed that acylation was the rate-limiting step[21]. Based on experimental findings, the reaction of joining of m-A^2pm^3 residue to m-A^2pm^3, involves acylation and deacylation[21]. The acylation stage is characterised by the formation of a thiolate/imidazole ion-pair (a zwitterion) and a nucleophilic attack on the carboxyl carbon of the substrate subsequently resulting in the peptide bond breaking. Silva *et al.* also conducted a study on the inactivation of Ldt_{Mt2} by the carbapenems, imipenem and meropenem using QM/MM simulations and an umbrella sampling[19]. Using density functional tight binding/molecular mechanics (DFTB/MM), a four-membered ring transition state was obtained and the theoretical energetics confirmed the previously reported experimental results[67]. Another theoretical study aimed at determining the mode of interactions of different carbapenems within the active site of Ldt_{Mt2} was performed using the MM-GBSA and SIE binding free energy approach[18]. Results from the study revealed a direct correlation between the energy of the inhibitor-Ldt_{Mt2} pre-complexes and the free energies of the covalently bound inhibitor-Ldt_{Mt2} complexes. This was however contrary to what was demonstrated by experimental data[21].

Using the DFT approach, Fakhar *et al.* conducted a mechanistic study of the carbapenems with Ldt_{Mt2} and came up with an acylation step model of the *β*-lactam ring. The study propounded three reaction pathways involving four-membered rings (TS-4, TS-4-His and TS-4-water) and one pathway involving a six-membered ring (TS-6-water). All the four suggested pathways revealed different transition states. It was concluded that the TS-6-water model best described the reaction mechanics. A study on the flap dynamics of Ldt_{Mt2} was also performed through MD simulations to evaluate the impact of induced conformational changes of the flap region during the binding process[22]. The MM-GBSA method had revealed greater binding energy for values imipenem complex with Ldt_{Mt2} as compared to the complexes with ertapenem and meropenem[23]. However, according to the dynamic cross-correlation matrix (DCCM) analysis there were strong anti-correlated motions in the imipenem-Ldt_{Mt2} flap whereas binding to ertapenem and meropenem induced a shift to correlation motion within flap units[22]. Various other experimental[16, 21, 68-73] and theoretical studies[6, 19, 20, 22, 23, 74, 75] have been performed on Ldt_{Mt2}. Our group has recently proposed a plausible mechanism for the interaction between the Ldt_{Mt2} enzyme and carbapenems. A theoretical investigation of the same computational model on Ldt_{Mt5} will provide a better understanding on why carbapenems inhibit Ldt_{Mt2}, but not Ldt_{Mt5}.

1.2 Computational methods

Computer-aided drug design (CADD) techniques have been crucial in the discovery and development of small molecules with therapeutic importance. There are basically two categories i.e. ligand-based and structure-based methods[76, 77]. Ligand-based methods make use of ligand information only, to predict activity based on similarity to known active ligands and tools such as homology modelling are utilised. Structure-based use both target and ligand structure information and utilities such as molecular docking are commonly employed[76, 77]. Ultimately compound databases are virtually screened to obtain ligands with potent therapeutic properties.

1.2.1 Virtual Screening

Virtual screening (VS) is a crucial computational technique in contemporary drug design and discovery to explore compound libraries, aimed at identifying putative binders for a specific drug target. It is effective in reducing the immense chemical space of huge databases to a smaller size that can be evaluated experimentally[78]. Structure-based virtual screening (SBVS) also known as neighbourhood behaviour search is the computational screening of small molecules for potential candidate ligands through docking into the binding structure of a protein receptor[79]. The technique offers greater possibility to discover novel ligands, however its success heavily relies on the quality of the receptor structure and the accuracy of the scoring function used to measure the binding affinity between a ligand and a receptor[80]. Modern technological advances in computational and bioinformatics have allowed for rapid chemical and biological data mining in search of novel compounds in a short space of time and limited computational expense. Structure-based virtual screening normally uses docking techniques and both free and commercially available docking software can be used to perform the ligand docking[81].

Docking principally involves the prediction of ligand orientation within a receptor binding site[82]. Fundamentally, all docking programs have conformational search algorithm which scouts for the best fit of inhibitors in the active site of the enzyme and a scoring function which ranks the various conformations as intermolecular binding energy[60]. The docking process is essential for the 3-dimensional (3D) structure modelling of the receptor-ligand complex and it is useful for analysing the strength of the interactions which determine molecular recognition. It is used for exploring conformations of a ligand within the binding pocket and estimation of their binding affinities[82]. This process is referred to as virtual screening when it is automated

for a large data set of ligands. Rigid docking and flexible docking are the two main forms of the docking technique. Rigid docking is a procedure that performs rigid body search and it is reliable only if the ligand molecule has a few rotatable bonds and does not assume multiple conformations within the active site. Flexible docking allows for ligand flexibility of both the ligand and the enzyme. The multiple rotatable bonds of the ligand and also of the amino acid residues are allowed to freely orient themselves to attain the best conformation possible[82, 83].

A review by Honarparvar *et al*. comprehensively discusses the molecular docking process[60]. It emphases the importance of confirming the flexibility of both the ligand molecule and the enzyme target when docking. It was revealed that flexible targets could undergo conformational changes upon binding a ligand, thus potentially affect the docking accuracy. The number of active sites on an enzyme is also of paramount importance since it is bound to affect the binding of ligand molecules. It was further highlighted in the review that the binding affinities of ligand molecules to the enzyme obtained from docking provide a general insight on the correlation on the activity of an inhibitor on an enzyme, but this approach has not always been reliable, since these are estimations[60]. Docking algorithms of SBVS are generally classified into three categories based on the search method i.e. algorithms that search the conformational space during docking (Monte Carlo algorithm and Genetic algorithm); algorithms searching the space before docking and algorithms performing incremental docking[84]. There are two types of failures protein-ligand docking predictions namely, soft and hard failures. A soft failure is a result of limitations in the search algorithm whereby the algorithm fails to locate the global energy minimum which corresponds to the crystal structure. A hard failure arises when the global energy minimum is corresponding to a mis-docked structure and the energy being lower than that of the minimized crystal structure. Such a failure emanates from inaccuracies in reproducing variability in the energies of other binding modes[85].

Scoring functions serve to distinguish the different poses (conformations) assumed by a ligand within the binding pocket of a receptor and following a docking procedure, the functions predict the binding affinities of various receptor-ligand complexes through ranking[83]. The scoring functions utilised in docking software applications apply certain assumptions in the evaluation of modelled complexes, therefore they are not able to account for the physical interactions that facilitate ligand binding such as hydrogen bonding, hydrophobic and solvation effects, Van der Waal's, steric and electrostatic interactions which are governed by kinetic and thermodynamic principles[86]. Scoring functions improve the effectiveness of docking

algorithms, however the binding affinities are estimated. There are four types of scoring functions available: consensus scoring, empirical-based, force-field based and knowledge-based scoring[84]. The review by Reddy *et al.* performed an appraisal on the available virtual screening methods and recent developments of the docking and similarity based methods[84]. Another review evaluated the various available docking software programs[87].

It is however important to realise that virtual screening has its draw backs. A review by Scior *et al.* critically evaluated the virtual screening technique and four major categories of classical limitations were highlighted and further discussed in detail. These limitations regard inaccurate assumptions and expectations; data design and content; some relate to the software choice and others are due to conformational sampling as well as protein and ligand flexibility[88]. In spite of the limitations highlighted, virtual screening plays an important role in drug discovery and development.

1.2.2 Molecular Dynamics (MD) Simulation

Molecular dynamics simulations are calculations which seek to describe the complex interactions (fluctuations and conformational changes of molecules) in biomolecular systems through computational models. A number of review articles[89-103] and textbooks[104-107] describe in detail the theory behind MD free energy calculations and its application to biomolecular systems. Different computational software such as Amber[108], ICM[109], and NAMD[110] can be used to perform MD simulations. Generally, a molecular system is initially modelled from either experimental structures or comparative modelling data[111]. All the forces exerted on the atoms in the system are then estimated from molecular mechanics principles. Simulations are typically performed on clusters or supercomputers because of the enormous amount of calculations required. The model which best reproduces the actual molecular interactions is the atomistic representation, which includes aspects such as bond angles, bond length and bond rotations[112]. Bonded and non-bonded atomic interactions, which produce Van der Waals and electrostatic forces, need to be taken into consideration and these are governed by quantum-mechanical laws such as Coulomb's law, Lennard-Jones potentials and Newtonian laws[113, 114]. Solvent representation is of paramount importance in system definition. In order to characterise the solvation effects of a real solvent such as hydrophobic effects, explicit solvation needs to be considered[112]. Force-fields are complicated equations which are aimed at deducing potential energy from the molecular structure. They are computational parameters summing up the various atomic forces that govern molecular dynamics of a particular system.

Different force fields are employed in MD simulations and they are fine-tuned with different parameters but generally giving similar results[115]. Common examples include AMBER[108], CHARMM[116] and GROMOS[117].

In the present study the AMBER MD software package will be utilised for various simulations. The AMBER force fields are described as follows[113]:

$$E_{AMBER} = E_{angle} + E_{bond} + E_{dihedral} + E_{non\text{-}bonded} \qquad \textbf{(1)}$$

E_{angle} are bond angle approximations whereas and E_{bond} are strain energies. The $E_{dihedral}$ is the energy interaction involving the dihedral angles of four atoms linearly-bonded. $E_{non\text{-}bonded}$ denotes the systems' non-bonded interactions composed of an electrostatic potential; Lennard-Jones potential for the van der Waals forces and the Pauli repulsion potential[114]. The AMBER force field (GAFF) has parameters fine-tuned for simulations involving proteins, nucleic acids and small organic compounds such as enzyme inhibitors[118]. Molecular dynamics simulations are important in describing molecular interactions, however their utility should not be overemphasised. There is need to perform studies comparing the simulations with experimental data in order to validate the computational model[111].

1.2.3 Molecular Mechanics (MM)

Molecular mechanics utilise the established traditional approach to estimate the total energy of a molecule with relation to its conformation[119]. It is very useful in deducing the potential energy for molecular dynamics simulations on complex molecules. Aspects such as transition states and geometries can be predicted and the relative energies between molecules can also be deduced[120, 121]. The greatest advantage of this method is that the computational cost of molecular mechanics is minimum. However, force field methods disregard the influence of electrons, electronic rearrangements (charge transfer, and/or electronic excitation) and bond breaking/formation, as a result this makes them inadequate to describe complex systems[120-122]. Considering the limitations of both approaches (QM and MM), hybrid methods have become popular and effective solutions for dealing with complex systems.

1.2.4 Quantum Mechanics (QM)

Quantum mechanics play a crucial role in investigating the mechanisms, which are involved in biochemical systems[121]. Owing to the rapid advancement in the development of super computers, QM can be harnessed to accurately predict the physical properties of reactions and provide reliable information on electronic properties, energies, geometries and reactivities of molecules[121, 122]. However, to accurately model complex systems such as protein structures,

the quantum mechanics method is limited in terms of high computational cost. In a bid to avert this challenge, a small but most significant portion of the system such as the active site only, is often considered at the QM level for the modelling[120]. The major setback of this approach is that it often leads to insufficient description of the system as a whole, which may result in misleading conclusions. Several textbooks discuss the principles and applications of quantum mechanics[123-126].

1.2.5 Hybrid quantum mechanics/molecular mechanics (QM/MM)

Quantum mechanics/molecular mechanics simulations are hybrid molecular simulation methods which incorporate the precision of quantum mechanics and the speed of molecular mechanics to evaluate chemical reactions in condensed phases[127, 128]. This allows the study of complex biochemical systems i.e. enzymes. In principle the system separates into compartments in which the reaction centre is subjected to the more precise and costly QM approach and the 'spectator' system is evaluated using the less accurate but efficient MM classical approach[119, 122]. Electrostatic interactions between the QM and MM region are categorised as either mechanical embedding or electrostatic embedding. Mechanical (classical) embedding is simple, and it deals with electrostatic interactions using low level theory at the MM level[120, 122]. The disadvantage of this method is that it is difficult to assign appropriate MM properties (*e.g.* atom centred point charges) to the QM region and its inability to consider the effects of electrostatic interactions on the electronic structure of the QM system[119]. Electrostatic embedding is an alternative method in which there is direct coupling of the QM wave function and the MM region[129]. Electronic interactions of the QM and MM region are integrated over the QM charge density[119, 120]. Based on the partitioning strategy, there exists two different forms of QM/MM of Hamiltonian known as subtractive and additive forms[130].

For the subtractive approach, the total energy $E_{QM/MM}$ is derived in a three-phase process. Firstly, at the MM level, the energy E_{MM} (QM+MM) of the whole system (comprising both QM and MM sections) is estimated. This is then followed by the addition of the QM energy of the separated QM sub-region which is denoted $E_{QM}(QM)$[120]. Thirdly, the MM energy of the QM sub-region $E_{MM}(QM)$ is then calculated and deducted. The equation below sums up the subtractive QM/MM method as follows:

$$E_{QM/MM} = E_{MM}\,(QM+MM) + E_{QM}(QM) - E_{MM}(QM) \qquad \textbf{(2)}$$

The advantages of this method are that it is very efficient and simple to implement since there no contact is necessary within the QM and MM aspects of the system[120, 121]. However, the

main setback of the approach is the limited availability of the force field to the QM portion and its lack of insufficient flexibility to describe certain changes occurring in chemical reactions[122]. The most popular subtractive QM/MM method is ONIOM (our Own N-layer Integrated molecular Orbital molecular Mechanics)[121, 131]. A review on the principles and applications of these methods appeared in 2012[130].

1.2.5.1 ONIOM

ONIOM is a reliable hybrid subtractive QM/MM method capable of performing a high-level QM calculation on a small selected region of the system while incorporating the environmental (lower-level) effects thus producing a consistent energy expression[121, 131]. This means that large and complex molecular systems can be calculated to produce energy and geometry with accuracy highly comparable to smaller systems, using limited computational resources through simple linear extrapolation[121]. The ONIOM method is flexible and versatile since approximations can be easily defined and performed as two-layer ONIOM (QM1:QM2), three-layer ONIOM (QM1:QM2:MM), or multi-layer model[128, 131, 132]. This hierarchical application of method makes it a unique hybrid QM/MM method[128, 132]. A recent review on the ONIOM method discussed the parameterization procedures and applications to varying classes of molecules and systems[121].

1.3 Experimental Methods

The main goal of pharmaceutical research is to discover and develop novel compounds capable of the influencing structure and regulating the function of disease-associated proteins[133]. Accurate knowledge of the structure and function of such proteins is of paramount importance in drug development. The initial step in contemporary drug discovery is the identification of biomolecules such as essential proteins which are directly involved in disease initiation and progression. This is then followed by the discovery of novel pharmaceutical compounds through searching for small drug-like molecules, (with small molecular weight) with 'promising' therapeutic effects[133]. These drug compounds can exhibit their therapeutic potential by inhibiting specific proteins or activating biomolecular signals via protein-protein and/or protein-DNA interactions. *In vitro* and *in vivo* tests are then carried out to evaluate the inhibitory effects of the identified compounds. The most common targets of drugs are enzymes since they take part in important biochemical events.

Advances in bioinformatics, genomics and proteomics have facilitated the application of various recombinant DNA techniques to evaluate the protein of interest[134]. Protein expression

together with protein purification are important tools extensively used in biopharmaceutical research for the preparation of pure proteins for various purposes such as antibody production, crystallization and kinetic studies. The success of any drug discovery study relies on the appropriate selection of an expression system as well as the optimization of experimental conditions[135]. In the current study, the aforementioned techniques will be used to prepare the enzyme, Ldt$_{Mt5}$ of *M.tb* to evaluate the binding of the computationally screened compounds.

1.3.1 Protein expression

Protein expression involves transcription and translation that is the creation of a copy of genetic information in the nucleus and copying of information to synthesize protein respectively[136]. It is one of the most important processes in biological systems. Important in heterologous protein expression procedures is the host bacterium *Escherichia coli* (*E. coli*) which because it is relatively easy to manipulate and economical, yet yields high-levels of recombinant protein production, a process commonly known as overexpression[137, 138]. A recent review evaluates genetic approaches for improvement of plasmid based expression of recombinant protein in *E. coli*[139]. Albeit, there are other bacteria which can be used for the same purpose such as *Lactococcus lactis*[140] and *Bacilli* (*Bacillus subtilis* and *Brevibacillus choshinensis*)[141, 142]. Other non-*E.coli* expression systems for heterologous proteins are yeast cell (*Kluyveromyces lactis*, *Pichia pastoris, Saccharomyces cerevisiae* and *Schizosaccharomyces pombe*), insect cell, mammalian cell and cell-free (CF) expression systems[140, 143, 144]. Furthermore, fungi and protozoa have been developed as alternative recombinant protein expression systems[145]. A review on the latest approaches on efficient production of protein for use in drug discovery critically evaluates these expression systems[146]. Protein expression using *E. coli* is cost effective in that cells can be grown to very high densities within a short period of time in inexpensive growth media[138]. There are many strains of *E. coli* which can be used for protein expression with peculiar advantages and disadvantages, therefore the choice of the strain is governed by the specialty of a strain. The BL21 (DE3) strain and its derivatives are the most popular strains for first expression screen and protein expression in general[136]. Common challenges associated with recombinant protein expression in *E. coli* are no or low expression, inclusion body formation and protein inactivity which were discussed critically in review[136, 139]. A typical protein expression workflow includes cloning, transformation, plasmid isolation clone confirmation through sequencing, induction and cell lysis. After lysis, a crude mixture of proteins is obtained that needs to be purified.

1.3.2 Protein purification

Protein purification principles and applications has been reviewed in several textbooks and reviews[147-151]. It is a systematic sequence of procedures aimed at isolating the protein of interest from a concoction of tissues or cells[147]. Purification of protein is important in the structure evaluation, function characterization and interaction assessment of the desired protein. Protein purification can be categorized as either *preparative* or *analytical*. Preparative purifications are aimed at producing proteins such as biopharmaceuticals, enzymes and nutritional proteins for especially for subsequent commercial applications. In this study analytical purification will be performed. The purpose of producing small amounts of protein in research is mainly for identification, quantification, and evaluation of the protein's structure and function. Different purification strategies can be employed based on the physicochemical characteristics, size, biological activity and binding affinity of the proteins in the mixture[147]. Chromatography is best applied for the purpose of protein purification[152]. There are various chromatographic techniques which are based on different exclusion properties. High performance liquid chromatography (HPLC) is a chromatographic technique harnessing high pressure to elute solutes by gradient through a column fast, thus limiting diffusion but improving resolution[147, 153]. Size exclusion chromatography is used to separate protein in solution by size through the use of porous gels. Free-flow electrophoresis, ion exchange chromatography and hydrophobic interaction chromatography are chromatographic techniques, which separate proteins on the basis of differences in charge or hydrophobicity[147, 152, 153].

The most widely used protein purification method for recombinant proteins expressed in bacteria is affinity chromatography[153]. This separation technique is based on molecular conformation, and it involves the use of specific resins and it includes immunoprecipitation, metal binding chromatography and immunoaffinity chromatography[147, 153]. The metal binding strategy is a technique in which six to eight histidines are engineered into the N- or C-terminal of a protein creating a polyhistidine tag and the protein is made to pass through a column with immobilized metal ions such as cobalt or nickel which bind strongly to the tag. The untagged proteins pass freely through the column whereas the tagged protein remains bound to the column. The desired protein is eluted with a chemical which competes for binding to the column with the histidine tag such as imidazole[147]. There are many challenges involved when microbial hosts are harnessed to express recombinant proteins. These include changes in conformation, structural flexibility and stability issues, protein insolubility, low purification yields and host cell toxicity[136]. However fusion tags coupled with affinity techniques address

these challenges of production and purification efficiency[150]. Enzymes are such proteins which are required to undergo the same treatment for use in biopharmaceutical engineering and testing, more specifically for enzyme inhibition assays.

1.3.3 Enzyme inhibition assays

In drug discovery target proteins are usually enzymes and inhibitors are generally small molecules that bind to the active site, thereby hindering the natural function of the enzyme. Competitive inhibitors are molecules which mimic the enzyme substrate and compete for the active site of the enzyme. Non-competitive inhibitors are compounds that can bind to an enzyme alongside or without a substrate, thereby changing the conformation of both the active site and the substrate[154]. The inhibition constant (Ki) is the concentration of inhibitor needed for half maximum inhibition and it is an indicator of the potency of an inhibitor. It is sometimes presented as dissociation constant KD or IC_{50}[155]. However, the difference between Ki and IC_{50} is that in enzymatic binding especially competitive binding, the inhibitor is competing with the substrate for the active site, so the concentration required for a 50 % enzyme activity reduction depends on the substrate and how tightly the inhibitor binds to the enzyme. The IC_{50} is usually greater than the Ki, however in low substrate concentration it tends to equal the Ki[154, 155].

Protein-ligand binding can be evaluated through various experimental techniques with varying basis of detection, sensitivity and interaction information output. Hydrodynamic and calorimetric methods of analysis include equilibrium dialysis and rate dialysis; affinity gel chromatography; analytical size exclusion chromatography; analytical ultracentrifugation; capillary electrophoresis; surface plasmon resonance; electro-optics; x-ray and neutron scattering; isothermal titration calorimetry and differential scanning calorimetry[156, 157]. Structural and spectroscopic techniques to study enzyme interactions with inhibitors include X-ray crystallography, circular dichroism; various fluorescence methods; mass spectroscopy; nuclear magnetic resonance; electron paramagnetic resonance and atomic force microscopy[156, 157]. In this present study, the method that will be considered for evaluating protein-ligand binding affinity is ITC which will be introduced and reviewed.

1.3.3.1 Isothermal Titration Calorimetry

To understand the structure-function relationship in biomolecules, thermodynamics need to be evaluated. One relevant technique for such evaluation is isothermal titration calorimetry[158]. This is a technique which measures binding of molecules through the detection of heat changes in solution. Several reviews and textbooks have discussed the characteristics, applications,

advantages and the challenges of this technique[159-166]. When performing this experiment, a solution containing the protein is titrated by a solution with the ligand (reactant) to attain heat exchange[158, 159]. Binding either produces an exothermic or endothermic reaction. The solution is kept at a constant temperature by a thermostat and the reaction is assessed through the amount of energy required to maintain the constant temperature. In ITC, the ligand concentration is the independent variable under experimental control. Data which can be processed and analysed from a single titration in ITC include the number of binding sites (*g*), the equilibrium/binding constant (K*b*), Gibbs free energy of binding (ΔG), binding enthalpy (ΔH), binding entropy (ΔS), and the stoichiometry (n) of binding[157-159, 167]. Furthermore, ITC experiments reveal information on electrostatic interactions, hydrophobic interactions and the type of reaction[159]. The advantages of using ITC are (a) high accuracy and duplicability with a limited degree of error[168]; (b) high robustness and responsiveness ranging from 10^{-2} to 10^{3} μM[169]; (c) it is a non-destructive technique with no molecular weight restrictions[166].

Several drug development studies targeting a specific protein have employed the assay[170-173]. It is suggested that ITC is the only technique capable of resolving the entropic and enthalpic elements of binding affinity which are paramount in evaluating high-affinity binding ligands[157, 160, 174, 175]. Isothermal titration calorimetry is an important assay to validate computationally attained structure-based predictions of binding energies and to establish detailed structure/energy correlations. It is possible to directly compare entropic and enthalpic elements between the computational simulations and the experimental if explicit solvation of the protein-ligand complex is performed on the model[160].

Aims and Objectives

Aim (Paper 1):

Computational screening of potential inhibitors against Ldt_{Mt5} and validation of the screened inhibitors through *in vitro* experiments.

Specific objectives of the study (Chapter 2)

- To perform virtual screening for potential inhibitors of Ldt_{Mt5} using computational applications
- To investigate the interactions and binding free energy between Ldt_{Mt5} and potential inhibitors using Molecular Dynamics (MD) simulations
- To express, purify and perform inhibition studies on Ldt_{Mt5} **(Chapter 4)**

Aim (Paper 2)

To determine a computational model employing Quantum Mechanics technique that explains the activity and activation energy of β-lactams against Ldt_{Mt5}.

Specific objectives of the study (Chapter 3)

- To investigate the nature of the transition state structure involved in the mechanism
- To determine the activation free energies of the mechanism using ONIOM through the thermodynamics and energetics of the reaction path

Thesis Outline

The current project evaluates the computational screening of potent lead compounds against Ldt_{Mt5} and the mechanism of interaction and experimental validation of screened compounds.

Chapter 2 outlines the virtual screening of compounds and molecular dynamics simulations to determine the calculated binding energies using AMBER 14.

Chapter 3 outlines the mechanism of action of selected β-lactams against Ldt_{Mt5} using ONIOM.

Chapter 4 evaluates the experimental binding thermodynamics of a selected β-lactam compound using ITC to validate the computational model.

Chapter 5 discusses the conclusion and the significance of the study.

References

[1] Organization, W. H. (2017) Antibacterial agents in clinical development: an analysis of the antibacterial clinical development pipeline, including tuberculosis.

[2] Crick, D. C., Mahapatra, S., and Brennan, P. J. (2001) Biosynthesis of the arabinogalactan-peptidoglycan complex of Mycobacterium tuberculosis, *Glycobiology 11*, 107R-118R.

[3] Organization, W. H. (1993) WHO declares tuberculosis a global emergency, In *WHO declares tuberculosis a global emergency*, pp 2-2.

[4] (WHO), W. H. O. (2016) World Health Organisation. *Global tuberculosis report* 2016 (cited 12 June 2017); available from http://apps.who.int/iris/bitstream/10665/250441/1/9789241565394-eng.pdf?ua=1.

[5] Filippova, E. V., Kieser, K. J., Luan, C. H., Wawrzak, Z., Kiryukhina, O., Rubin, E. J., and Anderson, W. F. (2016) Crystal structures of the transpeptidase domain of the Mycobacterium tuberculosis penicillin-binding protein PonA1 reveal potential mechanisms of antibiotic resistance, *The FEBS journal 283*, 2206-2218.

[6] Billones, J. B., Carrillo, M. C. O., Organo, V. G., Macalino, S. J. Y., Sy, J. B. A., Emnacen, I. A., Clavio, N. A. B., and Concepcion, G. P. (2016) Toward antituberculosis drugs: in silico screening of synthetic compounds against Mycobacterium tuberculosis L,D-transpeptidase 2, *Drug design, development and therapy 10*, 1147.

[7] Adewumi, O. A. (2012) Treatment outcomes in patients infected with multidrug resistant tuberculosis and in patients with multidrug resistant tuberculosis coinfected with human immunodeficiency virus at Brewelskloof Hospital.

[8] Seung, K. J., Keshavjee, S., and Rich, M. L. (2015) Multidrug-resistant tuberculosis and extensively drug-resistant tuberculosis, *Cold Spring Harbor perspectives in medicine*, a017863.

[9] Gandhi, N. R., Moll, A., Sturm, A. W., Pawinski, R., Govender, T., Lalloo, U., Zeller, K., Andrews, J., and Friedland, G. (2006) Extensively drug-resistant tuberculosis as a cause of death in patients co-infected with tuberculosis and HIV in a rural area of South Africa, *The Lancet 368*, 1575-1580.

[10] Migliori, G. B., Dheda, K., Centis, R., Mwaba, P., Bates, M., O'Grady, J., Hoelscher, M., and Zumla, A. (2010) Review of multidrug-resistant and extensively drug-resistant TB: global perspectives with a focus on sub-Saharan Africa, *Tropical Medicine & International Health 15*, 1052-1066.

[11] Dheda, K., Shean, K., Zumla, A., Badri, M., Streicher, E. M., Page-Shipp, L., Willcox, P., John, M. A., Reubenson, G., and Govindasamy, D. (2010) Early treatment outcomes and HIV status of patients with extensively drug-resistant tuberculosis in South Africa: a retrospective cohort study, *The Lancet 375*, 1798-1807.

[12] Calver, A. D., Murray, M., Strauss, O. J., Streicher, E. M., Hanekom, M., Liversage, T., Masibi, M., Van Helden, P. D., Warren, R. M., and Victor, T. C. (2010) Emergence of increased resistance and extensively drug-resistant tuberculosis despite treatment adherence, South Africa, *Emerging infectious diseases 16*, 264.

[13] Klopper, M., Warren, R. M., Hayes, C., van Pittius, N. C. G., Streicher, E. M., Müller, B., Sirgel, F. A., Chabula-Nxiweni, M., Hoosain, E., and Coetzee, G. (2013) Emergence and spread of extensively and totally drug-resistant tuberculosis, South Africa, *Emerging infectious diseases 19*, 449.

[14] Mlambo, C., Warren, R., Poswa, X., Victor, T., Duse, A., and Marais, E. (2008) Genotypic diversity of extensively drug-resistant tuberculosis (XDR-TB) in South Africa, *The international journal of tuberculosis and lung disease 12*, 99-104.

[15] Kana, B. D., Karakousis, P. C., Parish, T., and Dick, T. (2014) Future target-based drug discovery for tuberculosis?, *Tuberculosis 94*, 551-556.

[16] Cordillot, M., Dubée, V., Triboulet, S., Dubost, L., Marie, A., Hugonnet, J. E., Arthur, M., and Mainardi, J. L. (2013) In vitro cross-linking of Mycobacterium tuberculosis peptidoglycan by l,d-transpeptidases and inactivation of these enzymes by carbapenems, *Antimicrobial agents and chemotherapy 57*, 5940-5945.

[17] Basta, L. A. B., Ghosh, A., Pan, Y., Jakoncic, J., Lloyd, E. P., Townsend, C. A., Lamichhane, G., and Bianchet, M. A. (2015) Loss of a functionally and structurally distinct ld-transpeptidase, LdtMt5,

compromises cell wall integrity in mycobacterium tuberculosis, *Journal of Biological Chemistry 290*, 25670-25685.

[18] Silva, J. R. A., Bishai, W. R., Govender, T., Lamichhane, G., Maguire, G. E., Kruger, H. G., Lameira, J., and Alves, C. N. (2015) Targeting the cell wall of Mycobacterium tuberculosis: a molecular modeling investigation of the interaction of imipenem and meropenem with L,D-transpeptidase 2, *Journal of Biomolecular Structure and Dynamics 34*, 304-317.

[19] Silva, J. R. A., Govender, T., Maguire, G. E., Kruger, H. G., Lameira, J., Roitberg, A. E., and Alves, C. N. (2015) Simulating the inhibition reaction of Mycobacterium tuberculosis L,D-transpeptidase 2 by carbapenems, *Chemical Communications 51*, 12560-12562.

[20] Silva, J. R. R. A., Roitberg, A. E., and Alves, C. U. N. (2014) Catalytic mechanism of L,D-transpeptidase 2 from Mycobacterium tuberculosis described by a computational approach: insights for the design of new antibiotics drugs, *Journal of chemical information and modeling 54*, 2402-2410.

[21] Erdemli, S. B., Gupta, R., Bishai, W. R., Lamichhane, G., Amzel, L. M., and Bianchet, M. A. (2012) Targeting the cell wall of Mycobacterium tuberculosis: structure and mechanism of L,D-transpeptidase 2, *Structure 20*, 2103-2115.

[22] Fakhar, Z., Govender, T., Lamichhane, G., Maguire, G. E., Kruger, H. G., and Honarparvar, B. (2017) Computational model for the acylation step of the β-lactam ring: Potential application for l,d-transpeptidase 2 in mycobacterium tuberculosis, *Journal of Molecular Structure 1128*, 94-102.

[23] Fakhar, Z., Govender, T., Maguire, G. E., Lamichhane, G., Walker, R. C., Kruger, H. G., and Honarparvar, B. (2017) Differential flap dynamics in l,d-transpeptidase2 from mycobacterium tuberculosis revealed by molecular dynamics, *Molecular BioSystems 13*, 1223-1234.

[24] Ernst, J. D. (2012) The immunological life cycle of tuberculosis, *Nature reviews. Immunology 12*, 581.

[25] Kang, D. D., Lin, Y., Moreno, J. R., Randall, T. D., and Khader, S. A. (2011) Profiling early lung immune responses in the mouse model of tuberculosis, *PloS one 6*, e16161.

[26] Wolf, A. J., Linas, B., Trevejo-Nuñez, G. J., Kincaid, E., Tamura, T., Takatsu, K., and Ernst, J. D. (2007) Mycobacterium tuberculosis infects dendritic cells with high frequency and impairs their function in vivo, *The Journal of Immunology 179*, 2509-2519.

[27] Manca, C., Paul, S., Barry, C. E., Freedman, V. H., and Kaplan, G. (1999) Mycobacterium tuberculosis catalase and peroxidase activities and resistance to oxidative killing in human monocytes in vitro, *Infection and immunity 67*, 74-79.

[28] O'Brien, S., and Andrew, P. W. (1991) Guinea-pig alveolar macrophage killing of Mycobacterium tuberculosis, in vitro, does not require hydrogen peroxide or hydroxyl radical, *Microbial pathogenesis 11*, 229-236.

[29] Long, R., Jones, R., Talbot, J., Mayers, I., Barrie, J., Hoskinson, M., and Light, B. (2005) Inhaled nitric oxide treatment of patients with pulmonary tuberculosis evidenced by positive sputum smears, *Antimicrobial agents and chemotherapy 49*, 1209-1212.

[30] Rhoades, E. R., and Orme, I. M. (1997) Susceptibility of a panel of virulent strains of Mycobacterium tuberculosis to reactive nitrogen intermediates, *Infection and immunity 65*, 1189-1195.

[31] Russell, D. G. (2001) Mycobacterium tuberculosis: here today, and here tomorrow, *Nature reviews. Molecular cell biology 2*, 569.

[32] van der Wel, N., Hava, D., Houben, D., Fluitsma, D., van Zon, M., Pierson, J., Brenner, M., and Peters, P. J. (2007) M. tuberculosis and M. leprae translocate from the phagolysosome to the cytosol in myeloid cells, *Cell 129*, 1287-1298.

[33] Balcewicz-Sablinska, M. K., Keane, J., Kornfeld, H., and Remold, H. G. (1998) Pathogenic Mycobacterium tuberculosis evades apoptosis of host macrophages by release of TNF-R2, resulting in inactivation of TNF-α, *The journal of Immunology 161*, 2636-2641.

[34] Chen, M., Gan, H., and Remold, H. G. (2006) A mechanism of virulence: virulent Mycobacterium tuberculosis strain H37Rv, but not attenuated H37Ra, causes significant mitochondrial inner membrane disruption in macrophages leading to necrosis, *The Journal of Immunology 176*, 3707-3716.

[35] Kwan, C. K., and Ernst, J. D. (2011) HIV and tuberculosis: a deadly human syndemic, *Clinical microbiology reviews 24*, 351-376.

[36] Harris, J., and Keane, J. (2010) How tumour necrosis factor blockers interfere with tuberculosis immunity, *Clinical & Experimental Immunology 161*, 1-9.

[37] Alderwick, L. J., Harrison, J., Lloyd, G. S., and Birch, H. L. (2015) The Mycobacterial cell wall-peptidoglycan and Arabinogalactan, *Cold Spring Harbor perspectives in medicine 5*, a021113.

[38] Daffe, M., and Draper, P. (1997) The envelope layers of mycobacteria with reference to their pathogenicity, *Advances in microbial physiology 39*, 131-203.

[39] Mikušová, K. N., Yagi, T., Stern, R., McNeil, M. R., Besra, G. S., Crick, D. C., and Brennan, P. J. (2000) Biosynthesis of the galactan component of the mycobacterial cell wall, *Journal of Biological Chemistry 275*, 33890-33897.

[40] Brennan, P. J. (2003) Structure, function, and biogenesis of the cell wall of Mycobacterium tuberculosis, *Tuberculosis 83*, 91-97.

[41] Besra, G. S., Khoo, K. H., McNeil, M. R., Dell, A., Morris, H. R., and Brennan, P. J. (1995) A new interpretation of the structure of the mycolyl-arabinogalactan complex of Mycobacterium tuberculosis as revealed through characterization of oligoglycosylalditol fragments by fast-atom bombardment mass spectrometry and 1H nuclear magnetic resonance spectroscopy, *Biochemistry 34*, 4257-4266.

[42] Pan, F., Jackson, M., Ma, Y., and McNeil, M. (2001) Cell wall core galactofuran synthesis is essential for growth of mycobacteria, *Journal of bacteriology 183*, 3991-3998.

[43] Talip, B. A., Sleator, R. D., Lowery, C. J., Dooley, J. S., and Snelling, W. J. (2013) An update on global tuberculosis (TB), *Infectious Diseases: Research and Treatment 6*, IDRT. S11263.

[44] Raymond, J. B., Mahapatra, S., Crick, D. C., and Pavelka, M. S. (2005) Identification of the namH gene, encoding the hydroxylase responsible for the N-glycolylation of the mycobacterial peptidoglycan, *Journal of Biological Chemistry 280*, 326-333.

[45] Nikaido, H., and Brennan, P. (1995) The envelope of mycobacteria, *Annu. Rev. Biochem 64*, 29-63.

[46] Pavelka, M. S. (2007) Another brick in the wall, *Trends in microbiology 15*, 147-149.

[47] Durand, P., Golinelli-Pimpaneau, B., Mouilleron, S., Badet, B., and Badet-Denisot, M. A. (2008) Highlights of glucosamine-6P synthase catalysis, *Archives of biochemistry and biophysics 474*, 302-317.

[48] Jagtap, P. K. A., Soni, V., Vithani, N., Jhingan, G. D., Bais, V. S., Nandicoori, V. K., and Prakash, B. (2012) Substrate-bound crystal structures reveal features unique to Mycobacterium tuberculosis N-acetyl-glucosamine 1-phosphate uridyltransferase and a catalytic mechanism for acetyl transfer, *Journal of Biological Chemistry 287*, 39524-39537.

[49] Zhang, W., Jones, V. C., Scherman, M. S., Mahapatra, S., Crick, D., Bhamidi, S., Xin, Y., McNeil, M. R., and Ma, Y. (2008) Expression, essentiality, and a microtiter plate assay for mycobacterial GlmU, the bifunctional glucosamine-1-phosphate acetyltransferase and N-acetylglucosamine-1-phosphate uridyltransferase, *The international journal of biochemistry & cell biology 40*, 2560-2571.

[50] Kim, D. H., Lees, W. J., Kempsell, K. E., Lane, W. S., Duncan, K., and Walsh, C. T. (1996) Characterization of a Cys115 to Asp substitution in the Escherichia coli cell wall biosynthetic enzyme UDP-GlcNAc enolpyruvyl transferase (MurA) that confers resistance to inactivation by the antibiotic fosfomycin, *Biochemistry 35*, 4923-4928.

[51] Barreteau, H., Kovač, A., Boniface, A., Sova, M., Gobec, S., and Blanot, D. (2008) Cytoplasmic steps of peptidoglycan biosynthesis, *FEMS microbiology reviews 32*, 168-207.

[52] Falk, P. J., Ervin, K. M., Volk, K. S., and Ho, H. T. (1996) Biochemical evidence for the formation of a covalent acyl-phosphate linkage between UDP-N-acetylmuramate and ATP in the Escherichia coli UDP-N-acetylmuramate: L-alanine ligase-catalyzed reaction, *Biochemistry 35*, 1417-1422.

[53] Bouhss, A., Dementin, S., van Heijenoort, J., Parquet, C., and Blanot, D. (1999) Formation of adenosine 5'-tetraphosphate from the acyl phosphate intermediate: a difference between the MurC and MurD synthetases of Escherichia coli, *FEBS letters 453*, 15-19.

[54] Mahapatra, S., Crick, D. C., and Brennan, P. J. (2000) Comparison of the UDP-N-Acetylmuramate: l-Alanine Ligase Enzymes from Mycobacterium tuberculosis and Mycobacterium leprae, *Journal of bacteriology 182*, 6827-6830.

[55] Feng, Z., and Barletta, R. G. (2003) Roles of Mycobacterium smegmatis D-alanine: D-alanine ligase and D-alanine racemase in the mechanisms of action of and resistance to the peptidoglycan inhibitor D-cycloserine, *Antimicrobial agents and chemotherapy 47*, 283-291.

[56] Butler, E. K., Davis, R. M., Bari, V., Nicholson, P. A., and Ruiz, N. (2013) Structure-function analysis of MurJ reveals a solvent-exposed cavity containing residues essential for peptidoglycan biogenesis in Escherichia coli, *Journal of bacteriology 195*, 4639-4649.

[57] Mohamed, Y. F., and Valvano, M. A. (2014) A Burkholderia cenocepacia MurJ (MviN) homolog is essential for cell wall peptidoglycan synthesis and bacterial viability, *Glycobiology 24*, 564-576.

[58] Hett, E. C., Chao, M. C., and Rubin, E. J. (2010) Interaction and modulation of two antagonistic cell wall enzymes of mycobacteria, *PLoS pathogens 6*, e1001020.

[59] Triboulet, S., Arthur, M., Mainardi, J. L., Veckerlé, C., Dubée, V., NGuekam-Moumi, A., Gutmann, L., Rice, L. B., and Hugonnet, J. E. (2011) Inactivation kinetics of a new target of β-lactam antibiotics, *Journal of Biological Chemistry 286*, 22777-22784.

[60] Honarparvar, B., Govender, T., Maguire, G. E., Soliman, M. E., and Kruger, H. G. (2013) Integrated approach to structure-based enzymatic drug design: molecular modeling, spectroscopy, and experimental bioactivity, *Chemical reviews 114*, 493-537.

[61] Mainardi, J. L., Fourgeaud, M., Hugonnet, J. E., Dubost, L., Brouard, J. P., Ouazzani, J., Rice, L. B., Gutmann, L., and Arthur, M. (2005) A novel peptidoglycan cross-linking enzyme for a β-lactam-resistant transpeptidation pathway, *Journal of Biological Chemistry 280*, 38146-38152.

[62] Lavollay, M., Arthur, M., Fourgeaud, M., Dubost, L., Marie, A., Veziris, N., Blanot, D., Gutmann, L., and Mainardi, J. L. (2008) The peptidoglycan of stationary-phase Mycobacterium tuberculosis predominantly contains cross-links generated by L,D-transpeptidation, *Journal of bacteriology 190*, 4360-4366.

[63] Hugonnet, J. E., Tremblay, L. W., Boshoff, H. I., Barry, C. E., and Blanchard, J. S. (2009) Meropenem-clavulanate is effective against extensively drug-resistant Mycobacterium tuberculosis, *Science 323*, 1215-1218.

[64] Hugonnet, J. E., and Blanchard, J. S. (2007) Irreversible inhibition of the Mycobacterium tuberculosis β-lactamase by clavulanate, *Biochemistry 46*, 11998-12004.

[65] Correale, S., Ruggiero, A., Capparelli, R., Pedone, E., and Berisio, R. (2013) Structures of free and inhibited forms of the L, D-transpeptidase LdtMt1 from Mycobacterium tuberculosis, *Acta Crystallographica Section D: Biological Crystallography 69*, 1697-1706.

[66] Li, W. J., Li, D. F., Hu, Y. L., Zhang, X. E., Bi, L. J., and Wang, D. C. (2013) Crystal structure of L,D-transpeptidase Ldt Mt2 in complex with meropenem reveals the mechanism of carbapenem against Mycobacterium tuberculosis, *Cell research 23*, 728.

[67] Ackerman, S. H., and Gatti, D. L. (2013) Biapenem inactivation by B2 metallo β-lactamases: energy landscape of the hydrolysis reaction, *PloS one 8*, e55136.

[68] Bianchet, M. A., Pan, Y. H., Basta, L. A. B., Saavedra, H., Lloyd, E. P., Kumar, P., Mattoo, R., Townsend, C. A., and Lamichhane, G. (2017) Structural insight into the inactivation of Mycobacterium tuberculosis non-classical transpeptidase Ldt Mt2 by biapenem and tebipenem, *BMC biochemistry 18*, 8.

[69] Böth, D., Steiner, E. M., Stadler, D., Lindqvist, Y., Schnell, R., and Schneider, G. (2013) Structure of LdtMt2, an L,D-transpeptidase from Mycobacterium tuberculosis, *Acta Crystallographica Section D: Biological Crystallography 69*, 432-441.

[70] Schoonmaker, M. K., Bishai, W. R., and Lamichhane, G. (2014) Non-classical transpeptidases of Mycobacterium tuberculosis alter cell size, morphology, cytosolic matrix, protein localization, virulence and resistance to β-lactams, *Journal of bacteriology*, JB. 01396-01313.

[71] Kumar, P., Kaushik, A., Lloyd, E. P., Li, S. G., Mattoo, R., Ammerman, N. C., Bell, D. T., Perryman, A. L., Zandi, T. A., and Ekins, S. (2017) Non-classical transpeptidases yield insight into new antibacterials, *Nature chemical biology 13*, 54.

[72] Kim, H. S., Kim, J., Im, H. N., Yoon, J. Y., An, D. R., Yoon, H. J., Kim, J. Y., Min, H. K., Kim, S. J., and Lee, J. Y. (2013) Structural basis for the inhibition of Mycobacterium tuberculosis L, D-transpeptidase by meropenem, a drug effective against extensively drug-resistant strains, *Acta Crystallographica Section D: Biological Crystallography 69*, 420-431.

[73] Steiner, E. M., Schneider, G., and Schnell, R. (2017) Binding and processing of β-lactam antibiotics by the transpeptidase LdtMt2 from Mycobacterium tuberculosis, *The FEBS journal 284*, 725-741.

[74] Silva, J. R. A., Bishai, W. R., Govender, T., Lamichhane, G., Maguire, G. E., Kruger, H. G., Lameira, J., and Alves, C. N. (2016) Targeting the cell wall of Mycobacterium tuberculosis: a molecular modeling investigation of the interaction of imipenem and meropenem with L,D-transpeptidase 2, *Journal of Biomolecular Structure and Dynamics 34*, 304-317.

[75] Baldin, S., Misiura, N., and Švedas, V. (2017) Building a full-atom model of l,d transpeptidase 2 from Mycobacterium tuberculosis for screening new inhibitors, *Acta Naturae (англоязычная версия) 9*.

[76] Sliwoski, G., Kothiwale, S., Meiler, J., and Lowe, E. W. (2014) Computational methods in drug discovery, *Pharmacological reviews 66*, 334-395.

[77] Leelananda, S. P., and Lindert, S. (2016) Computational methods in drug discovery, *Beilstein journal of organic chemistry 12*, 2694.

[78] Dilip, A., Lešnik, S., Štular, T., Janežič, D., and Konc, J. (2016) Ligand-based virtual screening interface between PyMOL and LiSiCA, *Journal of cheminformatics 8*, 46.

[79] Yang, Y., Zhan, J., and Zhou, Y. (2016) SPOT-Ligand: Fast and effective structure-based virtual screening by binding homology search according to ligand and receptor similarity, *Journal of computational chemistry 37*, 1734-1739.

[80] Cheng, T., Li, Q., Zhou, Z., Wang, Y., and Bryant, S. H. (2012) Structure-based virtual screening for drug discovery: a problem-centric review, *The AAPS journal 14*, 133-141.

[81] Vyas, V., Ukawala, R., Ghate, M., and Chintha, C. (2012) Homology modeling a fast tool for drug discovery: current perspectives, *Indian journal of pharmaceutical sciences 74*, 1.

[82] Kitchen, D. B., Decornez, H., Furr, J. R., and Bajorath, J. (2004) Docking and scoring in virtual screening for drug discovery: methods and applications, *Nature reviews Drug discovery 3*, 935-949.

[83] Halperin, I., Ma, B., Wolfson, H., and Nussinov, R. (2002) Principles of docking: An overview of search algorithms and a guide to scoring functions, *Proteins: Structure, Function, and Bioinformatics 47*, 409-443.

[84] Reddy, A. S., Pati, S. P., Kumar, P. P., Pradeep, H., and Sastry, G. N. (2007) Virtual screening in drug discovery-a computational perspective, *Current Protein and Peptide Science 8*, 329-351.

[85] Verkhivker, G. M., Bouzida, D., Gehlhaar, D. K., Rejto, P. A., Arthurs, S., Colson, A. B., Freer, S. T., Larson, V., Luty, B. A., and Marrone, T. (2000) Deciphering common failures in molecular docking of ligand-protein complexes, *Journal of computer-aided molecular design 14*, 731-751.

[86] Rester, U. (2006) Dock around the clock–current status of small molecule docking and scoring, *Molecular Informatics 25*, 605-615.

[87] Pagadala, N. S., Syed, K., and Tuszynski, J. (2017) Software for molecular docking: a review, *Biophysical reviews 9*, 91-102.

[88] Scior, T., Bender, A., Tresadern, G., Medina-Franco, J. L., Martínez-Mayorga, K., Langer, T., Cuanalo-Contreras, K., and Agrafiotis, D. K. (2012) Recognizing pitfalls in virtual screening: a critical review, *Journal of chemical information and modeling 52*, 867-881.

[89] Cozzini, P., Fornabaio, M., Marabotti, A., Abraham, D. J., Kellogg, G. E., and Mozzarelli, A. (2004) Free energy of ligand binding to protein: evaluation of the contribution of water molecules by computational methods, *Current medicinal chemistry 11*, 3093-3118.

[90] Hu, H., and Yang, W. (2008) Free energies of chemical reactions in solution and in enzymes with ab initio quantum mechanics/molecular mechanics methods, *Annu. Rev. Phys. Chem. 59*, 573-601.

[91] van Gunsteren, W. F., Daura, X., and Mark, A. E. (2002) Computation of free energy, *Helvetica Chimica Acta 85*, 3113-3129.

[92] Brandsdal, B. O., Österberg, F., Almlöf, M., Feierberg, I., Luzhkov, V. B., and Åqvist, J. (2003) Free energy calculations and ligand binding, In *Advances in protein chemistry*, pp 123-158, Elsevier.

[93] Rodinger, T., and Pomès, R. (2005) Enhancing the accuracy, the efficiency and the scope of free energy simulations, *Current opinion in structural biology 15*, 164-170.

[94] Shirts, M. R., and Pande, V. S. (2005) Solvation free energies of amino acid side chain analogs for common molecular mechanics water models, *The Journal of chemical physics 122*, 134508.

[95] Wang, J., Hou, T., and Xu, X. (2006) Recent advances in free energy calculations with a combination of molecular mechanics and continuum models, *Current Computer-Aided Drug Design 2*, 287-306.

[96] Foloppe, N., and Hubbard, R. (2006) Towards predictive ligand design with free-energy based computational methods?, *Current medicinal chemistry 13*, 3583-3608.

[97] Blumberger, J. (2008) Free energies for biological electron transfer from QM/MM calculation: method, application and critical assessment, *Physical Chemistry Chemical Physics 10*, 5651-5667.

[98] Meirovitch, H., Cheluvaraja, S., and White, R. P. (2009) Methods for calculating the entropy and free energy and their application to problems involving protein flexibility and ligand binding, *Current Protein and Peptide Science 10*, 229-243.

[99] Steinbrecher, T., and Labahn, A. (2010) Towards accurate free energy calculations in ligand protein-binding studies, *Current medicinal chemistry 17*, 767-785.

[100] Söderhjelm, P., Kongsted, J., Genheden, S., and Ryde, U. (2010) Estimates of ligand-binding affinities supported by quantum mechanical methods, *Interdisciplinary Sciences: Computational Life Sciences 2*, 21-37.

[101] Christ, C. D., Mark, A. E., and Van Gunsteren, W. F. (2010) Basic ingredients of free energy calculations: a review, *Journal of computational chemistry 31*, 1569-1582.

[102] Gorham, R. D., Kieslich, C. A., and Morikis, D. (2011) Electrostatic clustering and free energy calculations provide a foundation for protein design and optimization, *Annals of biomedical engineering 39*, 1252-1263.

[103] Noy, E., and Senderowitz, H. (2011) Molecular simulations for the evaluation of binding free energies in lead optimization, *Drug Development Research 72*, 36-44.

[104] Christov, C. (2016) *Insights into Enzyme Mechanisms and Functions from Experimental and Computational Methods*, Vol. 105, Academic Press.

[105] Reddy, M. R., and Erion, M. D. (2001) *Free energy calculations in rational drug design*, Springer Science & Business Media.

[106] Frenkel, D., and Smit, B. (2002) Understanding molecular simulations: from algorithms to applications, Academic press.

[107] Chipot, C., and Pohorille, A. (2007) *Free energy calculations*, Springer.

[108] Case, D. A., Cheatham, T. E., Darden, T., Gohlke, H., Luo, R., Merz, K. M., Onufriev, A., Simmerling, C., Wang, B., and Woods, R. J. (2005) The Amber biomolecular simulation programs, *Journal of computational chemistry 26*, 1668-1688.

[109] Schapira, M., Totrov, M., and Abagyan, R. (1999) Prediction of the binding energy for small molecules, peptides and proteins, *Journal of Molecular Recognition 12*, 177-190.

[110] Phillips, J. C., Braun, R., Wang, W., Gumbart, J., Tajkhorshid, E., Villa, E., Chipot, C., Skeel, R. D., Kale, L., and Schulten, K. (2005) Scalable molecular dynamics with NAMD, *Journal of computational chemistry 26*, 1781-1802.

[111] Durrant, J. D., and McCammon, J. A. (2011) Molecular dynamics simulations and drug discovery, *BMC biology 9*, 71.

[112] Hospital, A., Goñi, J. R., Orozco, M., and Gelpí, J. L. (2015) Molecular dynamics simulations: advances and applications, *Advances and applications in bioinformatics and chemistry: AABC 8*, 37.

[113] Cornell, W. D., Cieplak, P., Bayly, C. I., Gould, I. R., Merz, K. M., Ferguson, D. M., Spellmeyer, D. C., Fox, T., Caldwell, J. W., and Kollman, P. A. (1995) A second generation force field for the simulation

of proteins, nucleic acids, and organic molecules, *Journal of the American Chemical Society 117*, 5179-5197.

[114] Jones, J. E. (1924) On the determination of molecular fields. II. From the equation of state of a gas, In *Proceedings of the Royal Society of London A: Mathematical, Physical and Engineering Sciences*, pp 463-477, The Royal Society.

[115] Rueda, M., Ferrer-Costa, C., Meyer, T., Pérez, A., Camps, J., Gelpí, J. L., and Orozco, M. (2007) A consensus view of protein dynamics, *Proceedings of the National Academy of Sciences 104*, 796-801.

[116] Vanommeslaeghe, K., Hatcher, E., Acharya, C., Kundu, S., Zhong, S., Shim, J., Darian, E., Guvench, O., Lopes, P., and Vorobyov, I. (2010) CHARMM general force field: A force field for drug-like molecules compatible with the CHARMM all-atom additive biological force fields, *Journal of computational chemistry 31*, 671-690.

[117] van Gunsteren, W. F., Daura, X., and Mark, A. E. (2002) GROMOS force field, *Encyclopedia of computational chemistry 2*.

[118] Wang, J., Wolf, R. M., Caldwell, J. W., Kollman, P. A., and Case, D. A. (2004) Development and testing of a general amber force field, *Journal of computational chemistry 25*, 1157-1174.

[119] van der Kamp, M. W., and Mulholland, A. J. (2013) Combined quantum mechanics/molecular mechanics (QM/MM) methods in computational enzymology, *Biochemistry 52*, 2708-2728.

[120] Lin, H., and Truhlar, D. G. (2007) QM/MM: what have we learned, where are we, and where do we go from here?, *Theoretical Chemistry Accounts 117*, 185.

[121] Chung, L. W., Sameera, W., Ramozzi, R., Page, A. J., Hatanaka, M., Petrova, G. P., Harris, T. V., Li, X., Ke, Z., and Liu, F. (2015) The ONIOM method and its applications, *Chemical reviews 115*, 5678-5796.

[122] Groenhof, G. (2013) Introduction to QM/MM simulations, In *Biomolecular Simulations*, pp 43-66, Springer.

[123] Zettili, N. (2003) Quantum mechanics: concepts and applications, AAPT.

[124] McGervey, J. D. (2017) *Quantum mechanics: concepts and applications*, Academic Press.

[125] Tannor, D. J. (2007) *Introduction to quantum mechanics: a time-dependent perspective*, University Science Books.

[126] Lewars, E. G. (2010) *Computational chemistry: introduction to the theory and applications of molecular and quantum mechanics*, Springer Science & Business Media.

[127] Singh, U. C., and Kollman, P. A. (1986) A combined ab initio quantum mechanical and molecular mechanical method for carrying out simulations on complex molecular systems: Applications to the CH3Cl+ Cl− exchange reaction and gas phase protonation of polyethers, *Journal of Computational Chemistry 7*, 718-730.

[128] Maseras, F., and Morokuma, K. (1995) IMOMM: A new integrated ab initio+ molecular mechanics geometry optimization scheme of equilibrium structures and transition states, *Journal of Computational Chemistry 16*, 1170-1179.

[129] Hratchian, H. P., Parandekar, P. V., Raghavachari, K., Frisch, M. J., and Vreven, T. (2008) QM: QM electronic embedding using Mulliken atomic charges: Energies and analytic gradients in an ONIOM framework, *The Journal of chemical physics 128*, 034107.

[130] Xu, D., Zheng, M., and Wu, S. (2012) Principles and Applications of Hybrid Quantum Mechanical and Molecular Mechanical Methods, In *Quantum Simulations of Materials and Biological Systems*, pp 155-168, Springer.

[131] Vreven, T., Byun, K. S., Komáromi, I., Dapprich, S., Montgomery Jr, J. A., Morokuma, K., and Frisch, M. J. (2006) Combining quantum mechanics methods with molecular mechanics methods in ONIOM, *Journal of Chemical Theory and Computation 2*, 815-826.

[132] Svensson, M., Humbel, S., Froese, R. D., Matsubara, T., Sieber, S., and Morokuma, K. (1996) ONIOM: a multilayered integrated MO+ MM method for geometry optimizations and single point energy predictions. A test for Diels– Alder reactions and Pt (P (t-Bu) 3) 2+ H2 oxidative addition, *The Journal of Physical Chemistry 100*, 19357-19363.

[133] Ideker, T., and Sharan, R. (2008) Protein networks in disease, *Genome research 18*, 644-652.

[134] Young, C. L., Britton, Z. T., and Robinson, A. S. (2012) Recombinant protein expression and purification: a comprehensive review of affinity tags and microbial applications, *Biotechnology journal 7*, 620-634.

[135] Gräslund, S., Nordlund, P., Weigelt, J., Hallberg, B. M., Bray, J., Gileadi, O., Knapp, S., Oppermann, U., Arrowsmith, C., and Hui, R. (2008) Protein production and purification, *Nature methods 5*, 135.

[136] Rosano, G. L., and Ceccarelli, E. A. (2014) Recombinant protein expression in Escherichia coli: advances and challenges, *Frontiers in microbiology 5*, 172.

[137] Sezonov, G., Joseleau-Petit, D., and D'Ari, R. (2007) Escherichia coli physiology in Luria-Bertani broth, *Journal of bacteriology 189*, 8746-8749.

[138] Shiloach, J., and Fass, R. (2005) Growing E. coli to high cell density—a historical perspective on method development, *Biotechnology advances 23*, 345-357.

[139] Singha, T. K., Gulati, P., Mohanty, A., Khasa, Y. P., Kapoor, R. K., and Kumar, S. (2017) Efficient genetic approaches for improvement of plasmid based expression of recombinant protein in Escherichia coli: A review, *Process Biochemistry 55*, 17-31.

[140] Chen, R. (2012) Bacterial expression systems for recombinant protein production: E. coli and beyond, *Biotechnology advances 30*, 1102-1107.

[141] Tanio, M., Tanaka, T., and Kohno, T. (2008) 15N isotope labeling of a protein secreted by Brevibacillus choshinensis for NMR study, *Analytical biochemistry 1*, 164-166.

[142] Tanio, M., Tanaka, R., Tanaka, T., and Kohno, T. (2009) Amino acid-selective isotope labeling of proteins for nuclear magnetic resonance study: proteins secreted by Brevibacillus choshinensis, *Analytical biochemistry 386*, 156-160.

[143] Sugiki, T., Shimada, I., and Takahashi, H. (2008) Stable isotope labeling of protein by Kluyveromyces lactis for NMR study, *Journal of biomolecular NMR 42*, 159-162.

[144] Sato, Y., Aizawa, K., Ezure, T., Ando, E., and Uozumi, N. (2012) A simple fed-batch method for transcription and insect cell-free translation, *Journal of bioscience and bioengineering 114*, 677-679.

[145] Fernandez, F. J., and Vega, M. C. (2013) Technologies to keep an eye on: alternative hosts for protein production in structural biology, *Current opinion in structural biology 23*, 365-373.

[146] Sugiki, T., Fujiwara, T., and Kojima, C. (2014) Latest approaches for efficient protein production in drug discovery, *Expert opinion on drug discovery 9*, 1189-1204.

[147] Scopes, R. K. (2013) *Protein purification: principles and practice*, Springer Science & Business Media.

[148] Cutler, P. (2004) *Protein purification protocols*, Vol. 244, Springer Science & Business Media.

[149] Burgess, R. R., and Deutscher, M. P. (2009) *Guide to protein purification*, Vol. 463, Academic Press.

[150] Waugh, D. S. (2005) Making the most of affinity tags, *Trends in biotechnology 23*, 316-320.

[151] Yang, H., Viera, C., Fischer, J., and Etzel, M. R. (2002) Purification of a large protein using ion-exchange membranes, *Industrial & engineering chemistry research 41*, 1597-1602.

[152] Harrison, R. (1993) *Protein purification process engineering*, Vol. 18, CRC Press.

[153] Schmitt, J., Hess, H., and Stunnenberg, H. G. (1993) Affinity purification of histidine-tagged proteins, *Molecular biology reports 18*, 223-230.

[154] Yung-Chi, C., and Prusoff, W. H. (1973) Relationship between the inhibition constant (Ki) and the concentration of inhibitor which causes 50 per cent inhibition (I50) of an enzymatic reaction, *Biochemical pharmacology 22*, 3099-3108.

[155] Gilson, M. K. (2009) BindingDB: Background.

[156] Chowdhry, B. Z., and Harding, S. E. (2001) Protein-ligand interactions and their analysis, *Protein–ligand interactions: hydrodynamics and calorimetry: a practical approach. Oxford University Press, Oxford, UK*.

[157] Du, X., Li, Y., Xia, Y. L., Ai, S. M., Liang, J., Sang, P., Ji, X. L., and Liu, S. Q. (2016) Insights into protein–ligand interactions: Mechanisms, models, and methods, *International journal of molecular sciences 17*, 144.

[158] Freire, E., Mayorga, O. L., and Straume, M. (1990) Isothermal titration calorimetry, *Analytical chemistry 62*, 950A-959A.

[159] Saboury, A. (2006) A review on the ligand binding studies by isothermal titration calorimetry, *Journal of the Iranian Chemical Society 3*, 1-21.

[160] Leavitt, S., and Freire, E. (2001) Direct measurement of protein binding energetics by isothermal titration calorimetry, *Current opinion in structural biology 11*, 560-566.

[161] Jelesarov, I., and Bosshard, H. R. (1999) Isothermal titration calorimetry and differential scanning calorimetry as complementary tools to investigate the energetics of biomolecular recognition, *Journal of molecular recognition 12*, 3-18.

[162] Feig, A. L. (2007) Applications of isothermal titration calorimetry in RNA biochemistry and biophysics, *Biopolymers: Original Research on Biomolecules 87*, 293-301.

[163] Doyle, M. L. (1997) Characterization of binding interactions by isothermal titration calorimetry, *Current Opinion in Biotechnology 8*, 31-35.

[164] Falconer, R. J., and Collins, B. M. (2011) Survey of the year 2009: applications of isothermal titration calorimetry, *Journal of Molecular Recognition 24*, 1-16.

[165] Ladbury, J. E. (2004) Application of isothermal titration calorimetry in the biological sciences: things are heating up!, *Biotechniques 37*, 885-887.

[166] Bouchemal, K. (2008) New challenges for pharmaceutical formulations and drug delivery systems characterization using isothermal titration calorimetry, *Drug Discovery Today 13*, 960-972.

[167] Pierce, M. M., Raman, C., and Nall, B. T. (1999) Isothermal titration calorimetry of protein–protein interactions, *Methods 19*, 213-221.

[168] Krell, T. (2008) Microcalorimetry: a response to challenges in modern biotechnology, *Microbial biotechnology 1*, 126-136.

[169] Freyer, M. W., and Lewis, E. A. (2008) Isothermal titration calorimetry: experimental design, data analysis, and probing macromolecule/ligand binding and kinetic interactions, *Methods in cell biology 84*, 79-113.

[170] Sarver, R. W., Yuan, P., Marshall, V. P., Petzold, G. L., Poorman, R. A., DeZwaan, J., and Stockman, B. J. (1999) Thermodynamic and circular dichroism studies differentiate inhibitor interactions with the stromelysin S 1–S 3 and S' 1–S' 3 subsites, *Biochimica et Biophysica Acta (BBA)-Protein Structure and Molecular Enzymology 1434*, 304-316.

[171] Bachhawat, K., Thomas, C. J., Surolia, N., and Surolia, A. (2000) Interaction of chloroquine and its analogues with heme: an isothermal titration calorimetric study, *Biochemical and biophysical research communications 276*, 1075-1079.

[172] Kožíšek, M., Bray, J., Řezáčová, P., Šašková, K., Brynda, J., Pokorná, J., Mammano, F., Rulíšek, L., and Konvalinka, J. (2007) Molecular analysis of the HIV-1 resistance development: enzymatic activities, crystal structures, and thermodynamics of nelfinavir-resistant HIV protease mutants, *Journal of molecular biology 374*, 1005-1016.

[173] Zhang, Y. L., Yao, Z. J., Sarmiento, M., Wu, L., Burke, T. R., and Zhang, Z. Y. (2000) Thermodynamic study of ligand binding to protein-tyrosine phosphatase 1B and its substrate-trapping mutants, *Journal of Biological Chemistry 275*, 34205-34212.

[174] Perozzo, R., Folkers, G., and Scapozza, L. (2004) Thermodynamics of protein–ligand interactions: history, presence, and future aspects, *Journal of Receptors and Signal Transduction 24*, 1-52.

[175] Bronowska, A. K. (2011) Thermodynamics of ligand-protein interactions: implications for molecular design, In *Thermodynamics-Interaction Studies-Solids, Liquids and Gases*, InTech.

Chapter 2

Identification of potent L,D-transpeptidase 5 inhibitors for *Mycobacterium tuberculosis* as potential anti-TB leads: Virtual Screening and Molecular Dynamics Simulations

Victor T. Sabe[1], Gideon F. Tolufashe[1], Sibusiso B. Maseko[1], Collins U. Ibeji,[1] Thavendran Govender [1], Glenn E. M. Maguire[1,2], Gyanu Lamichhane[3], Bahareh Honarparvar[1]* and Hendrik G. Kruger[1]*

[1]Catalysis and Peptide Research Unit, School of Health Sciences, University of KwaZulu-Natal, Durban 4001, South Africa.

[2]School of Chemistry and Physics, University of KwaZulu-Natal, 4001 Durban, South Africa.

[3]Center for Tuberculosis Research, Division of Infectious Diseases, School of Medicine, Johns Hopkins University, Baltimore, MD 21205, USA.

*Corresponding authors: kruger@ukzn.ac.za (Prof. Hendrik G. Kruger), Honarparvarb@ukzn.ac.za (Dr Bahareh Honarparvar), Telephone: + 27 31 2601845, Fax: +27 31 2603091, Catalysis and Peptide Research Unit, School of Health Sciences, University of KwaZulu-Natal, Durban 4041, South Africa.

Abstract

Virtual screening is a useful *in silico* approach to identify potential leads against various targets. It is known that carbapenems (doripenem and faropenem) do not show any reasonable inhibitory activities against L,D-transpeptidase 5 (Ldt_{Mt5}) and also an adduct of meropenem exhibited slow acylation. Since these drugs are active against L,D-transpeptidase 2 (Ldt_{Mt2}), understanding the differences between these two enzymes are essential. In this study, a ligand-based virtual screening of 12766 compounds followed by molecular dynamics (MD) simulations were applied to identify potential leads against Ldt_{Mt5}. To further validate the obtained virtual screening ranking for Ldt_{Mt5}, we screened the same libraries of compounds against Ldt_{Mt2} which had more experimentally reported and calculated binding energies. The observed consistency between the binding affinities of Ldt_{Mt2} validates the obtained virtual screening binding scores for Ldt_{Mt5}. We subjected 37 compounds with docking scores ranging from -7.2 to -9.9 kcal mol^{-1} obtained from virtual screening for further MD analysis. A final set of compounds (n = 10) from four antibiotic classes with $\leq$ -30 kcal mol^{-1} Molecular Mechanics/Generalized Born Surface Area (MM-GBSA) binding free energies (ΔG_{bind}) were characterised. The outcome of this study provides insight into the design of potential novel leads for Ldt_{Mt5}.

Keywords: Virtual Screening; Molecular dynamics (MD); *Mycobacterium tuberculosis* (*M.tb*); L,D-transpeptidase 5 (Ldt_{Mt5}); Molecular Mechanics/Generalized Born Surface Area (MM-GBSA)

2.0 Introduction

The alarming rise of multi and extensively drug-resistant tuberculosis (TB) has become a serious global health threat [1]. The emergence of resistant strains is partly due to the poor patient compliance to the extensive treatment regimen [2,3]. Thus, the identification of new anti-TB leads, particularly $Ldt_{Mt5,}$ that can shorten the treatment regimen and target the resistant TB strains are urgently needed. *Mycobacterium tuberculosis* possess a peptidoglycan (PG) layer that encapsulates the cytoplasmic membrane and is essential for cellular growth and viability [4]. The peptidoglycan structure of *M.tb* from a stationary-phase culture revealed a high content (80 %) of nonclassical 3→3 cross-links generated by L,D-transpeptidation [5], whereas there classical 4→3 cross-links are predominantly formed by the D,D-transpeptidation activity of penicillin-binding proteins (PBPs) during the exponential phase of growth [6-9]. L,D-transpeptidases (Ldt) and PBPs are structurally similar [10] and contain the catalytic active-site cysteine and serine residues, respectively [11]. Five Ldt paralogues have been identified for *M.tb*, Ldt_{Mt1} to Ldt_{Mt5}. The reported experimental and theoretical studies revealed that both Ldt_{Mt1} and Ldt_{Mt2} can be inactivated by carbapenems, a class of β-lactam antibiotics [6,8,5,12]. The enzymes, Ldt_{Mt1} and Ldt_{Mt2} also have distinct functions *in vivo* [9,5] and it has been shown that Ldt_{Mt1} may have a role in adaptation to the non-replicative state of the bacilli [5], while Ldt_{Mt2} is essential for virulence in a mouse model of acute infection [9]. For *M.tb*, Ldt_{Mt5} is required for properly maintaining cell wall integrity [4] and a more recent study also revealed that four L,D paralogues, with the exception of Ldt_{Mt3}, are active in *in vitro* peptidoglycan cross-linking assays, and that all but Ldt_{Mt5} are inhibited by carbapenems [7].

The single crystal X-ray structure of the extra-cellular portion of Ldt_{Mt5} was recently published [4]. Modest enhancement in susceptibility of *M.tb* to certain carbapenems (doripenem and faropenem) was observed presumably due to synthetic lethality, as these β-lactams may inactivate other targets. Meanwhile, a meropenem-adduct crystal structure was formed which supports very slow acylation of Ldt_{Mt5} over many days. The structures of apo-Ldt_{Mt5} and its meropenem-Ldt_{Mt5} (**Fig. 1**) demonstrate that, despite overall structural similarity to Ldt_{Mt2}, the Ldt_{Mt5} active site residues are different [4].
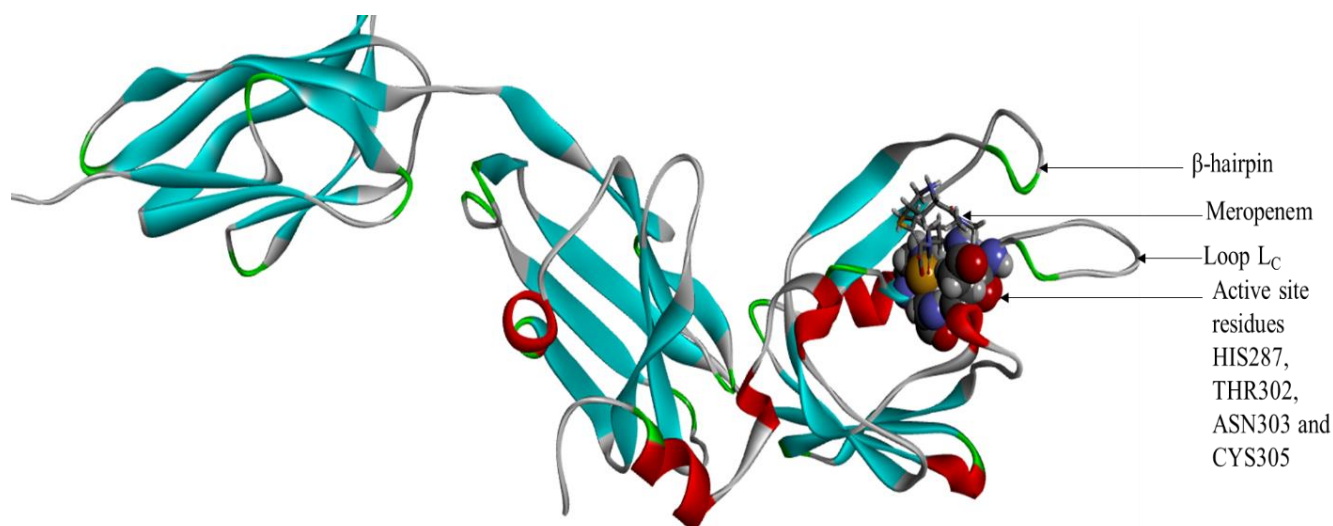
Fig. 1 The rendering of MERO-Ldt_{Mt5} crystal X-ray structure. Shown is a β-hairpin flap (312-330) and Lc loop (338-358) and active site pocket in CPK form [HIS287 (342), THR302 (357), ASN303 (358) and CYS305 (360)] and meropenem (inhibitor) in stick form [13]

The presence of a structurally divergent catalytic site and a proline-rich C-terminal subdomain suggest that this protein may have a distinct role in PG metabolism, perhaps involving other cell wall anchored proteins. Also, *M.tb* lacking a functional copy of Ldt_{Mt5} displays aberrant growth, and is more susceptible to killing by osmotic shock, select carbapenem antibiotics and crystal violet [4]. The *β*-lactam and oxazolidinone compounds will most likely be able to form covalent bonds with the catalytic cysteine of Ldt_{Mt5} probably due to the carbonyl and amide functional group in the structural backbone. Hence, in case any promising inhibitors from the other classes are identified, they will most likely act as competitive [14] inhibitors.
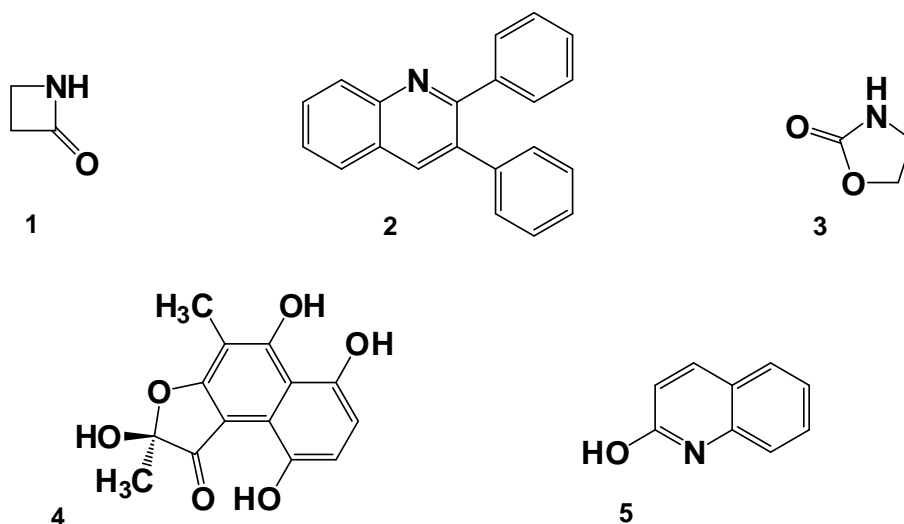
Fig. 2 2D scaffold structures of (1) *β*-lactam (2) Diarylquinoline (3) Oxazolidinone (4) Rifamycin (5) Quinolone classes of TB antibiotics

Carbapenems gave insignificant binding of Ldt_{Mt5} experimentally using isothermal titration calorimetry (ITC). Carbapenems are considered the last resort antibiotics to treat resistant bacterial infections in humans [15-22]. This fact motivated us to perform a virtual screening of five classes of known TB antibiotics (**Fig. 2**). Virtual screening with both AutoDock Vina and Schrödinger Maestro software programs was performed as a benchmark for the automated docking. Molecular dynamics and binding free energy studies were performed on each of the screened compounds from the five classes of anti-TB agents. To the best of our knowledge, a computational model to identify and rank the different anti-TB agents against Ldt_{Mt5} has not yet been reported.

2.1 Materials and methods

The following *in silico* approaches were used to screen five classes of known TB antibiotics (**Fig. 2**) against Ldt$_{Mt5}$. The automated docking process was perfomed using Autodock Vina [23] and Schrödinger Maestro [24] programs which implement the quasi-flexible docking method to perform the screening [25]. The docked energies followed by visual inspection of the inhibitor pose was performed to ensure the close proximity of the selected compounds with the catalytic cysteine. This was followed by molecular dynamics simulations/MD trajectory analyses using CPPTRAJ module [26] implimented in Amber 14 [27] package.

2.1.1 System preparation

The 3D crystal structure of the meropenem-bound Ldt$_{Mt5}$ (PDB code: 4ZFQ [13]) was retrieved from the Protein Data Bank [28]. The missing residues (the *β*-hairpin flap is missing having the loop LC and the ex-CTSD being disordered) [13] of the Ldt$_{Mt5}$ enzyme were refined using MODELLER v9.15 [29]. Assignment of the protonation states of the enzyme residues at pH = 7 was performed by recalculating the standard pKa values of the titratable amino acids using the empirical propKa server [30], similar to a study on Ldt$_{Mt2}$ [31]. These protonation states of the titratable residues were used for the virtual screening and for the subsequent modelling.

The chemical compounds used for the screening were retrieved from the ZINC [32] database. This database is available for free download (http://zinc.docking.org) in different formats usable for computational studies [32]. Compounds from five classes of known TB antibiotics were subjected for the initial screening-based on their mode of action. Each scaffold of the five classes was drawn using the 2D Sketcher tool implemented in ZINC GUI. A structural similarity index of 99 % was set for all compounds except for rifamycin in which ligand mining could only be performed at a similarity index of 50 %. All the screened compounds obeyed Lipinski's rule [33] of drug-likeness to filter the compound molecules and Veber's criteria for oral bioavailability of drug candidates [34]. The considered Lipinski's parameters [33] are as follows: molecular weight; xlogP; net charge; rotatable bonds; polar surface area; hydrogen donors; hydrogen acceptors; polar and apolar solvation (**Table 1**).

Table 1 Parameters set for all screened compounds which were subjected to Lipinski's rules and Veber's drug-like filter

Parameter	Minimum	Maximum
Molecular weight (g/mol)	32	500
xlogP	-4.00	5
Net charge	-5	5
Rotatable bonds	0	10
Polar surface area (Å^2)	0	140
Hydrogen donors	0	5
Hydrogen acceptors	0	10
Polar solvation (kcal mol^{-1})	-400	1
Apolar solvation (kcal mol^{-1})	-100	40

2.1.2 Virtual screening using AutoDock Vina

AutoDock Vina is a program for molecular docking and virtual screening. The prepared 3D structure of Ldt_{Mt5} [13] in PDB format was converted to pdbqt format using raccoon [23], likewise the library of compounds downloaded from ZINC database in mol2 format were converted to pdbqt format. Virtual Screening using automated docking involves the preparation of the receptor (this includes assigning of Kollman charges [35] and Gasteiger partial charges [36] to all atoms and assignment of AD4 types to atoms of the protein structure), ligands and a config file in which grid center, a grid box size, and a docking run number are assigned. AutoDock tools 1.5.6 [37] were employed to determine the proper size of the grid box for the potential binding site for the lead compounds and the receptor grid centre was set on Cys305 (360) (active site reactive residue) [13]. The grid box was determined as centre (X = 3.9 Y = -39.5 Z = 12.1) and dimension (X = 45 Y = 45 Z = 45) with the grid spacing of 0.375 Å were considered for each of the following atom types: A C H HD N OA and SA representing all probable atom types in the target enzyme. Created finally, was a conf.txt file which includes receptor in pdbqt format, a grid center with x, y, z coordinates, a grid box size in Å, and a docking run number of 10. The virtual screening was carried out using the python script, VS.bash executable on AutoDock Vina. Docked results were ranked based on the binding affinities and visual inspection to ensure an acceptable drug/enzyme interaction is present. Visual inspection of the selected ligands inside the enzyme was performed using the Discovery Studio [38] software program.

2.1.3 Virtual screening using Schrödinger Maestro

Schrödinger Maestro software program was applied for the docking studies. Protein/ligand preparation and virtual screening were all performed in the Maestro 11.2 graphical user interface [24]. The Protein Preparation Wizard [39] of the Schrödinger Maestro software program was used to prepare the 3D protein structure. The pre-processing of the protein was performed which includes assigning of bond orders; adding of hydrogens; creating zero-order bonds to metals; creating disulphide bonds; deleting crystallographic waters beyond 5.00 Å from hetero groups and generating hetero states using Epik[40]: pH 7.0+/-2.0. In the 3D protein structure refinement, the alignment of H-bonds was done using PROPKA pH: 7.0 and waters with less than three hydrogen bonds to non-waters were removed. Restrained minimization was performed to converge heavy atoms to RMSD of 0.30Å.

The 2D compound sketches were imported onto the Schrödinger Maestro project table and they were converted into a 3D model using the pre-set option. The LigPrep module [24] was used to refine the structures using default parameters. Ionization was performed to generate possible states at target pH:7.0+/-2.0 using Epik [40] and tautomers were generated. The compounds were subjected to OPLS3 [41] (optimized potentials for liquid simulations) force field for energy optimisation. For ligand preparation, the system was set to retain specified chiralities to 10 per ligand and the output format was Maestro from Schrödinger software program. The grid box was positioned at the centre and the receptor grid centre was set on Cys305 (360) (active site reactive residue) [13] with grid spacing minimum distance of 1 Å and maximum distance of 3.5 Å. The XYZ coordinates were -31.88; 23.5 and -46.48 respectively. Default settings of Maestro 11.2 were used for other parameters such as constraints, rotatable groups, and sites.

Using a predetermined receptor grid, quasi-flexible docking [14,42,25] was performed via the Glide [43] mode of Schrödinger Maestro (Schrödinger, Inc). The system was set to resume post-docking minimization, setting the number of poses per ligand to 5. For filtering, default settings were employed and this includes applying the Epik

state penalty parameters [24] for docking and the scaling of ligand van der Waals radii for nonpolar atoms using the scaling factor 0.80 [44,45] and partial charge cut-off 0.15 [45,44]. Ligand docking was done using the three incremental stages of ranking accuracy *i.e.* high throughput virtual screening (HTVS), Glide simple precision (SP) and Glide extra precision (XP) [24]. The docking score (Glide GScore) from Glide extra precision (XP) was used to evaluate specific protein-ligand interactions within the active site of the enzyme.

The difference with these programs lies in the docking algorithm in which Schrödinger Maestro uses the Glide module which employs the Monte Carlo algorithm [46] that makes random moves and accepts or rejects each conformation based on Boltzmann probability while AutoDock Vina utilizes the AutoDock module. This program applies the genetic algorithm [47], which maintains a selective pressure towards an optimal solution, with randomized information exchange permitting exploration of the search space [25]. However, both software modules (Glide and AutoDock) identify multiple top-ranked docked poses per ligand. They both use hierarchical algorithms that are an exhaustive systematic search for the best ligand conformations within the protein active site, therefore visual inspection for one best conformation per ligand, based on known interactions was performed to identify a single best conformation per ligand for MD simulations.

2.1.4 Molecular dynamics simulation

MD simulations were performed to investigate the stability and dynamics of the complexes using the AMBER 14 package. The ff99SB [48] force field was used to describe the protein-ligand interactions whereas the general AMBER force field (GAFF) [49] was used to describe solvent-ligand interactions. System solvation for the complexes was performed in a 10 Å cubic box by using TIP3P water model. To neutralize the system negative value, sodium ions were added accordingly. The protein-ligand complexes were parametrized by the Leap [49] module of Amber14 package using the GAFF force field. All simulations were performed using a 2 fs timestep (based on a study with similar protein size) and the rest of the process was also based on the same study [31]. The partial Mesh Ewald (PME) [50] summation method was used to calculate the electrostatic forces with space cut-off of 12 Å. Using the SHAKE algorithm [51] all bonds were constrained to hydrogen (H) atoms. A two-stage energy minimization process, which is characterised by 2500 steps of steepest decent minimization and 2500 steps of conjugated gradient was carried out to get rid of steric clashes. The solute molecule was first restrained at 500 kcal mol^{-1} whereas the water molecules and the ions were relaxed. The harmonic restraint was removed on the second stage thus the whole system was relaxed. Heating of the system to a constant temperature of 300 K followed with a restraint of 10 kcal mol^{-1} for 200 ps, to keep the solute fixed. Density equilibration for 50 ps was performed and MD simulations ran at a constant temperature and pressure (1 atm). The Ldt$_{Mt5}$-ligand complexes were simulated for 20 ns [52]. The post-dynamics trajectory analysis including radius of gyration (Rg) and root mean square deviation (RMSD) was evaluated. In addition to that, triplicate MD simulations were also performed with varying initial atomic coordinates to validate the simulations.

2.1.5 Binding free energy calculation

MM-GBSA is a widely accepted method to compare the binding affinities and to gain rational insights about inhibitors by analysing the binding mechanism [53]. The average binding free energies (ΔG_{bind}) of the protein-ligand complexes was calculated for the last 10 ns using MM-GBSA method [54]. Counter ions and water molecules were removed. Entropy penalty ($-T\Delta S$) for the complexes was obtained using normal mode analysis (nmode). The PTRAJ and CPPTRAJ modules [26] were used to analyse the MD trajectories.

2.2 Results and discussions

2.2.1 Data set preparation

A total of 12766 antibacterial lead compounds in five categories listed in **Table 2** were derived from ZINC database were screened.

Table 2 The selected five categories of antibacterial compounds from ZINC database

Class	Mode of action	Number of screened compounds
β-lactam	Cell wall biosynthesis (inhibition of transpeptidase and inhibition of β-lactamase by clavulanic acid)	2707
Diarylquinoline	ATP synthesis inhibition (subunit c of ATP synthase)	4309
Oxazolidinone	Protein synthesis inhibition	3065
Rifamycin	RNA synthesis inhibition (inhibition of RNA polymerase).	2678
Quinolone	DNA synthesis inhibition (inhibition of gyrase).	7

2.2.2 Ligand-based virtual screening and docking

Structural parameters were set to filter the compounds for screening based on Lipinski's rule-of-five (**Table 1**). Virtual screening of ligands was performed on a set of 98 docked poses and then considered for further visual inspection of the interaction [14] to determine the optimal ligand conformation per compound in the active pocket of Ldt_{Mt5}. A total of 46 top-ranked poses was obtained using AutoDock Vina, (**Table 3**) and 52 from Schrödinger Maestro (**Table 4**). From there a total of 37 compounds, (13 from AutoDock Vina, **Table 3** and 24 from Schrödinger Maestro **Table 4**), were selected for further MD analysis. **Fig. 3** shows the virtual screening workflow down to the final 10 lead compounds.


```
         ZINC COMPOUNDS (+35Million)

Filter 1        Virtual Screening
                12766 Compounds

Filter 2    Docking with AutoDock Vina and
                Schrödinger  Maestro
                98 Docked Poses

Filter 3      Reranking by Visual Inspection
                37 Compounds

Filter 4            Rescoring
                10 Final Compounds
```
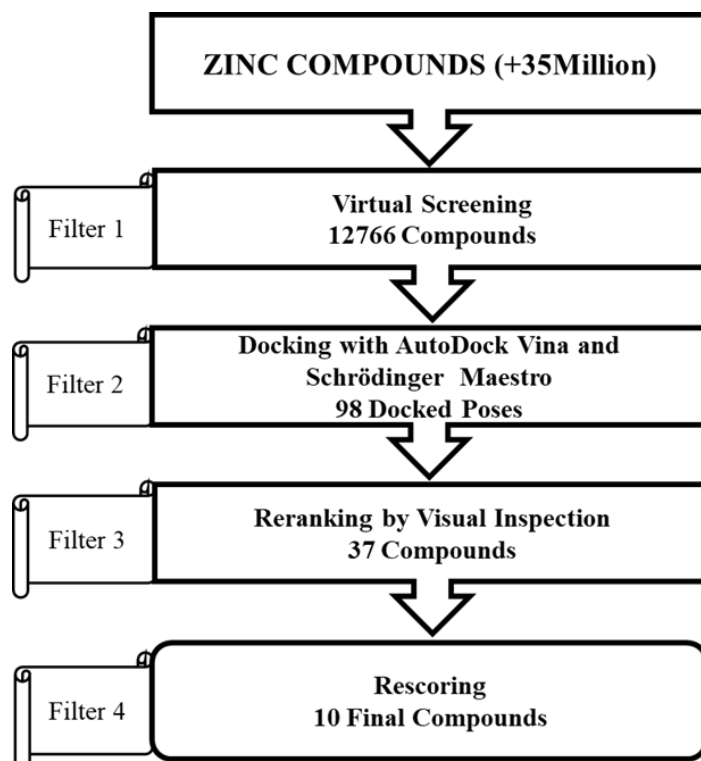
Fig. 3 Virtual screening workflow to the ten final lead compounds

The docking (consensus) scores for AutoDock Vina of the 10 top-ranked compounds across all classes lie between -7.4 and -9.0 kcal mol^{-1} (**Table 3**). The Schrödinger Maestro top-ranked docking scores were also considered, and the values are between -7.2 and -9.9 kcal mol^{-1} (**Table 4**). The docking scores of both software programs seem to be within the same range and both software programs optimize the ligand conformation during docking.

Table 3 The top 10 ligands per class based on the lowest docked energies were chosen for AutoDock Vina against Ldt$_{Mt5}$ (The optimal ligands in the active pocket, highlighted in blue, were selected for further MD analysis)

Antibiotic class	Ligand Identity	Docking score (kcal mol^{-1})
β-lactam		
1	ZINC 01662030	-8.4
2	ZINC 02475683	-8.4
3	ZINC 02475684	-8.4
4	ZINC 01662029	-8.3
5	ZINC 02462884	-8.3
6	ZINC 03791246	-8.3
7	ZINC 01412853	-8.3
8	ZINC 01385054	-8.2
9	ZINC 01412838	-8.2
10	ZINC 01412839	-8.2
Rifamycin		
1	ZINC 19569373	-8.6
2	ZINC 03197606	-8.4
3	ZINC 14828615	-8.4
4	ZINC 01551761	-8.4
5	ZINC 13125731	-8.2
6	ZINC 13125732	-8.2
7	ZINC 14693083	-8.2
8	ZINC 15216498	-8.2
9	ZINC 33832153	-8.2
10	ZINC 39227187	-8.2
Oxazolidinone		
1	ZINC 03921583	-8.7
2	ZINC 03921580	-8.5
3	ZINC 00586642	-8.4
4	ZINC 00003190	-8.3
5	ZINC 00594969	-8.3
6	ZINC 03785925	-8.3
7	ZINC 03921504	-8.3
8	ZINC 05774946	-8.2
9	ZINC 03791902	-8.2
10	ZINC 03921352	-8.2
Diarylquinoline		
1	ZINC 00022457	-9.0
2	ZINC 00022456	-8.7
3	ZINC 00057310	-8.2
4	ZINC 00075863	-8.2
5	ZINC 00097351	-8.2
6	ZINC 00152025	-8.2
7	ZINC 00236246	-8.1
8	ZINC 00254016	-8.1
9	ZINC 00118842	-8.0
10	ZINC 00192295	-8.0
Quinolone		
1	ZINC 80595608	-8.0
2	ZINC 80595598	-7.9
3	ZINC 80595612	-7.9
4	ZINC 78317542	-7.6
5	ZINC 80595606	-7.6
6	ZINC 79236395	-7.4

AutoDock Vina top-ranked docking scores were considered, and the values are between -7.4 and -9.0 kcal mol^{-1}

Table 4 The Schrödinger Maestro top ligands per class based on the lowest Glide docking score against Ldt$_{Mt5}$ (The optimal ligands in the active pocket, highlighted in blue, were selected for further MD analysis)

Antibiotic class	Ligand Identity	Docking score (kcal mol^{-1})
β-lactam		
1	ZINC 03788344	-9.9
2	ZINC 03788344	-9.7
3	ZINC 03788344	-9.4
4	ZINC 03788344	-9.2
5	ZINC 03808350	-8.8
6	ZINC 03788344	-8.9
7	ZINC 03808351	-8.7
8	ZINC 03808352	-8.7
9	ZINC 03826440	-8.4
10	ZINC 03826440	-8.4
11	ZINC 03788344	-8.4
12	ZINC 03785001	-8.2
13	ZINC 03785029	-8.2
14	ZINC 03808350	-8.1
15	ZINC 03784242	-7.9
Rifamycin		
1	ZINC 06483425	-9.3
2	ZINC 06483423	-9.3
3	ZINC 06483425	-9.2
4	ZINC 06483423	-9.2
5	ZINC 13532137	-8.0
6	ZINC 59077219	-7.9
7	ZINC 59077220	-7.9
8	ZINC 59077221	-7.9
9	ZINC 59077222	-7.9
10	ZINC 59077219	-7.9
11	ZINC 59077220	-7.9
12	ZINC 59077221	-7.9
Oxazolidinone		
1	ZINC 00108966	-8.0
2	ZINC 00108966	-8.0
3	ZINC 00108973	-8.0
4	ZINC 00108973	-8.0
5	ZINC 00108966	-7.9
6	ZINC 00108966	-7.9
7	ZINC 00108973	-7.9
8	ZINC 00108973	-7.9
9	ZINC 00052567	-7.5
10	ZINC 00052568	-7.5
11	ZINC 02512954	-7.3
12	ZINC 02512954	-7.2
13	ZINC 00108966	-7.2
14	ZINC 00108966	-7.2
Diarylquinolone		
1	ZINC 00096619	-8.1
2	ZINC 00002447	-7.7
3	ZINC 00002447	-7.7
4	ZINC 00007109	-7.5
5	ZINC 00060410	-7.7
6	ZINC 00060410	-7.7
7	ZINC 00060410	-7.7
8	ZINC 00060410	-7.7
9	ZINC 00060410	-7.7
10	ZINC 00060410	-7.7
Quinolone		
1	ZINC 80595598	-3.6

Schrödinger Maestro top-ranked docking scores were considered, and the values are between -7.2 and -9.9 kcal mol^{-1}. The class Quinolone was eliminated for further MD analysis because of its low docking score of -3.7 kcal mol^{-1}

2.2.3 Binding free energy analysis

Our group has reported that MD studies provide comparable binding free energies for Ldt_{Mt2} with several inhibitors [31] to experiment. Based on the calculated docking scores, the complexes showing the best score and best ligand conformations within the protein active site were subjected to further molecular dynamics simulations using the AMBER14 package. Similar protocol was carried out by John *et al.* and Islam *et al.* [52,55]. With a cut-off predicted binding energy (ΔG_{bind}) of $\leq$ -30 kcal mol^{-1}, a final set of lead compounds (n = 10) (marked in bold) from four antibiotic classes was selected from **Tables 5** and **6**.

Table 5 Binding free energies and their corresponding components for compounds against Ldt_{Mt5} screened by AutoDock Vina using the AMBER14 package

ZINC ID	ΔE_{vdw}	ΔE_{ele}	ΔG_{gas}	ΔG_{polar}	$\Delta G_{nonpolar}$	$\Delta G_{solvation}$	$-T\Delta S$	ΔG_{bind}
β-lactam								
02475683	**-59.68**	**-9.72**	**-69.41**	**27.7**	**-6.82**	**20.88**	**-31.01**	**-48.52**
02462884	**-54.07**	**-8.97**	**-63.03**	**22.7**	**-6.42**	**16.28**	**-27.53**	**-46.75**
03791246	-26.26	-123.11	96.85	-112.62	-3.1	-155.72	-18.6	-18.86
Rifamycin								
14693083	-42.27	-5.81	-48.07	22.49	-3.97	18.52	-2.03	-29.95
13125732	-30.71	-7.55	-38.26	18.27	-2.96	15.31	-15.55	-22.95
13125731	-28.75	-5.52	-34.27	19	-2.92	16.09	-20.68	-18.18
Oxazolidinone								
05774946	-30.17	-0.5	-30.67	8.68	-3.93	4.75	-20.58	-25.92
00003190	-32.67	-4.89	-37.57	15.9	-3.39	12.51	-17.07	-25.06
00594969	-26.73	-0.41	-26.32	9.77	-3.14	6.63	-3.58	-19.7
Diarylquinolone								
00022456	**-47.08**	**-4.08**	**-51.15**	**-14.65**	**-5.36**	**9.28**	**-18.42**	**-41.87**
00022457	**-44.53**	**-5.72**	**-50.25**	**-16.46**	**-5.01**	**11.45**	**-23.61**	**-38.8**
00192295	-35.19	-2.46	-37.65	14.48	-3.22	11.26	-21	-26.39
Quinolone								
78317542	-30.55	-278.11	-308.64	290.44	-3.91	286.52	-18.06	-22.12
79236395	-31.66	-154.13	-185.77	167.67	-3.79	163.88	-14.87	-21.89

Compounds in bold are the best binders within the -30 kcal mol^{-1} $\leq$ screening threshold and compounds in normal text are below the threshold

Table 6 Binding free energies and their corresponding components for compounds screened by Schrödinger Maestro using the AMBER14 package

ZINC ID	ΔE_{vdw}	ΔE_{ele}	ΔG_{gas}	ΔG_{polar}	$\Delta G_{nonpolar}$	$\Delta G_{solvation}$	$-T\Delta S$	ΔG_{bind}
β-lactam								
03784242	-28.18	-154.51	-182.69	160.28	-4.08	156.20	-21.11	-26.49
03785029	-27.18	-153.7	-180.88	159.8	-4.03	155.77	-24.48	-25.11
03785344	-19.65	-333.09	-352.74	339.3	-3.43	335.87	-18.24	-16.87
03785001	**-30.57**	**-175.27**	**-205.83**	**179.63**	**-4.48**	**175.15**	**-16.06**	**-30.68**
03808350	-30.12	-136.81	-166.93	150.41	-4.72	145.69	-19.04	-21.23
03808351	**-33.59**	**-188.02**	**-221.61**	**191.16**	**-4.87**	**186.29**	**-27.84**	**-35.32**
03808352	**-34.38**	**-167.3**	**-201.68**	**174.86**	**-5.36**	**169.5**	**-26.19**	**-32.18**
03826440	-26.83	-176.63	-203.45	184.25	-4.36	179.9	-18.32	-23.56
Rifamycin								
06483423	-37.88	-10.71	-48.59	26.03	-4.57	21.45	-17.91	-27.14
06483425	-39.5	-11.34	-50.85	27.31	-4.77	22.53	-11.67	-28.31
13532137	**-46.38**	**-12.24**	**-58.62**	**26.57**	**-5.16**	**21.41**	**-19.39**	**-37.21**
59077219	-9.81	-98.27	-108.1	103.06	-1.73	101.34	-14.14	-6.77
59077220	-17.38	-173.77	-191.17	176.93	-3.29	173.64	-22.4	-17.53
59077221	-20.37	-92.93	-113.32	104.55	-3.23	101.32	-17.38	-11.99
59077222	-33.2	-164.92	-196.14	176.58	-4.28	172.3	-22.59	-23.84
Oxazolidinone								
00052567	-26.43	-304.35	-330.78	315.3	-4.06	311.24	-22.5	-19.54
00052568	-32.74	-307.5	-340.24	316.29	-4.38	311.91	-9.02	-28.33
00108966	-30.59	-4.15	-34.74	12.44	-3.84	8.6	-18.77	-26.13
00108973	**-43.19**	**-3.93**	**-47.12**	**14.93**	**-5.02**	**9.91**	**-23.21**	**-37.21**
02512954	-21.99	-331.59	-353.58	332.66	-3.29	329.37	-20.23	-24.21
Diarylquinolone								
00002447	**-44.45**	**-257.63**	**-302.08**	**270.09**	**-5.69**	**264.4**	**-22.68**	**-37.68**
00007109	-22.67	-3.16	25.83	-3.16	12.22	9.45	-20.51	-16.38
00060410	-28.61	-4.13	-32.74	12.17	-3.48	8.69	-14.97	-24.05
00096619	-34.15	-4.99	-39.13	15.42	-4.18	11.24	-15.17	-27.89

Compounds in bold are the best binders within the -30 kcal mol^{-1} ≤ screening threshold and compounds in normal text are below the threshold

Two different classes of compounds were obtained as the best binders from utilizing the two docking programs. AutoDock Vina identified two lead compounds in terms of highest binding, both monobactams and these compounds showed greater predicted binding energies compared to the three carbapenems which were identified using Schrödinger Maestro (**Table 7**).

Table 7 Identified lead compounds with their antibacterial class, ZINC ID, calculated binding energies and the corresponding chemical structure, ten in total

Class	ZINC ID	ΔG_{bind} (kcal mol^{-1})	Structure
β-lactam	**02475683**	**-48.52**	
	02462884	**-46.75**	
	03808351	-35.32	
	03808352	-32.18	
	03785001	-30.68	
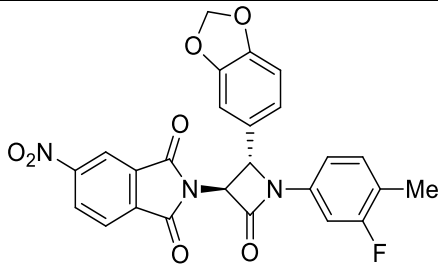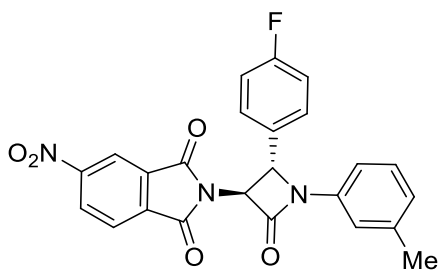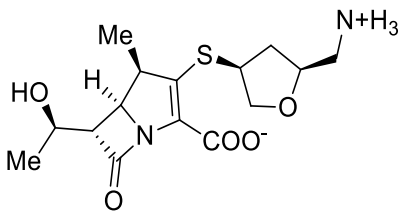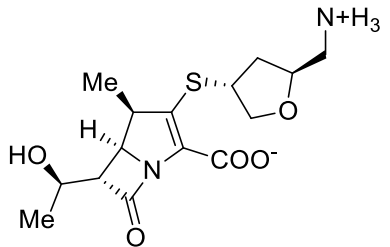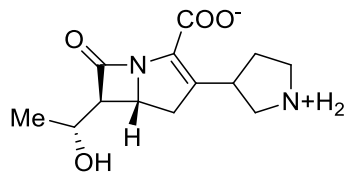
Diarylquinolone	**00022456**	**-41.87**	
	00022457	**-38.8**	
	00002447	-37.68	
Oxazolidinone	00108973	-37.21	
Rifamycin	13532137	-37.21	
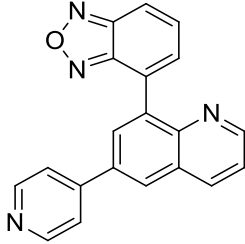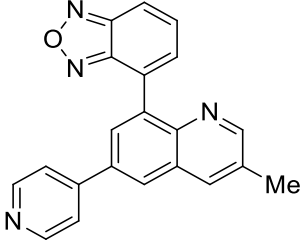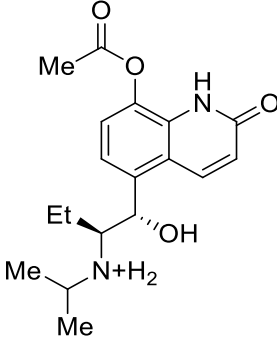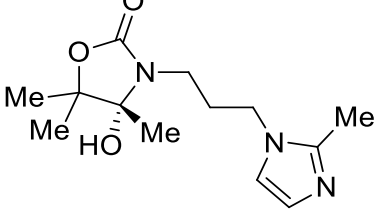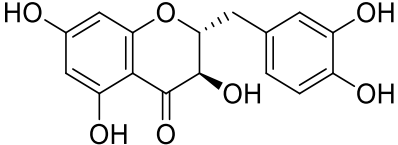
Compounds in bold were screened by AutoDock Vina [23] and compounds in normal text were screened by Schrödinger Maestro [24]

The final set of compounds (n = 10) had all parameters within the Lipinski's and Veber's constraints of drug-likeness (**Table 8**). It is noteworthy that all the screened compounds revealed a topological polar surface area (tPSA) > 150 Å^2, which is an indication of a high bioavailability [56].

Table 8 Drug-like properties of the 10 potential leads from the ZINC database

ZINC ID	xlogP	Apolar desolvation (kcal mol^{-1})	Polar desolvation (kcal mol^{-1})	H bond donors	H bond acceptors	Net charge	tPSA (Å^2)	Molecular weight (gmol^{-1})	Rotatable bonds
*02475683	4.37	11.33	-14.54	0	10	0	124	489.415	4
*02462884	4.53	12.58	-14.66	0	8	0	105	445.406	4
*03808351	-0.76	-8.64	-92.33	4	7	0	117	342.417	5
*03808352	-0.76	-8.61	-86.43	4	7	0	117	342.417	5
*03785001	4.73	1.62	-34.23	1	3	1	24	384.371	4
ᵛ00022456	4.06	1.31	-14.65	0	5	0	64	324.343	2
ᵛ00022457	4.49	1.62	-14.46	0	5	0	64	338.37	2
ᵛ00108973	0.69	-1.15	-18.45	1	6	0	67	267.329	4
ˣ00002447	1.43	-1.02	-53.74	4	6	1	96	333.408	7
ᶠⁱ13532137	0.92	-3.03	-13.32	5	7	0	127	318.281	2

Compounds in bold were screened by AutoDock Vina and compounds in normal text were screened by Schrödinger Maestro. Representations: * β-lactam; ᵛ Diarylquinolone; ˣ Oxazolidinone; ᶠⁱ Rifamycin

In light of the experimentally reported covalently bound interactions between L,D-transpeptidases and β-lactams, the subsequent section of this study focuses on better understanding of the binding interactions between the β-lactam class and Ldt$_{Mt5}$. To validate the virtual screening ranking and to compare the binding affinities, selected carbapenems known to inhibit Ldt$_{Mt2}$ were screened for both Ldt$_{Mt2}$ and Ldt$_{Mt5}$ (**Table 9**). According to the consistent trend observed in **Table 9**, the docking scores obtained seem to be valid.

Table 9 Comparison of the calculated binding energies for carbapenems on Ldt$_{Mt5}$ against the calculated and experimental [57,58] binding energies for Ldt$_{Mt2}$

Carbapenem	Ldt$_{Mt2}$ ΔG$_{exp}$ (kcal mol^{-1})	Ldt$_{Mt2}$ ΔG$_{docked}$ (kcal mol^{-1})	Ldt$_{Mt5}$ ΔG$_{docked}$ (kcal mol^{-1})
Biapenem	-9.0[57]	-6.7	-6.2
Imipenem	-9.8[58]	-6.5	-5.5
Meropenem	-8.2[58]	-7.1	-6.3
Tebipenem	-9.4[57]	-6.6	-6.0

The ZINC IDs for biapenem, imipenem, meropenem and tebipenem are 03784073, 03830927, 03808779 and 04072129 respectively

2.2.4 Trajectory analyses of *β*-lactam-Ldt$_{Mt5}$ complexes

2.2.4.1 Root mean square deviation (RMSD) analysis

RMSD is a measure of accuracy, comparing the differences between predicted values and observed values of a model [59]. The average values of the *β*-lactam-Ldt$_{Mt5}$ complexes (A-E) (**Fig. 4**) are 1.88, 1.75, 1.35, 2.25 and 1.55 Å respectively which lies in the accepted range of <2.5 Å [14] for stable simulation.
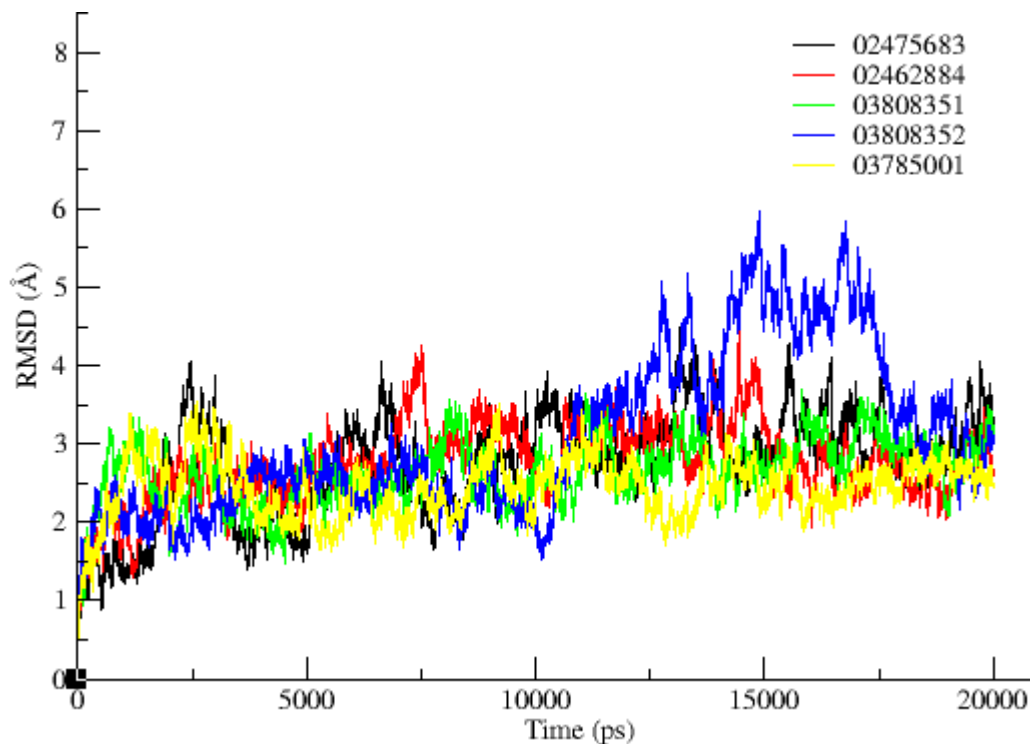

Fig. 4 Time evolution of the root mean square deviation (RMSD) of the *β*-lactam- Ldt$_{Mt5}$ complexes of **A** 02475683-Ldt$_{Mt5}$ (black), **B** 02462884-Ldt$_{Mt5}$ (red), **C** 03808351-Ldt$_{Mt5}$ (green), **D** 03808352-Ldt$_{Mt5}$ (blue) and **E** 03785001-Ldt$_{Mt5}$ (yellow) during 20 ns MD trajectories

2.2.4.2 Analysis of the radius of gyration (Rg)

The radius of gyration is defined as the moment of inertia of the C-α atoms from its centre of mass and it is used as an indicator of structural compactness of the protein-ligand complex [60,61]. **Fig. 5** shows the Rg plots for the β-lactam-Ldt$_{Mt5}$ complexes over a 20 ns trajectory. The average Rg values for complex A (02475683-Ldt$_{Mt5}$), B (02462884-Ldt$_{Mt5}$), C (03808351-Ldt$_{Mt5}$), D (03808352-Ldt$_{Mt5}$) and E (03785001-Ldt$_{Mt5}$) reveal great overal similarity. The values are 29.65 Å, 29.60 Å, 29.83 Å, 30.25Å and 29.60 Å respectively.
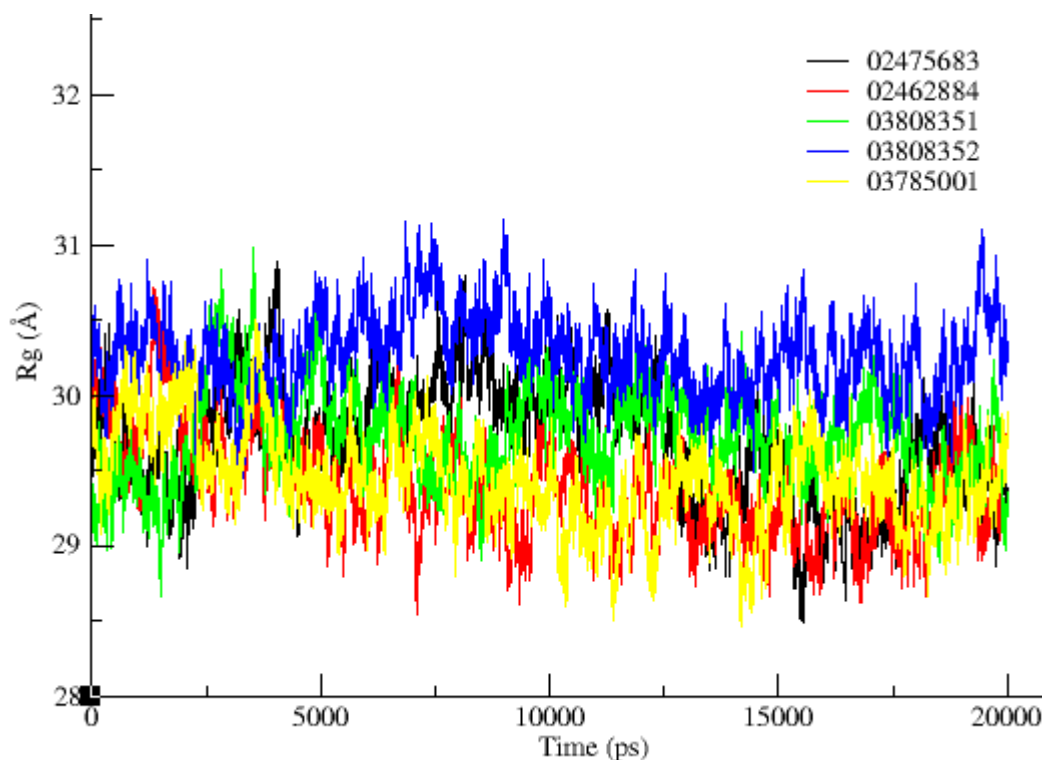
Fig. 5 The radius of gyration (Rg) of the β-lactam-Ldt$_{Mt5}$ complexes of **A** 02475683-Ldt$_{Mt5}$ (black), **B** 02462884-Ldt$_{Mt5}$ (red), **C** 03808351-Ldt$_{Mt5}$ (green), **D** 03808352-Ldt$_{Mt5}$ (blue) and **E** 03785001-Ldt$_{Mt5}$ (yellow) during 20 ns MD trajectories

2.2.4.3 Binding free energy (ΔG_{bind}) analysis of β-lactam-Ldt$_{Mt5}$ complexes

In this study, the calculated binding energies of β-lactam derivatives (meropenem and imipenem) against Ldt$_{Mt2}$ from previous studies [62,31] were used to validate the selection of lead compounds which demonstrated the best binding affinity for Ldt$_{Mt5}$. We hereby calculated the binding free energies (ΔG_{bind}) of the selected β-lactam-Ldt$_{Mt5}$ complexes using the MM-GBSA method by extracting 1000 snapshots at 10 ps interval from the last 10 ns production MD trajectories. The entropy (-TΔS) contributions were calculated using normal mode analysis [63,64] by extracting 100 snapshots from the MD trajectories. The contributing binding components upon complexation, namely, ΔE_{vdw}, ΔE_{ele}, ΔG_{gas}, ΔG_{polar}, $\Delta G_{nonpolar}$ and $\Delta G_{solvation}$ are shown in **Table 10**. The results reveal binding free energies (ΔG_{bind}) of -48.52 kcal mol^{-1} and -46.75 kcal mol^{-1} for complex A (02475683-Ldt$_{Mt5}$) and complex B (02462884-Ldt$_{Mt5}$) respectively. The binding free energies of complexes C (03808351-Ldt$_{Mt5}$), D (03808352-Ldt$_{Mt5}$) and E (03785001-Ldt$_{Mt5}$) are -35.32 kcal mol^{-1}, -32.18 kcal mol^{-1} and -30.68 kcal mol^{-1}, all between -30 kcal mol^{-1} and -40 kcal mol^{-1}. It was observed that compounds with a greater binding affinity (A and

B) are characterised by a more negative van der Waals value and they are less electronegative as compared to the other compounds (C-E).

Table 10 Calculated binding free energies and their corresponding components for the selected β-lactam-Ldt$_{Mt5}$ complexes using the AMBER14 package

Compound	ZINC ID	ΔE_{vdw}	ΔE_{ele}	ΔG_{gas}	ΔG_{polar}	$\Delta G_{nonpolar}$	$\Delta G_{solvation}$	$-T\Delta S$	ΔG_{bind}
A	**02475683**	**-59.68**	**-9.72**	**-69.41**	**27.7**	**-6.82**	**20.88**	**-31.01**	**-48.52**
B	**02462884**	**-54.07**	**-8.97**	**-63.03**	**22.7**	**-6.42**	**16.28**	**-27.53**	**-46.75**
C	03808351	-33.59	-188.02	-221.61	191.16	-4.87	186.29	-27.84	-35.32
D	03808352	-34.38	-167.3	-201.68	174.86	-5.36	169.5	-26.19	-32.18
E	03785001	-30.57	-175.27	-205.83	179.63	-4.48	175.15	-16.06	-30.68

Compounds in bold were screened by AutoDock Vina and compounds in normal text were screened by Schrödinger Maestro

2.2.4.4 Residue-inhibitor interaction analysis

To further elucidate the possible intermolecular hydrogen bonding and electrostatic interactions between β-lactam-Ldt$_{Mt5}$ complexes, we used LigPlot program [65]. The active site of Ldt$_{Mt5}$ is defined by four conserved residues (His287 (342), Thr302 (357), Asn303 (358) and Cys305 (360)) [13]. **Fig. 6** shows the schematic representations of core amino acid residues interaction modes between the β-lactam compounds (A-E) and Ldt$_{Mt5}$. It is important to note that the residue-inhibitor interaction of compound A with Ldt$_{Mt5}$ demonstrates close hydrogen bond interaction between the ligand and two active site residues Asn303 (358) and Cys305 (360), which can be a possible explanation to the highest binding free energy observed. Compound B interact with the residue Asn263 (318) and a water molecule which is within the active site (**Fig. 6**) and binding free energies (**Table 10**) of both compounds (A, B) are within the same range. Common among all 3 compounds (C-E) is the interaction with residue Arg242 (297). Compound C has other interactions with residues Glu284 (339) and Gly304 (359). Val244 (299) is a common residue between compound D and E while each compound interacts with Gly304 (359) and Asn243 (298) respectively. The other 3 compounds (C-E) also fall in a similar binding free energies range (**Table 10**) and they are unique in that they interact with different residues, although not with any of the active site residues.
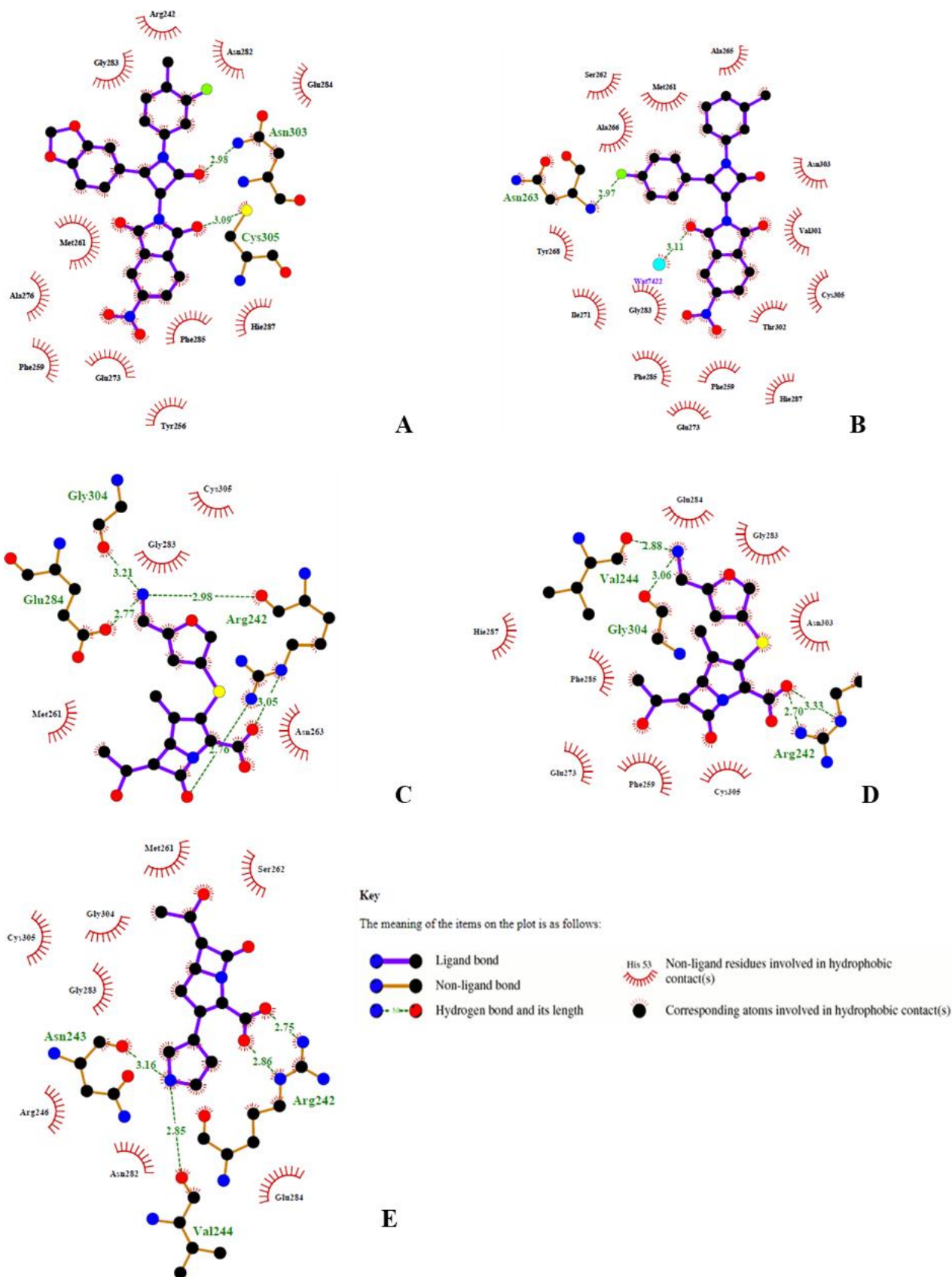
Fig. 6 2D schematic representations of the hydrogen and hydrophobic interactions between Ldt$_{Mt5}$ residues and the selected β-lactam compounds, ZINC ID (**A**) 02475683, (**B**) 02462884, (**C**) 03808351, (**D**) 03808352, and (**E**) 03785001. All structures are average conformations generated from the last 10 ns snapshots of each MD system

Results from virtual screening and docking studies demonstrated that several lead compounds from different classes of antibiotics potentially tend to bind to the active pocket of Ldt$_{Mt5}$. The binding free energies also demonstrate favourable binding potential of our lead compounds to Ldt$_{Mt5}$. It is known that β-lactams, specifically carbapenems, form covalent bonds with the catalytic cysteine (305) residue of Ldt$_{Mt5}$ due to the carbonyl functional group in the structural backbone. However, results from the model as highlighted by the residue-inhibitor interaction analysis seem to suggest that other compounds may interact differently with Ldt$_{Mt5}$. Instead of forming covalent interaction, other potential inhibitors of Ldt$_{Mt5}$ may perform competitive inhibition instead. It is also important to note that the closer the inhibitor interacts with the active site residues, the higher the binding affinity it may have as demonstrated compound A (**Fig. 6**).

2.3 Conclusion

In this study, virtual screening of compounds from ZINC database against Ldt$_{Mt5}$ was investigated with AutoDock Vina and Schrödinger Maestro software programs. The obtained docking scores presented a reasonable number of lead compounds which can be utilised as potential drug candidates against Ldt$_{Mt5}$. Despite the lack of overlap on the screened compounds using these two different software programs, both provided reasonable binding scores. The observed exclusiveness of each program to a certain class of compounds strongly suggests that the effectiveness of a computational technique is subject to the software program utilised. To improve the chances of getting a 'lead compound', different programs with alternative search algorithms need to be employed for the screening of compound libraries. It is essential to verify virtual screening results with MD free energy calculations as was demonstrated before [14]. The screened lead compounds were subjected to MM-GBSA approach. A final set of compounds (n = 10) from four antibiotic classes with ≤ -30 kcal mol^{-1} were obtained.

The computational model presented in this study is robust in that its accuracy was validated on both the docking stage as well as on the MD simulations stage. Such benchmarking offers baseline comparisons of experimental and computational data from a paralog of the enzyme under study which brings about comparable extrapolations applicable to the natural system. The model as expressed through the docking affinities and binding energy calculations from MD simulations, demonstrated strong binding ligands. It should also be noted however, that the residue-inhibitor interaction analysis further revealed that apart from the already known interactions, other compounds interact with other active site residues of the target. This certainly paves way to explore other β-lactam binding mechanisms and expresses the importance of molecular dynamics simulations in revealing other possible interactions within the active site of other transpeptidases. We therefore conclude that pharmacophore based virtual screening and molecular dynamics simulations are essential tools which will continue to play a significant role in drug design and identification of novel ligands.

Conflict of interest

Authors declare no conflict of interest.

References

1. Seung KJ, Keshavjee S, Rich ML (2015) Multidrug-resistant tuberculosis and extensively drug-resistant tuberculosis. Cold Spring Harbor perspectives in medicine:a017863

2. Billones JB, Carrillo MCO, Organo VG, Macalino SJY, Sy JBA, Emnacen IA, Clavio NAB, Concepcion GP (2016) Toward antituberculosis drugs: in silico screening of synthetic compounds against Mycobacterium tuberculosis L,D-transpeptidase 2. Drug design, development and therapy 10:1147

3. Adewumi OA (2012) Treatment outcomes in patients infected with multidrug resistant tuberculosis and in patients with multidrug resistant tuberculosis coinfected with human immunodeficiency virus at Brewelskloof Hospital.

4. Brammer BL, Ghosh A, Pan Y, Jakoncic J, Lloyd E, Townsend C, Lamichhane G, Bianchet M (2015) Loss of a Functionally and Structurally Distinct ld-Transpeptidase, LdtMt5, Compromises Cell Wall Integrity in Mycobacterium tuberculosis. The Journal of biological chemistry 290 (42):25670-25685

5. Lavollay M, Arthur M, Fourgeaud M, Dubost L, Marie A, Veziris N, Blanot D, Gutmann L, Mainardi JL (2008) The peptidoglycan of stationary-phase Mycobacterium tuberculosis predominantly contains cross-links generated by L,D-transpeptidation. Journal of bacteriology 190 (12):4360-4366

6. Dubée V, Triboulet S, Mainardi JL, Ethève-Quelquejeu M, Gutmann L, Marie A, Dubost L, Hugonnet JE, Arthur M (2012) Inactivation of Mycobacterium tuberculosis L,D-transpeptidase LdtMt1 by carbapenems and cephalosporins. Antimicrobial agents and chemotherapy 56 (8):4189-4195

7. Cordillot M, Dubée V, Triboulet S, Dubost L, Marie A, Hugonnet JE, Arthur M, Mainardi JL (2013) In vitro cross-linking of Mycobacterium tuberculosis peptidoglycan by l,d-transpeptidases and inactivation of these enzymes by carbapenems. Antimicrobial agents and chemotherapy 57 (12):5940-5945

8. Lecoq L, Dubée V, Triboulet SB, Bougault C, Hugonnet JE, Arthur M, Simorre JP (2013) Structure of Enterococcus faecium L,D-transpeptidase acylated by ertapenem provides insight into the inactivation mechanism. ACS chemical biology 8 (6):1140-1146

9. Gupta R, Lavollay M, Mainardi JL, Arthur M, Bishai WR, Lamichhane G (2010) The Mycobacterium tuberculosis protein LdtMt2 is a nonclassical transpeptidase required for virulence and resistance to amoxicillin. Nature medicine 16 (4):466-469

10. Biarrotte-Sorin S, Hugonnet JE, Delfosse V, Mainardi JL, Gutmann L, Arthur M, Mayer C (2006) Crystal structure of a novel β-lactam-insensitive peptidoglycan transpeptidase. Journal of molecular biology 359 (3):533-538

11. Mainardi JL, Fourgeaud M, Hugonnet JE, Dubost L, Brouard JP, Ouazzani J, Rice LB, Gutmann L, Arthur M (2005) A novel peptidoglycan cross-linking enzyme for a β-lactam-resistant transpeptidation pathway. Journal of Biological Chemistry 280 (46):38146-38152

12. Mainardi JL, Villet R, Bugg TD, Mayer C, Arthur M (2008) Evolution of peptidoglycan biosynthesis under the selective pressure of antibiotics in Gram-positive bacteria. FEMS microbiology reviews 32 (2):386-408

13. Basta LAB, Ghosh A, Pan Y, Jakoncic J, Lloyd EP, Townsend CA, Lamichhane G, Bianchet MA (2015) Loss of a functionally and structurally distinct ld-transpeptidase, LdtMt5, compromises cell wall integrity in mycobacterium tuberculosis. Journal of Biological Chemistry 290 (42):25670-25685

14. Honarparvar B, Govender T, Maguire GE, Soliman ME, Kruger HG (2013) Integrated approach to structure-based enzymatic drug design: molecular modeling, spectroscopy, and experimental bioactivity. Chemical reviews 114 (1):493-537

15. Bradley J, Garau J, Lode H, Rolston K, Wilson S, Quinn J (1999) Carbapenems in clinical practice: a guide to their use in serious infection. International journal of antimicrobial agents 11 (2):93-100

16. Paterson D (2000) Recommendation for treatment of severe infections caused by Enterobacteriaceae producing extended-spectrum β-lactamases (ESBLs). Clinical Microbiology and Infection 6 (9):460-463

17. Paterson DL Serious infections caused by enteric gram-negative bacilli--mechanisms of antibiotic resistance and implications for therapy of gram-negative sepsis in the transplanted patient. In: Seminars in respiratory infections, 2002. vol 4. pp 260-264

18. Paterson DL, Bonomo RA (2005) Extended-spectrum β-lactamases: a clinical update. Clinical microbiology reviews 18 (4):657-686

19. Torres JA, Villegas MV, Quinn JP (2007) Current concepts in antibiotic-resistant gram-negative bacteria. Expert review of anti-infective therapy 5 (5):833-843

20. Meletis G (2016) Carbapenem resistance: overview of the problem and future perspectives. Therapeutic advances in infectious disease 3 (1):15-21

21. Kattan J, Villegas M, Quinn J (2008) New developments in carbapenems. Clinical Microbiology and Infection 14 (12):1102-1111

22. El-Gamal MI, Brahim I, Hisham N, Aladdin R, Mohammed H, Bahaaeldin A (2017) Recent updates of carbapenem antibiotics. European journal of medicinal chemistry 131:185-195

23. Trott O, Olson AJ (2010) AutoDock Vina: improving the speed and accuracy of docking with a new scoring function, efficient optimization, and multithreading. Journal of computational chemistry 31 (2):455-461

24. Schrödinger Release 2018-1: Maestro S, LLC, New York, NY, 2018.

25. Reddy AS, Pati SP, Kumar PP, Pradeep H, Sastry GN (2007) Virtual screening in drug discovery-a computational perspective. Current Protein and Peptide Science 8 (4):329-351

26. Roe DR, Cheatham III TE (2013) PTRAJ and CPPTRAJ: software for processing and analysis of molecular dynamics trajectory data. Journal of chemical theory and computation 9 (7):3084-3095

27. Pearlman DA, Case DA, Caldwell JW, Ross WS, Cheatham III TE, DeBolt S, Ferguson D, Seibel G, Kollman P (1995) AMBER, a package of computer programs for applying molecular mechanics, normal mode analysis, molecular dynamics and free energy calculations to simulate the structural and energetic properties of molecules. Computer Physics Communications 91 (1-3):1-41

28. Berman HM, Westbrook J, Feng Z, Gilliland G, Bhat TN, Weissig H, Shindyalov IN, Bourne PE (2006) The protein data bank, 1999–. In: International Tables for Crystallography Volume F: Crystallography of biological macromolecules. Springer, pp 675-684

29. Sali A (1994) Modeller. A program for protein structure modeling by satisfaction of spatial restraints. http://guitar rockefeller edu/modiller/modeller html

30. Li H, Robertson AD, Jensen JH (2005) Very fast empirical prediction and rationalization of protein pKa values. Proteins: Structure, Function, and Bioinformatics 61 (4):704-721

31. Fakhar Z, Govender T, Maguire GE, Lamichhane G, Walker RC, Kruger HG, Honarparvar B (2017) Differential flap dynamics in l,d-transpeptidase2 from mycobacterium tuberculosis revealed by molecular dynamics. Molecular BioSystems 13 (6):1223-1234

32. Irwin JJ, Sterling T, Mysinger MM, Bolstad ES, Coleman RG (2012) ZINC: a free tool to discover chemistry for biology. Journal of chemical information and modeling 52 (7):1757-1768

33. Lipinski CA, Lombardo F, Dominy BW, Feeney PJ (2001) Experimental and computational approaches to estimate solubility and permeability in drug discovery and development settings1. Advanced drug delivery reviews 46 (1-3):3-26

34. Veber DF, Johnson SR, Cheng HY, Smith BR, Ward KW, Kopple KD (2002) Molecular properties that influence the oral bioavailability of drug candidates. Journal of medicinal chemistry 45 (12):2615-2623

35. Singh UC, Kollman PA (1984) An approach to computing electrostatic charges for molecules. Journal of Computational Chemistry 5 (2):129-145

36. Gasteiger J, Marsili M (1980) Iterative partial equalization of orbital electronegativity—a rapid access to atomic charges. Tetrahedron 36 (22):3219-3228

37. Morris GM, Huey R, Lindstrom W, Sanner MF, Belew RK, Goodsell DS, Olson AJ (2009) AutoDock4 and AutoDockTools4: Automated docking with selective receptor flexibility. Journal of computational chemistry 30 (16):2785-2791

38. BIOVIA DS (2017) BIOVIA Discovery Studio 2017 R2: A comprehensive predictive science application for the Life Sciences. San Diego, CA, USA http://accelrys com/products/collaborative-science/biovia-discovery-studio

39. Sastry GM, Adzhigirey M, Day T, Annabhimoju R, Sherman W (2013) Protein and ligand preparation: parameters, protocols, and influence on virtual screening enrichments. Journal of computer-aided molecular design 27 (3):221-234

40. Shelley JC, Cholleti A, Frye LL, Greenwood JR, Timlin MR, Uchimaya M (2007) Epik: a software program for pK a prediction and protonation state generation for drug-like molecules. Journal of computer-aided molecular design 21 (12):681-691

41. Harder E, Damm W, Maple J, Wu C, Reboul M, Xiang JY, Wang L, Lupyan D, Dahlgren MK, Knight JL (2015) OPLS3: a force field providing broad coverage of drug-like small molecules and proteins. Journal of chemical theory and computation 12 (1):281-296

42. Jones G, Willett P, Glen RC, Leach AR, Taylor R (1997) Development and validation of a genetic algorithm for flexible docking. Journal of molecular biology 267 (3):727-748

43. Friesner RA, Murphy RB, Repasky MP, Frye LL, Greenwood JR, Halgren TA, Sanschagrin PC, Mainz DT (2006) Extra precision glide: Docking and scoring incorporating a model of hydrophobic enclosure for protein–ligand complexes. Journal of medicinal chemistry 49 (21):6177-6196

44. Enyedy IJ, Egan WJ (2008) Can we use docking and scoring for hit-to-lead optimization? Journal of computer-aided molecular design 22 (3-4):161-168

45. Repasky MP, Shelley M, Friesner RA (2007) Flexible ligand docking with Glide. Current Protocols in Bioinformatics:8.12. 11-18.12. 36

46. Metropolis N, Rosenbluth AW, Rosenbluth MN, Teller AH, Teller E (1953) Equation of state calculations by fast computing machines. The journal of chemical physics 21 (6):1087-1092

47. Taylor RD, Jewsbury PJ, Essex JW (2002) A review of protein-small molecule docking methods. Journal of computer-aided molecular design 16 (3):151-166

48. Hornak V, Abel R, Okur A, Strockbine B, Roitberg A, Simmerling C (2006) Comparison of multiple Amber force fields and development of improved protein backbone parameters. Proteins: Structure, Function, and Bioinformatics 65 (3):712-725

49. Wang J, Wolf RM, Caldwell JW, Kollman PA, Case DA (2004) Development and testing of a general amber force field. Journal of computational chemistry 25 (9):1157-1174

50. Harvey M, De Fabritiis G (2009) An implementation of the smooth particle mesh Ewald method on GPU hardware. Journal of chemical theory and computation 5 (9):2371-2377

51. Kräutler V, Van Gunsteren WF, Hünenberger PH (2001) A fast SHAKE algorithm to solve distance constraint equations for small molecules in molecular dynamics simulations. Journal of computational chemistry 22 (5):501-508

52. John A, Sivashanmugam M, Umashankar V, Natarajan SK (2017) Virtual screening, molecular dynamics, and binding free energy calculations on human carbonic anhydrase IX catalytic domain for deciphering potential leads. Journal of Biomolecular Structure and Dynamics 35 (10):2155-2168

53. Sun H, Li Y, Tian S, Xu L, Hou T (2014) Assessing the performance of MM/PBSA and MM/GBSA methods. 4. Accuracies of MM/PBSA and MM/GBSA methodologies evaluated by various simulation protocols using PDBbind data set. Physical Chemistry Chemical Physics 16 (31):16719-16729

54. Miller III BR, McGee Jr TD, Swails JM, Homeyer N, Gohlke H, Roitberg AE (2012) MMPBSA. py: an efficient program for end-state free energy calculations. Journal of chemical theory and computation 8 (9):3314-3321

55. Islam MA, Pillay TS (2017) Identification of promising DNA GyrB inhibitors for Tuberculosis using pharmacophore-based virtual screening, molecular docking and molecular dynamics studies. Chemical biology & drug design 90 (2):282-296

56. Martin YC (2005) A bioavailability score. Journal of medicinal chemistry 48 (9):3164-3170

57. Bianchet MA, Pan YH, Basta LAB, Saavedra H, Lloyd EP, Kumar P, Mattoo R, Townsend CA, Lamichhane G (2017) Structural insight into the inactivation of Mycobacterium tuberculosis non-classical transpeptidase Ldt Mt2 by biapenem and tebipenem. BMC biochemistry 18 (1):8

58. Erdemli SB, Gupta R, Bishai WR, Lamichhane G, Amzel LM, Bianchet MA (2012) Targeting the cell wall of Mycobacterium tuberculosis: structure and mechanism of L,D-transpeptidase 2. Structure 20 (12):2103-2115

59. Hyndman RJ, Koehler AB (2006) Another look at measures of forecast accuracy. International journal of forecasting 22 (4):679-688

60. Lobanov MY, Bogatyreva N, Galzitskaya O (2008) Radius of gyration as an indicator of protein structure compactness. Molecular Biology 42 (4):623-628

61. Peterson K, Zimmt M, Linse S, Domingue R, Fayer M (1987) Quantitative determination of the radius of gyration of poly (methyl methacrylate) in the amorphous solid state by time-resolved fluorescence depolarization measurements of excitation transport. Macromolecules 20 (1):168-175

62. Silva JRA, Bishai WR, Govender T, Lamichhane G, Maguire GE, Kruger HG, Lameira J, Alves CN (2016) Targeting the cell wall of Mycobacterium tuberculosis: a molecular modeling investigation of the interaction of imipenem and meropenem with L,D-transpeptidase 2. Journal of Biomolecular Structure and Dynamics 34 (2):304-317

63. Kassem S, Ahmed M, El-Sheikh S, Barakat KH (2015) Entropy in bimolecular simulations: A comprehensive review of atomic fluctuations-based methods. Journal of Molecular Graphics & Modelling 62:105-117. doi:10.1016/j.jmgm.2015.09.010

64. Chiba S, Harano Y, Roth R, Kinoshita M, Sakurai M (2012) Evaluation of protein-ligand binding free energy focused on its entropic components. Journal of Computational Chemistry 33 (5):550-560. doi:10.1002/jcc.22891

65. Wallace AC, Laskowski RA, Thornton JM (1995) LIGPLOT: a program to generate schematic diagrams of protein-ligand interactions. Protein engineering, design and selection 8 (2):127-134

Chapter 3

Inhibition Mechanism of L,D-transpeptidase 5 in presence of the *β*-lactams using ONIOM Method

Gideon F. Tolufashe,[a] Victor T. Sabe,[a] Collins U. Ibeji,[a,c] Monsurat M. Lawal,[a] Thavendran Govender,[a] Glenn E. M. Maguire,[a,b] Gyanu Lamichhane,[d] Hendrik G. Kruger[a*] and Bahareh Honarparvar[a*]

[a]Catalysis and Peptide Research Unit, School of Health Sciences, University of KwaZulu-Natal, Durban 4001, South Africa.

[b]School of Chemistry and Physics, University of KwaZulu-Natal, 4001 Durban, South Africa.

[c]Department of Pure and Industrial Chemistry, Faculty of Physical Sciences, University of Nigeria, Nsukka 410001, Enugu State, Nigeria.

[d]Center for Tuberculosis Research, Division of Infectious Diseases, School of Medicine, Johns Hopkins University, Baltimore, MD 21205, USA.

*Corresponding authors: baha.honarparvar@gmail.com, Honarparvarb@ukzn.ac.za (Dr Bahareh Honarparvar), (Prof. Hendrik G. Kruger) kruger@ukzn.ac.za, Telephone: + 27 31 2601845, Fax: +27 31 2603091, Catalysis and Peptide Research Unit, School of Health Sciences, University of KwaZulu-Natal, Durban 4041, South Africa.

Abstract

Tuberculosis (TB) is one of the world's deadliest diseases caused by the bacterium, *Mycobacterium tuberculosis* (*M.tb*). The L,D-transpeptidase enzymes catalyze the most dominant 3→3 peptidoglycan cross-links of the *M.tb* cell wall and specific *β*-lactam antibiotics have been reported to inhibit its action. Carbapenems inactivate L,D-transpeptidases (LDTs) by acylation, although differences in antibiotic side chains modulate drug binding and acylation rates. Herein, we used a two-layered our Own N-layer integrated Molecular Mechanics ONIOM method to investigate the catalytic mechanism of L,D-transpeptidase 5 (Ldt$_{Mt5}$) by *β*-lactam derivatives. Ldt$_{Mt5}$ complexes with six *β*-lactams, ZINC03788344 (**1**), ZINC02462884 (**2**), ZINC03791246 (**3**), ZINC03808351 (**4**), ZINC03784242 (**5**) and ZINC02475683 (**6**) were simulated. The QM region (high-level) comprises the *β*-lactam, one water molecule and the Cys360 catalytic residue, while the rest of the Ldt$_{Mt5}$ residues were treated with AMBER force field. The activation energies ($\Delta G^{\#}$) were calculated with B3LYP, M06-2X and *ω*B97X density functionals with 6-311++G(2d, 2p) basis set. The $\Delta G^{\#}$ for the acylation of Ldt$_{Mt5}$ by

the selected β-lactams, were calculated as 13.67, 20.90, 22.88, 24.29, 27.86 and 28.26 kcal mol^{-1} respectively. Several of the compounds showed an improved $\Delta G^{\#}$ when compared to the previously calculated for imipenem and meropenem for the acylation step for Ldt$_{Mt5}$. This model provides further validation of the catalytic inhibition mechanism of LDTs with atomistic detail.

Keywords: *Mycobacterium tuberculosis* (*M.tb*), L,D-transpeptidase 5 (Ldt$_{Mt5}$), QM/MM, ONIOM, Catalytic mechanism.

3.0 Introduction

The understanding of the enzyme-catalysed reactions mechanisms is essential to the study of biochemical processes. Possibly, an improved understanding can add to the development of novel inhibitors with greater therapeutic potential[1]. In *M.tb* peptidoglycan is required for major cell division, growth and recovery from dormancy. This is a metabolically inactive state that allows the mycobacterium to endure hostile physical-chemical situations or nutrient malnourishment[2]. This inactive state subsequently leads to latent infection which affects one-third of world's population[2]. The β-lactam antibiotics, an effective therapeutic category of antibacterial[3] agents for the inhibition of transpeptidases, which are required in cell wall biosynthesis[4]. Majority of the cross-linkage has been reported to occur via 3→3 linkages catalysed by L,D-transpeptidases which bypass the D,D-transpeptidase activity of penicillin-binding proteins (PBPs), leading to high-levels of resistance to the drugs[5-8]. The second type of cross-linkage occurs via 4→3 linkages catalysed by D,D-transpeptidase (also PBPs). This group of antibacterial drugs inactivate both transpeptidase enzymes[2, 3, 5, 9-12]. Carbapenems are one group of β-lactam antibiotics showed to have inactivated L,D-transpeptidase activity[2, 5, 10-12]. As is the case for all cysteine proteases[13], L,D-transpeptidases hydrolyse the peptide bonds by two catalytic processes that are required to start enzyme acylation by the second last peptide of the donor stem leading to the release of the C-terminal residue. This is tailed by deacylation of this acyl-enzyme intermediate by an acceptor stem[10, 14].

Unique to *M.tb*, the majority of the cross-links are generated by L,D-transpeptidation reaction, making this enzyme essential in the adaptation of *M.tb* to the stationary phase[5]. Combined inhibition of both transpeptidases (L,D and D,D) will permanently hinder the synthesis of the peptidoglycan sheet and therefore, destroy the bacteria[15]. Erdemli and co-workers[10] proposed mechanism of acylation of L,D-transpeptidase to be built on cysteine protease

mechanism. This mechanism for Ldt$_{Mt2}$ proceeds in two phases. Firstly, is the acylation step, where the Cys352 thiolate is produced via abstraction of proton bonds on the acyl carbon of the substrate resulting in a tetrahedral intermediate. Secondly, in the deacylation step, additional peptide stem goes into the catalytic pocket, and binds to the residues with the side chain amide of the m-A2pm3′ residue. In this step, His336 plays the role of the catalytic base via abstraction of a proton from the amine group of the mA2pm3′ residue, which in turn makes an attack (nucleophilic) on the carbonyl carbon of the acyl-enzyme[10].

Computational applications has been employed to investigate this mechanism, which corroborates experimental observations for the catalytic mechanism of L,D-transpeptidase 2, a commonly studied enzyme from *M.tb*[16, 17]. The first computational study on the inhibition mechanism of L,D-transpeptidase 2 was carried out using a hybrid DFTB/MM potential[16]. The peptidoglycan fragment bound with the initial coordinates of the extramembrane portion of Ldt$_{Mt2}$ (ex-Ldt$_{Mt2}$) (PDB code: 3TUR) was replaced *in silico*, for the natural substrate. Based on the results obtained, the formation of His336-imidazolium/Cys354-thiolate initiated a four-membered ring acylation step. This is then followed by a single step attack of Cys354 on the carbonyl carbon of the substrate. The aforementioned is the rate-limiting step, and it agrees with the experimental results for cysteine proteases. The attack on the acyl-enzyme complex by amine group of the subsequent substrate and results in the formation of 3→3 peptide bond (deacylation step) [16]. Fakhar *et al*.[17] using a *β*-lactam model investigated the acylation of *β*-lactam ring by Ldt$_{Mt2}$ in *M.tb* with B3LYP/6-31 + G(d). The acylation mechanism employed four-membered and six-membered ring transition states. The calculated thermochemical quantities for the proposed models specified that the activation free energy for the six-membered ring transition states model was significantly lower in comparison to other models[17].

The crystal structure of Ldt$_{Mt5}$ was recently solved both for apo (PDB code: 4Z7A[12]) and meropenem bound (PDB code: 4ZFQ[12]). Any *M.tb* strain with a deletion of Ldt$_{Mt5}$, displays abnormal growth phenotype and is more vulnerable to killing by cell wall perturbing agents including carbapenems which are considered the last resort antibiotics to combat resistant bacterial infections in humans[12].

Herein we have investigated the acylation reaction of some selected *β*-lactam derivatives from our on-going virtual screening against Ldt$_{Mt5}$ *via* a 6-membered ring mechanism. These results we hope will provide a reasonable computational model for designing of new anti-tuberculosis

drugs. This present work will adopt the protocol reported by Fakhar *et al.*[17]. The selected *β*-lactams are shown in **Fig. 1**. A water molecule will be evaluated as well as the active pocket of Ldt$_{Mt5}$ at the quantum mechanical (QM) level, and the other portion of the enzyme at molecular mechanics (MM) level. Compounds **1, 3, 4** and **5** are carbapenems while compounds **2** and **6** are monobactams.
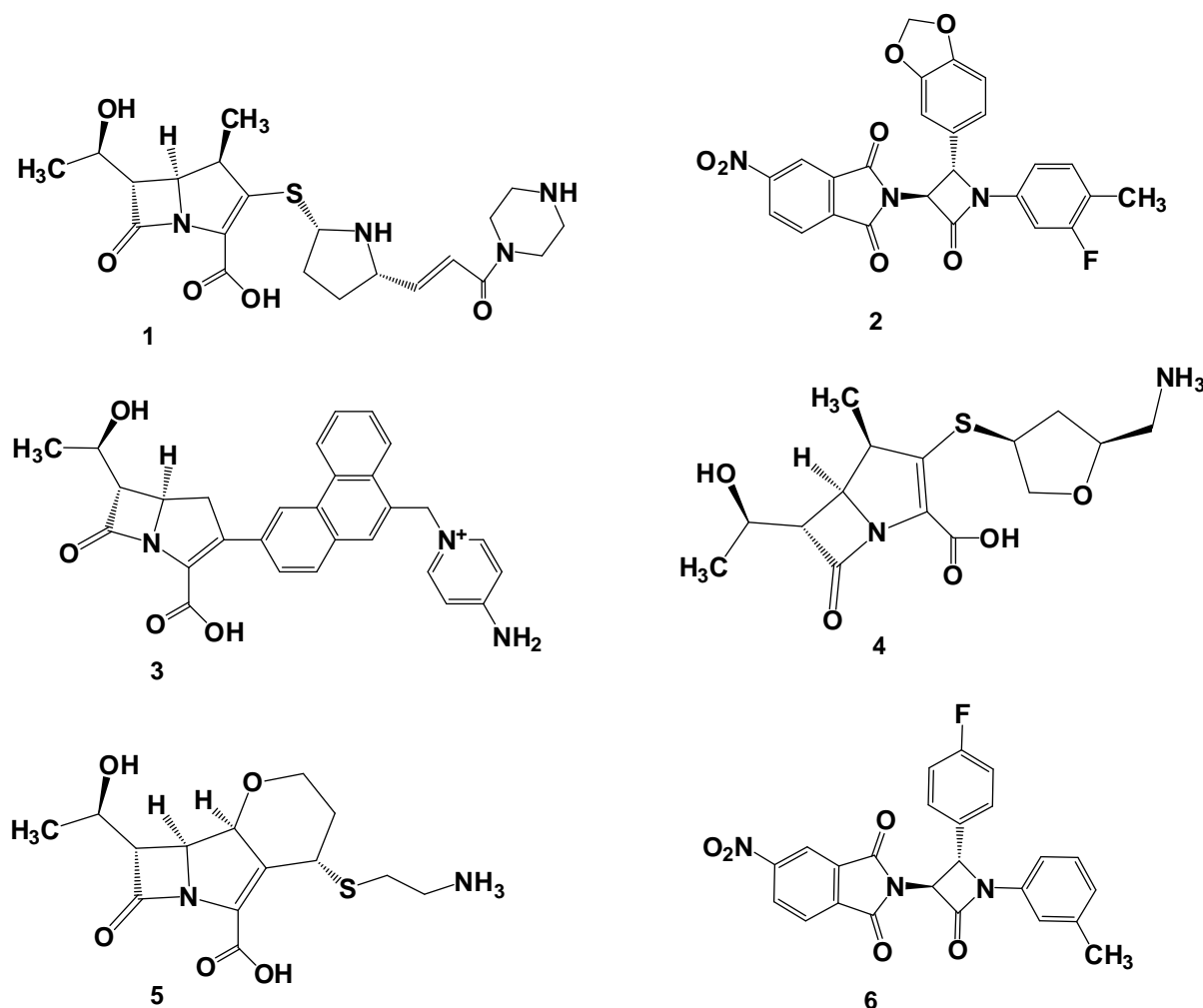
Fig. 1. 2D structures of the selected *β*-lactam derivatives

3.1 Computational methods

A 6-membered ring transition state mechanism[18, 19] for the acylation of carbapenems by Ldt$_{Mt5}$ (from *M.tb*) was investigated with a water molecule within the active pocket. QM/MM (ONIOM[20]) method calculations were applied. The influence of catalytic water has been reported to play a vital role in enzymatic reactions[17] using ONIOM method[20].

3.1.1 System preparation

The crystal structure of meropenem bond (PDB code: 4ZFQ, 2.8 Å resolution)[12] was retrieved from RCSB PDB[21] (**Fig. S1**) and complexed with the selected β-lactam derivatives from ZINC database[22] as described in our on going virtual screening study. The catalytic water molecule was manually inserted at the active site and was constrained (Modred) at a sufficiently close distance for a nucleophilic attack to occur[23]. We, therefore, took these complexes and performed partial and full geomtric minimizations using parm99 force field to remove clangs and bad connections. The partial minimization was performed for counterions water and molecules only, where the protein was fixed in a 10 Å box. In the full minimization, all atoms were geometrically optimized. A suitable snapshot from the minimization stage was partitioned into two layers and Our Own N-layered Integrated molecular Orbital and molecular Mechanics, ONIOM[24-26] (QM/MM) method was used to investigate the mechanism of the reaction. All counterions and the explicit water box were removed. The QM/MM regions, amino acids and water molecules around 6 Å around the active site were fully optimized, while others more than 6 Å were held fixed[27, 28]. Construction of starting structures for finding the respective transition states was obtained as follows: Crucial transition state (TS) interatomic distances (**Fig. 2**) were constrained using similar distances as previously reported[29] for Ldt_{Mt2}, followed by partial optimization. The cysteine catalytic active site (Cys360), all the selected β-lactams and water molecule were placed at a high layer [B3LYP/6-31+G(d)4] while the other residues were at the low layer (AMBER) for geometry optimization. The intrinsic reaction coordinates (IRC) calculations were computed to verify the calculated transition states proceeded from the reactant to the product. A full geometry optimization of the obtained transition states, reactant and product were performed. Thereafter, the stationary points were geometrically optimized vibrational frequency calculations carried to verify that the transition state and minimized one and no imaginary frequencies, respectively. Single-point energy calculations were performed on the optimized structures of the transition states, reactant and product, resorting to the electronic embedding scheme with the different functionals (B3LYP, MO6, wb97X) and a higher 6-311+G(2d,2p) basis set which combinations have been known to be excellent for thermodynamics and kinetics calculations[26, 30, 31]. To obtain the frontier orbital (HOMO, LUMO) of β-lactams 1-6 complexed with Ldt_{Mt5}, we used B3LYP/6 31G(d,p) functional. The donor–acceptor interactions in the systems was evaluated using the natural bond orbital (NBO) calculations.
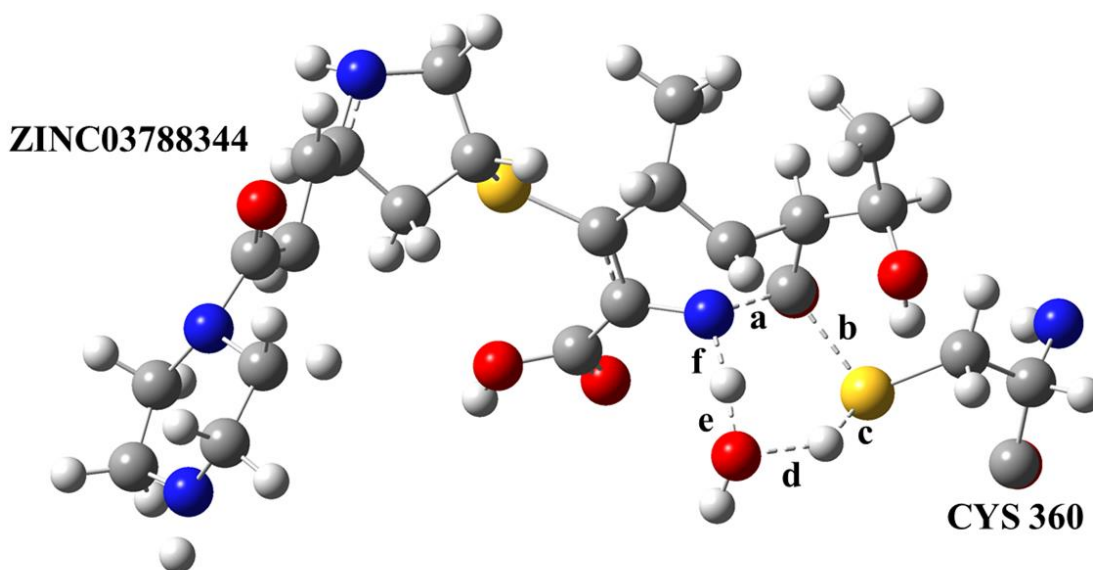
Fig. 2. 2D structure of the 6-membered ring transition states starting structures obtained using constraints with ONIOM (B3LYP/6-31+G(d):AMBER), where a = 1.64 Å, b = 2.14 Å, c = 1.60 Å, d = 1.58 Å, e = 1.3 Å, f = 1.3 Å. The TS optimized coordinates of all enzyme-inhibitor complexes are provided in the supplementary material)

3.1.2 Second-order perturbation analysis

NBO analysis is used to interpret the extent and function of intermolecular orbital interactions in the molecular system, principally charge transfer[32, 33]. The second-order perturbation theory is applied to estimate the energetic importance of all interactions between filled donor and empty acceptor NBOs. For each donor NBO (*i*) and acceptor NBO (*j*), the stabilization energy *E*(*2*) associated with delocalization is estimated as:

$$E^2 = \Delta E_{ij} = q_j \frac{F(i,j)^2}{\varepsilon_j - \varepsilon_i}$$

Where q_j is the donor orbital occupancy, ε_i and ε_j are diagonal matrix elements and $F(i,j)$ is the off-diagonal Fock matrix element.

3.1.3 Frontier molecular (FMO) orbitals

The electronic interaction between the donor and acceptor as well as the electron transfer in the molecular system principally relies on the spatial position of the FMO[34]. The kinetic characteristics of reactants and reactions are assessed by considering only FMO interactions[35]. To achieve this, the highest occupied molecular orbitals (HOMOs) and lowest unoccupied molecular orbitals (LUMOs) energies and the molecular orbital contributions were calculated using DFT[36-38].

3.2 Results and discussion

3.2.1 Mechanistic study

The activation free energies, enthalpies and entropies of the selected compounds, complexed with Ldt_{Mt5} for the 6-membered ring reaction pathway of the acylation are listed in **Table 1**. To investigate the accuracy and sensitivity of different functionals and method used, single point energy calculations of the respective structures (reactants, transition states and products) were performed using electronic embedding with B3LYP, M06-2X and ωB97X with 6-311++G(2d, 2p) basis set which have been reported to perform reasonable for kinetic and thermodynamic analysis[26, 30, 31]. In our previous study, the critical catalytic role of water, known to play an vital role in reaction mechanism has been demonstrated[9, 17]. The kinetic parameters obtained from the proposed model with water (TS-6-water) showed a lower activation barrier when compared with the model without water in Ldt_{Mt2}[17]. The catalytic behaviour of the acylation of Cys360 in Ldt_{Mt5} with one water molecule in the binding pocket against the selected β-lactams compounds was investigated. As shown in **Table 1**, the lowest activation energy ($\Delta G^{\#}$) is obtained with B3LYP/6-311++G(2d,2p) basis set, and thus our elucidation will be based on the results from this functional. The 6-membered ring transition state $\Delta G^{\#}$ of compounds **2**-**6** differs by about 1 kcal mol^{-1} while compound **1** showed the lowest activation barrier (**Table 1**). A comparison of the ΔH values of the transition states for compounds **1**-**6** revealed that they are consistent with the results obtained for the calculated $\Delta G^{\#}$.

Our results also reveal that our proposed 6-membered ring transition state mechanism is comparable to the activation energies of the 6-membered ring TS of Ldt_{Mt2} achieved previously[29] in our group using the same functional and basis set. In addition, the results revealed that this TS model with thermal corrections has a smaller value (between 14 and 28 kcal mol^{-1}) for Ldt_{Mt5} compared to the $\Delta G^{\#}$ 19.98 and 24.55 kcal mol^{-1} for a similar concerted pathway for imipenem and meropenem complexed with Ldt_{Mt2}[29]. Meanwhile, a higher $\Delta G^{\#}$ 53.29 and 91.08 kcal mol^{-1} for imipenem and meropenem against Ldt_{Mt5} respectively was previously observed[39]. Meropenem and imipenem were tested experimentally against Ldt_{Mt5}, both drugs were reported to show slow acylation which indicates possibly higher activation energies.

Table 1. Relative energy, **ΔH** (kcal mol^{-1}) and **ΔS** (kcal mol^{-1}) of Ldt$_{Mt5}$ for the 6-membered ring reaction pathway of the acylation step obtained in ONIOM model using different density functionals at 6-311++G(2d,2p):AMBER

Compounds		B3LYP[a]				M06[a]				ωB97X[a]			
		ΔE	ΔG#	ΔH	ΔS	ΔE	ΔG#	ΔH	ΔS	ΔE	ΔG#	ΔH	ΔS
1	R	0	0	0	0	0	0	0	0	0	0	0	0
	TS	17.36	13.67	13.41	0.26	21.71	18.03	17.77	0.26	23.08	19.39	19.13	0.26
	Pr	-19.39	-19.36	-18	-1.36	-18.75	-18.72	-17.35	-1.37	-18.94	-18.91	-17.54	-1.37
2	R	0	0	0	0	0	0	0	0	0	0	0	0
	TS	22.62	20.9	18.75	2.15	25.89	23.02	22.02	1.00	28.19	26.46	24.32	2.14
	Pr	-19.66	-16.79	-19.75	2.96	12.12	14.99	12.03	2.96	13.66	16.54	13.57	2.97
3	R	0	0	0	0	0	0	0	0	0	0	0	0
	TS	23.65	22.88	18.9	3.98	27.5	26.73	28.78	-2.05	28.69	27.92	23.95	3.97
	Pr	-14.23	-12.96	-14.28	1.32	-11.6	-10.32	-11.65	1.33	-13.74	-12.47	-13.79	1.32
4	R	0	0	0	0	0	0	0	0	0	0	0	0
	TS	25.01	24.29	21.68	2.61	27.33	26.62	24.01	2.61	30.77	30.05	27.44	2.61
	Pr	-6.26	-4.69	-4.93	0.24	-4.48	-2.91	-3.16	0.25	-5.26	-3.68	-3.93	0.25
5	R	0	0	0	0	0	0	0	0	0	0	0	0
	TS	29.3	27.86	25.62	2.24	32.15	30.71	28.47	2.24	34.12	32.69	30.44	2.25
	Pr	-9.88	-8.46	-8.41	-0.05	-7.69	-6.27	-6.22	-0.05	-9.11	-7.68	-7.64	-0.04
6	R	0	0	0	0	0	0	0	0	0	0	0	0
	TS	28.33	28.26	21.54	6.72	33	32.91	26.2	6.71	38.22	38.14	31.42	6.72
	Pr	-24.68	-23.23	-22.06	-1.17	-21.83	-20.38	-19.22	-1.16	-20.18	-18.73	-17.57	-1.16

[a]Energies relative to reactant for total electronic energy (ΔE) and activation free energy (ΔG#, with thermal correction) using B3LYP, M06, ωB97X/6-311++G(d,p):AMBER//B3LYP/6-31G(d,p):AMBER. R = reactant, TS = transition state and Pr = product. (The TS optimized coordinates of enzyme-inhibitor complexes are provided in the supplementary material)

Based on the results shown in **Table 1** and **Fig. 3**, compound **1** is the most reactive inhibitor in comparison to the other compounds.
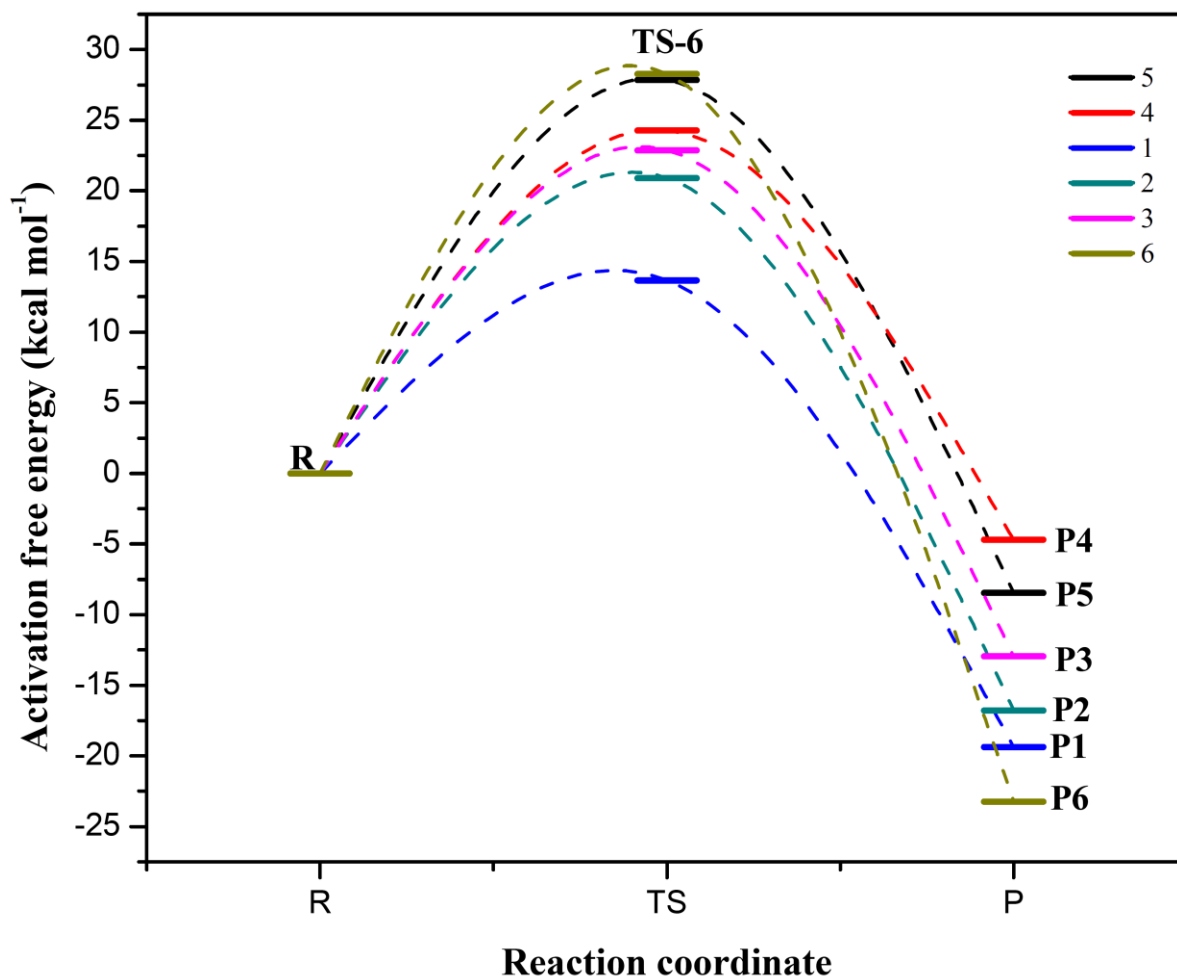

Fig. 3. Gibbs free energy pathway for the 6-membered ring mechanism of inhibition of L,D-transpeptidase (Ldt$_{Mt5}$) by the β-lactams compounds obtained at (ONIOM) B3LYP/6-311++G(2d,2p):AMBER, extrapolated from **Table 1**. See **Fig. 1** for the structure of the inhibitors

3.2.2 Frontier molecular orbitals and electrostatic potential mapping

The difference in the LUMO-HOMO, also known as the energy gap helps to characterize the chemical reactivity and kinetic stability of a molecule[40]. The frontier molecular orbitals (LUMO-HOMO) of β-lactams plot is shown in **Fig. S3**. This energy gap for the studied compounds calculated by B3LYP/6-31G(d,p) is presented in **Table S1**. The order of reactivity ranges from the lowest to highest in the order **2 < 1 < 3 < 4 < 5 < 6**. This order relatively follows the same order base on the $\Delta G^{\#}$ of the covalently bonded product formed after the acylation (**Table 1**), which indicates how fast or slow the kinetics of the reaction are. Molecular electrostatic potential (ESP) calculations of the transition states structures were surface mapped and this parameter was then used to depict the size, shape, charge density and reactive sites of the molecules[41, 42]. The mapped surface of the different compounds is presented in **Fig. 4**.

The values of the electrostatic potential are signified by various colours; red denotes the regions of the most negative electrostatic potential, blue signifies the regions of the most positive electrostatic potential and green represents the region of zero potential[43]. **Fig. 4** gives a pictorial representation of the nucleophilic sites and relative reactivity of atoms. It is evident in all the compounds that the site of nucleophilic attack between the Sγ and C3 atoms (red region) of cysteine and lactam ring respectively react with the electrophilic sites.
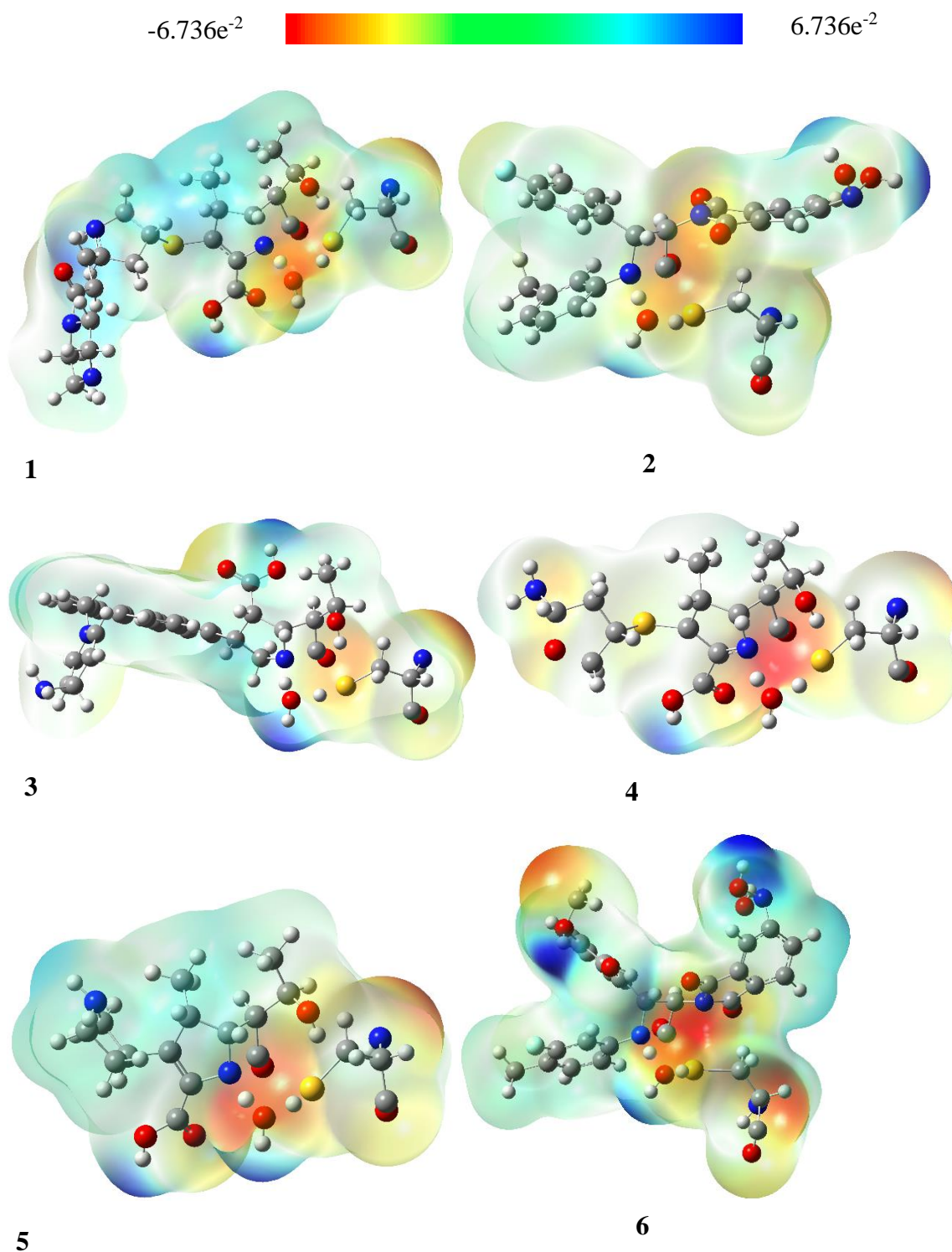
Fig. 4. Molecular electrostatic potential surface of selected compounds

3.2.3 Natural bond orbital (NBO) analysis

Charge transfer, viz from donor (bond or lone pair) to acceptor corresponding to a stabilizing donor-acceptor interaction can be calculated using NBO analysis. The charge transfer between the β-lactam-Ldt$_{Mt5}$ complexes is of paramount importance. The resulted donor, acceptor orbitals and energy of stabilization E^2 is derived from the second-perturbation theory[44, 45].

A larger E^2 value indicates a stronger interaction between the electron-donors and electron-acceptors, *i.e.* the more donating tendency from donors to acceptors the greater the extent of conjugation of the whole system[46]. In other words, a larger E^2 value contributes to a lower energy. The pictorial representation of the electron transfer for lactams-Ldt$_{Mt5}$ complexes derived from this analysis is shown in **Fig. 5**.
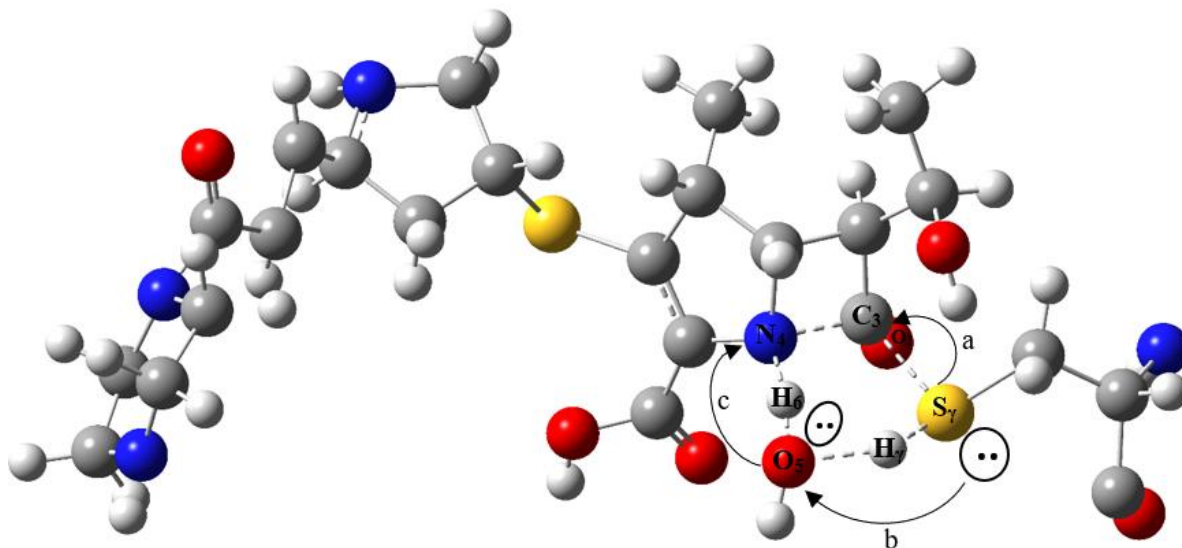

Fig. 5. Depiction of electron transfer for β-lactams/Ldt$_{Mt5}$ complexes derived from second-order perturbation theory of NBO analysis. The curved arrows (a, b and c) depict the direction of charge transfer from lone pair to antibonding (LP→σ*). (The TS optimized coordinates are provided in the supplementary material)

As presented in **Table 2**, the 6-membered ring, stabilization energy E^2 for the nucleophilic attack on the carbonyl group of compounds **4**, **3**, **5**, **6**, **2** and **1** by the thio group of Cys360 are 8.01, 6.16, 5.49, 3.40, 1.87 and 0.91 kcal mol^{-1} respectively. These values showed that the carbapenems have more nucleophilic attack in comparison to the monobactam. The E^2 value of the 6-membered ring transition states for each complex from a lone pair (LP) of the Sγ atom of the donor to the acceptor (C3). The concerted proton transfer to the β-lactam nitrogen [LP(N$_\beta$)-LP*(H$_e$)] revealed compound **5** and **6** (1.64 and 1.49 kcal mol^{-1}, respectively) as the highest while compound **2** (1.00 kcal mol^{-1}) the lowest. The result follows a similar trend with the activation energies of compound **5** and **6** having lower activation energies.

Table 2. Second-order perturbation stabilization energies corresponding to the core intermolecular charge transfer interaction (Donor to Acceptor) of the Ldt_{Mt5} for 6-membered transition states of carbapenems obtained at B3LYP/6-311++G(d,p)

Donor	Acceptor	E2 (kcal mol^{-1})
ZINC03788344		
LP (Sγ)	δ*(C3-O2)	0.91
LP (H42)	δ*(N6-C7)	1.06
ZINC02462884		
LP (Sγ)	δ*(C3-O2)	1.87
LP*(H21)	δ*(N2-C3)	1
ZINC03791246		
LP (Sγ)	δ*(C3-O2)	6.16
LP*(H21)	δ*(N2-C30)	1.17
ZINC03808351		
LP (Sγ)	δ*(C3-O2)	8.01
LP*(O-H21)	δ*(N2-C3)	0.14
ZINC03784242		
LP (Sγ)	δ*(C3-O2)	5.49
LP (H41)	δ*(N5-C9)	1.64
ZINC02475683		
LP (Sγ)	δ*(C3-O2)	3.4
LP* (H20)	δ*(N1-C4)	1.49

3.3 Conclusion

Due to the relatively weak *in vitro* inhibition of Ldt_{Mt5} by carbapenem drugs currently employed, we used the *β*-lactam ring as a scaffold to screen similar compounds in the ZINC database to see their kinetic behaviour with this enzyme. In this study, we investigated the acylation step of Ldt_{Mt5} by employing QM/MM (ONIOM) calculations. The 6-membered ring mechanisms were investigated for the acylation reaction path of Ldt_{Mt5} with six selected *β*-lactams from the ZINC database. The activation free energy (ΔG$^{\#}$) obtained from the 6-membered ring TS revealed that all the *β*-lactams were thermodynamically favourable than previously calculated ΔG$^{\#}$ for imipenem and meropenem complexed with Ldt_{Mt5}. Meropenem and imipenem were tested experimentally against Ldt_{Mt5}, both drugs were reported to show

slow acylation which indicate possibly higher activation energies. The obtained results are comparable to those observed for Ldt$_{Mt2}$ albeit, for compound **1** the activation energy is considerably lower than that obtained for meropenem and imipenem in complexed with Ldt$_{Mt2}$. This suggest that compound **1** should in theory be a very potent inhibitor of Ldt$_{Mt5}$.

The LUMO-HOMO energy gap values of the compounds are small suggestive of their structural stability. ESP revealed that the site of reaction are chemically active sites viz the interaction of the lactam ring with the cysteine of Ldt$_{Mt5}$. It is important to stress that this study has in addition to the previously reported efficacies for carbapenems, the selected *β*-lactam derivatives which showed a lower energy barrier difference found in acylation with Ldt$_{Mt5}$. Consequently, these findings should be subject to experimental bioactivities of this enzyme, more specifically binding thermodynamics assays i.e. isothermal titration calorimetry. Feedback from that will assist us to better validate our theorical model and aid rational design of new compounds and potential drug candidates with higher inhibitory activity against *M.tb*.

Competing interests
The authors declare no competing interests.

References

[1] R. Lonsdale, J.N. Harvey, A.J. Mulholland, A practical guide to modelling enzyme-catalysed reactions, Chemical Society Reviews 41(8) (2012) 3025-3038.

[2] S. Correale, A. Ruggiero, R. Capparelli, E. Pedone, R. Berisio, Structures of free and inhibited forms of the L,D-transpeptidase LdtMt1 from Mycobacterium tuberculosis, Acta Crystallographica Section D: Biological Crystallography 69(9) (2013) 1697-1706.

[3] J.F. Fisher, S.O. Meroueh, S. Mobashery, Bacterial resistance to β-lactam antibiotics: compelling opportunism, compelling opportunity, Chemical reviews 105(2) (2005) 395-424.

[4] J.E. Hugonnet, L.W. Tremblay, H.I. Boshoff, C.E. Barry, J.S. Blanchard, Meropenem-clavulanate is effective against extensively drug-resistant Mycobacterium tuberculosis, Science 323(5918) (2009) 1215-1218.

[5] M. Lavollay, M. Arthur, M. Fourgeaud, L. Dubost, A. Marie, N. Veziris, D. Blanot, L. Gutmann, J.L. Mainardi, The peptidoglycan of stationary-phase Mycobacterium tuberculosis predominantly contains cross-links generated by L, D-transpeptidation, Journal of bacteriology 190(12) (2008) 4360-4366.

[6] J.L. Mainardi, M. Fourgeaud, J.E. Hugonnet, L. Dubost, J.P. Brouard, J. Ouazzani, L.B. Rice, L. Gutmann, M. Arthur, A novel peptidoglycan cross-linking enzyme for a β-lactam-resistant transpeptidation pathway, Journal of Biological Chemistry 280(46) (2005) 38146-38152.

[7] J.L. Mainardi, J.E. Hugonnet, F. Rusconi, M. Fourgeaud, L. Dubost, A.N. Moumi, V. Delfosse, C. Mayer, L. Gutmann, L.B. Rice, Unexpected inhibition of peptidoglycan ld-transpeptidase from Enterococcus faecium by the β-lactam imipenem, Journal of Biological Chemistry 282(42) (2007) 30414-30422.

[8] J.L. Mainardi, R. Villet, T.D. Bugg, C. Mayer, M. Arthur, Evolution of peptidoglycan biosynthesis under the selective pressure of antibiotics in Gram-positive bacteria, FEMS microbiology reviews 32(2) (2008) 386-408.

[9] D.J. Tipper, J.L. Strominger, Mechanism of action of penicillins: a proposal based on their structural similarity to acyl-D-alanyl-D-alanine, Proceedings of the National Academy of Sciences 54(4) (1965) 1133-1141.

[10] S.B. Erdemli, R. Gupta, W.R. Bishai, G. Lamichhane, L.M. Amzel, M.A. Bianchet, Targeting the cell wall of Mycobacterium tuberculosis: structure and mechanism of L,D-transpeptidase 2, Structure 20(12) (2012) 2103-2115.

[11] R. Gupta, M. Lavollay, J.L. Mainardi, M. Arthur, W.R. Bishai, G. Lamichhane, The Mycobacterium tuberculosis protein LdtMt2 is a nonclassical transpeptidase required for virulence and resistance to amoxicillin, Nature medicine 16(4) (2010) 466-469.

[12] B.L. Brammer, A. Ghosh, Y. Pan, J. Jakoncic, E. Lloyd, C. Townsend, G. Lamichhane, M. Bianchet, Loss of a Functionally and Structurally Distinct ld-Transpeptidase, LdtMt5, Compromises Cell Wall Integrity in Mycobacterium tuberculosis, The Journal of biological chemistry 290(42) (2015) 25670-25685.

[13] R. Vicik, M. Busemann, K. Baumann, T. Schirmeister, Inhibitors of cysteine proteases, Current topics in medicinal chemistry 6(4) (2006) 331-353.

[14] M. Cordillot, V. Dubée, S. Triboulet, L. Dubost, A. Marie, J.E. Hugonnet, M. Arthur, J.L. Mainardi, In vitro cross-linking of Mycobacterium tuberculosis peptidoglycan by l,d-transpeptidases and inactivation of these enzymes by carbapenems, Antimicrobial agents and chemotherapy 57(12) (2013) 5940-5945.

[15] M.A. Kohanski, D.J. Dwyer, J.J. Collins, How antibiotics kill bacteria: from targets to networks, Nature Reviews Microbiology 8(6) (2010) 423.

[16] J.R.R.A. Silva, A.E. Roitberg, C.U.N. Alves, Catalytic mechanism of L,D-transpeptidase 2 from Mycobacterium tuberculosis described by a computational approach: insights for the design of new antibiotics drugs, Journal of chemical information and modeling 54(9) (2014) 2402-2410.

[17] Z. Fakhar, T. Govender, G. Lamichhane, G.E. Maguire, H.G. Kruger, B. Honarparvar, Computational model for the acylation step of the β-lactam ring: Potential application for l, d-transpeptidase 2 in mycobacterium tuberculosis, Journal of Molecular Structure 1128 (2017) 94-102.

[18] Z. Fakhar, T. Govender, G. Lamichhane, G.E.M. Maguire, H.G. Kruger, B. Honarparvar, Computational model for the acylation step of the β-lactam ring: Potential application for l,d-transpeptidase 2 in mycobacterium tuberculosis, Journal of Molecular Structure 1128 (2017) 94-102.

[19] J.R. Silva, A.E. Roitberg, C.N. Alves, Catalytic mechanism of L,D-transpeptidase 2 from Mycobacterium tuberculosis described by a computational approach: insights for the design of new antibiotics drugs, Journal of chemical information and modeling 54(9) (2014) 2402-10.

[20] S. Dapprich, I. Komáromi, K.S. Byun, K. Morokuma, M.J. Frisch, A new ONIOM implementation in Gaussian98. Part I. The calculation of energies, gradients, vibrational frequencies and electric field derivatives, Journal of Molecular Structure: THEOCHEM 461 (1999) 1-21.

[21] H.M. Berman, J. Westbrook, Z. Feng, G. Gilliland, T.N. Bhat, H. Weissig, I.N. Shindyalov, P.E. Bourne, The protein data bank, 1999, International Tables for Crystallography Volume F: Crystallography of biological macromolecules, Springer2006, pp. 675-684.

[22] J.J. Irwin, B.K. Shoichet, ZINC − A free database of commercially available compounds for virtual screening, Journal of chemical information and modeling 45(1) (2005) 177-182.

[23] J.R.A. Silva, W.R. Bishai, T. Govender, G. Lamichhane, G.E. Maguire, H.G. Kruger, J. Lameira, C.N. Alves, Targeting the cell wall of Mycobacterium tuberculosis: a molecular modeling investigation of the interaction of imipenem and meropenem with L, D-transpeptidase 2, Journal of Biomolecular Structure and Dynamics 34(2) (2016) 304-317.

[24] M. Svensson, S. Humbel, R.D. Froese, T. Matsubara, S. Sieber, K. Morokuma, ONIOM: a multilayered integrated MO+ MM method for geometry optimizations and single point energy predictions. A test for Diels−Alder reactions and Pt (P (t-Bu) 3) 2+ H2 oxidative addition, The Journal of Physical Chemistry 100(50) (1996) 19357-19363.

[25] T. Vreven, K. Morokuma, Ö. Farkas, H.B. Schlegel, M.J. Frisch, Geometry optimization with QM/MM, ONIOM, and other combined methods. I. Microiterations and constraints, Journal of computational chemistry 24(6) (2003) 760-769.

[26] A.J. Ribeiro, L. Yang, M.J. Ramos, P.A. Fernandes, Z.X. Liang, H. Hirao, Insight into enzymatic nitrile reduction: QM/MM study of the catalytic mechanism of QueF nitrile reductase, ACS Catalysis 5(6) (2015) 3740-3751.

[27] J. Zhou, P. Tao, J.F. Fisher, Q. Shi, S. Mobashery, H.B. Schlegel, QM/MM studies of the matrix metalloproteinase 2 (MMP2) inhibition mechanism of (S)-SB-3CT and its oxirane analogue, Journal of chemical theory and computation 6(11) (2010) 3580-3587.

[28] Y. Cao, S. Han, L. Yu, H. Qian, J.Z. Chen, MD and QM/MM studies on long-chain L-α-hydroxy acid oxidase: substrate binding features and oxidation mechanism, The Journal of Physical Chemistry B 118(20) (2014) 5406-5417.

[29] C.G. Ibeji, T. Govender, T. Ntombela, G.E.M. Maguire, G. Lamichhane, H.G. Kruger, B. Honarparvar, Catalytic Role of Water in the Acylation Mechanism of L,D-Transpeptidase 2: A QM/MM (ONIOM) Modeling, ACS Catalysis, Submitted for publication (2018).

[30] B.O. Milhøj, S.P. Sauer, Kinetics and Thermodynamics of the Reaction between the OH Radical and Adenine: A Theoretical Investigation, The Journal of Physical Chemistry A 119(24) (2015) 6516-6527.

[31] L. Goerigk, S. Grimme, A thorough benchmark of density functional methods for general main group thermochemistry, kinetics, and noncovalent interactions, Physical Chemistry Chemical Physics 13(14) (2011) 6670-6688.

[32] R.P. Gangadharan, S.S. Krishnan, Natural Bond Orbital (NBO) Population Analysis of 1-Azanapthalene-8-ol, Acta Physica Polonica, A. 125(1) (2014).

[33] E.D. Glendening, C.R. Landis, F. Weinhold, Natural bond orbital methods, Wiley interdisciplinary reviews: computational molecular science 2(1) (2012) 1-42.

[34] S. Sitha, K. Bhanuprakash, Role of aromatic π-bridge on electron transport property in a donor–bridge–acceptor system: A computational study on frontier molecular orbitals, Journal of Molecular Structure: THEOCHEM 761(1-3) (2006) 31-38.

[35] J. Bradley, G. Gerrans, Frontier molecular orbitals. A link between kinetics and bonding theory, Journal of Chemical Education 50(7) (1973) 463.

[36] E. Runge, 52 (1984) 997; EK Gross, W. Kohn, Phys. Rev. Lett 55 (1985) 2850.

[37] V. Suendo, S. Viridi, Ab initio calculation of UV-Vis absorption spectra of a single molecule chlorophyll a: Comparison study between RHF/CIS, TDDFT, and semi-empirical methods, arXiv preprint arXiv:1105.3766 (2011).

[38] I. Adejoro, F. Tolufashe, C. Ibeji, Density Functional Theory (DFT) Study of a new 4-[(Z)-phenyldiazenyl]-2H-Chromen-2-one Dye for Its Use as Sensitizer in Molecular Photovoltaics.

[39] G.F. Tolufashe, A.K. Halder, C.U. Ibeji, M.M. Lawal, T.Ntombela, G.E.M. Maguire, G. Lamichhane, H.G. Kruger and B. Honarparvar, Inhibition of Mycobacterium tuberculosis L,D-transpeptidase 5 by carbapenems: MD and QM/MM Mechanistic Studies Journal of Computer-aided Molecular Design, Submitted for publication (2018).

[40] Y. Uesugi, M. Mizuno, A. Shimojima, H. Takahashi, Transient resonance Raman and ab initio MO calculation studies of the structures and vibrational assignments of the T1 state and the anion radical of coumarin and its isotopically substituted analogues, The Journal of Physical Chemistry A 101(3) (1997) 268-274.

[41] I. Alkorta, J.J. Perez, Molecular polarization potential maps of the nucleic acid bases, International Journal of Quantum Chemistry 57(1) (1996) 123-135.

[42] J.S. Murray, P. Politzer, Molecular electrostatic potentials, Computational Medicinal Chemistry for Drug Discovery, CRC Press2003, pp. 231-254.

[43] A. Sethi, R. Prakash, Novel synthetic ester of Brassicasterol, DFT investigation including NBO, NLO response, reactivity descriptor and its intramolecular interactions analyzed by AIM theory, Journal of Molecular Structure 1083 (2015) 72-81.

[44] C. James, A.A. Raj, R. Reghunathan, V. Jayakumar, I.H. Joe, Structural conformation and vibrational spectroscopic studies of 2, 6-bis (p-N, N-dimethyl benzylidene) cyclohexanone using density functional theory, Journal of Raman Spectroscopy 37(12) (2006) 1381-1392.

[45] J.N. Liu, Z.R. Chen, S.F. Yuan, Study on the prediction of visible absorption maxima of azobenzene compounds, Journal of Zhejiang University. Science. B 6(6) (2005) 584.

[46] V. Balachandran, K. Parimala, Tautomeric purine forms of 2-amino-6-chloropurine (N 9 H 10 and N 7 H 10): Structures, vibrational assignments, NBO analysis, hyperpolarizability, HOMO–LUMO study using B3 based density functional calculations, Spectrochimica Acta Part A: Molecular and Biomolecular Spectroscopy 96 (2012) 340-351.

Chapter 4

Experimental Validation

4.0 Introduction

Recombinant proteins are the backbone of the biopharmaceutical industry[1]. They are important primarily in the structural determination of drug targets and the development of small molecule novel drugs[1, 2]. Proteins are complex in structure and function therefore they can hardly be synthesised chemically, hence they require a biological host cell[2]. Bacterial hosts are common in the synthesis of recombinant proteins, and *E. coli* is so often the candidate because it is relatively easy to manipulate, economical and high yielding, in a process known as overexpression[3, 4]. The BL21 (DE3) strain is popular for protein expression[5]. After expression the protein needs to be isolated, a process known as purification. This enables the protein to be structurally evaluated and functionally characterised. Affinity chromatography (metal binding) is widely used to purify recombinant proteins expressed in bacteria[6]. A pure protein can easily be evaluated for structure-function relationships with other biological or chemical compounds. Thermodynamics are a good measure of protein-ligand interactions[7, 8]. Isothermal titration calorimetry (ITC) is an ideal technique to validate theoretical structure-based binding energies since it is capable of resolving the entropic and enthalpic elements of binding affinity[9].

In this chapter, the primary focus was on experimental validation. In order to validate the previously reported virtual screening model and the binding energies of the compounds which were obtained against Ldt_{Mt5}, one compound (with the highest binding energy) was selected and prepared for a further binding thermodynamics analysis. A lyophilised pET28a-Ldt_{Mt5} plasmid was obtained from Johns Hopkins University.

4.1 Materials and Methods

4.1.1 Expression and Extraction of Ldt$_{Mt5}$

The lyophilised pET28a-Ldt$_{Mt5}$ (10 µg) plasmid was reconstituted in 50 µL nuclease-free water. The plasmid was used to transform *E. coli* strain BL21 (DE3) using the heat shock method. A single colony from the transformation was used to inoculate 5mL of Luria-Bertani (LB) medium containing 34 µg/mL of kanamycin and 34 µg/mL of chloramphenicol (LBAC medium) and was incubated overnight at 37 °C in a shaker. From the overnight culture, 1 mL was transferred into 500 mL flasks containing 100 mL of fresh LBAC (initial OD600 = 0.05). Cell growth was regulated at 37 °C and to induce protein overexpression, 0.1 mM isopropyl 1-thio-β-D-galactopyranoside (IPTG) was added at early exponential phase (OD600 between 0.5 - 0.7). The flasks were then transferred to 16 °C and left to grow on a shaker incubator (200rpm) overnight. Following induction, cells were harvested by centrifugation at 5000 x *g* at 4 °C for 10 minutes, and 10 mL of buffer A [10 mM Tris-HCl, pH 7.9 containing 1 mM phenylmethylsulfonyl fluoride (PMSF)] was used to resuspend the pellet. Sonication (Omni International Sonic Ruptor 400 Ultrasonic homogenizer) at the frequency of 20 kHz was performed to prepare the crude cell extracts. To minimize thermal effects, the sonication sample was placed on ice and for a period of 10 minutes at 20 % amplitude, the homogenized sample was subjected to 30 seconds on / 30 seconds off pulses. The sonicated samples were then centrifuged for 20 minutes at 13,000 x *g* at 4 °C (Beckman Centrifuge).

4.1.2 Purification of the Protein

Purification of the protein was conducted using the AKTA purifier 100-950 (GE Health Care). A His Pur Cobalt column, 5 mL, (Thermo Scientific) was used to purify the fusion protein. Firstly, the column was equilibrated with a 10-column volume of equilibration buffer (50 mM Na$_2$PO$_4$, pH 7.5, 300 mM NaCl, 5 mM imidazole). The protein sample (20 mL) was loaded onto the column using a sample pump. The column was washed with 5 column volumes of the same buffer to remove unbound proteins. Bound proteins (Ldt$_{Mt5}$) were then eluted using elution buffer (50 mM Na$_2$PO4, pH 7.5, 300 mM NaCl, 150 mM imidazole). SDS-PAGE was used to verify the purity of the eluted protein fraction[10].

4.1.3 Molecular weight and protein profile determination by SDS-PAGE

The method by Laemmli (1970) was adopted to determine the protein profile[10]. An initial preparation of a resolving gel (composed of 10 % [v/v] acrylamide, 0.1 % [v/v] sodium dodecyl sulphate [SDS] in 1.5 M Tris-HCl, pH 8.8) was cast on a vertical slab and this was followed by a stacking gel (5 % [v/v] acrylamide, 0.1 % [v/v] SDS in 1 M Tris-HCl, pH 6.8) which was layered above the initial cast. A stock solution of acrylamide [30 % (w/v)] was formulated by adding 29 g of acrylamide and 1 g of N,N'-methylbisacrylamide to 80 mL dH$_2$O which was adjusted to a 100 mL final volume. A solution composed for 5 µL of 6X SDS loading dye and 25 µL protein samples was added into eppendorf tubes and the samples were boiled for 5 minutes in a water-bath. The solution was loaded onto the gel which was run at a voltage of 80 V in 1 X SDS running buffer (25 mM Tris, 192 mM glycine, 0.1 % SDS) for a period of 1.5 hours. For improved visibility, the gel was soaked in Coomassie staining solution for 2 hours. The gel was then destained in solution of 10 % (v/v) methanol containing 10 % (v/v) acetic acid. The protein profile in the gel was captured using a UV-transilluminator (Syngene; Syoptics Ltd, Cambridge, UK).

4.1.4 Calorimetric Studies

Ldt$_{Mt5}$ protein was dialysed overnight in a 5 L buffer of 25 mM Tris-HCl at pH 7.5, 100 mM NaCl at 4 °C. The dialysed protein was filtered through a 0.22 µm filter and diluted to a concentration of 10 µM buffer (25 mM Tris-HCl at pH 7.5, 100 mM NaCl, 1 mM DTT) with 2 % DMSO. Aliquots of ligand solutions were diluted to 100 µM in the protein dialysis buffer containing 2 % DMSO. The samples (protein and ligand) were then degassed for 10 minutes in a ThermaVac®. Ligand injections (10 µL) into the cell containing Ldt$_{Mt5}$ were performed with 240-second equilibrations between injections. Calorimetry experiments were performed at 20 °C. Data were analysed with NanoAnalyze® software (TA Instruments, New Castle, DE).

4.2 Results

4.2.1 Expression and Purification of Ldt$_{Mt5}$

Protein expression was achieved by growing a culture at 16 °C as seen by the thick band around 50 kDa, **Figure 1**. The expressed Ldt$_{Mt5}$ contained an N-Terminal His-tag, which was used for purification. Purification was achieved by loading the crude lysate into a cobalt column. The protein fusion protein was purified with a single step purification procedure. **Figure 1** shows a chromatogram of Ldt$_{Mt5}$ fusion protein and protein profile.
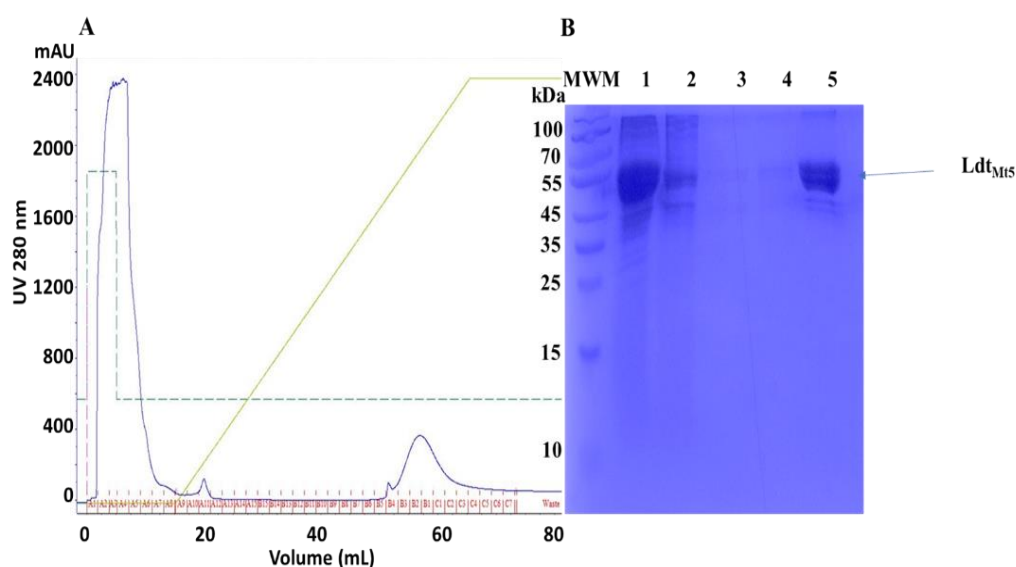

Figure 1. Purification of Ldt$_{Mt5}$ fusion protein using affinity chromatography. The cell lysate was loaded onto a His Pur cobalt column previously equilibrated with 50 mM Na$_2$PO$_4$, 300 mM, NaCl and 5 mM imidazole. Unbound proteins were washed out with 5 column volumes of the same buffer and bound proteins were eluted with same buffer but with 0-250 mM imidazole gradient. Purity was verified using SDS-PAGE. **A**; chromatogram showing bound and unbound fractions. **B**; SDS-PAGE of the collected fractions, MWM; Molecular weight marker; 1 crude protein, 2 unbound protein, 3-5 bound proteins

4.2.2 Isothermal Titration Calorimetry

The compound (ZINC02475683) with the highest calculated binding energy was selected for further binding thermodynamics analysis of binding to Ldt$_{Mt5}$ using ITC. The ligand (CAS 330960-03-7) compound name, 1H-Isoindole-1,3(2H)-dione, 2-[2-(1,3-benzodioxol-5-yl)-1-(3-chloro-4-methylphenyl)-4-oxo-3-azetidinyl]-4-nitro- was commercially available and the closest analogue which was used for the evaluation of the enzyme inhibition assay (**Figure 2**).
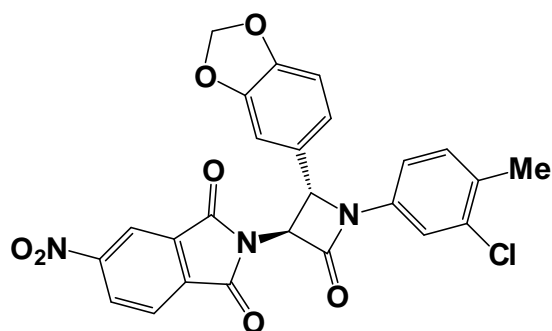
Figure 2. The chemical structure of the ligand used to evaluate the thermodynamics of binding to Ldt$_{Mt5}$ using ITC

The isothermal titration calorimetry results reveal that no significant heat exchange associated with binding was measured as shown in **Figure 3**.
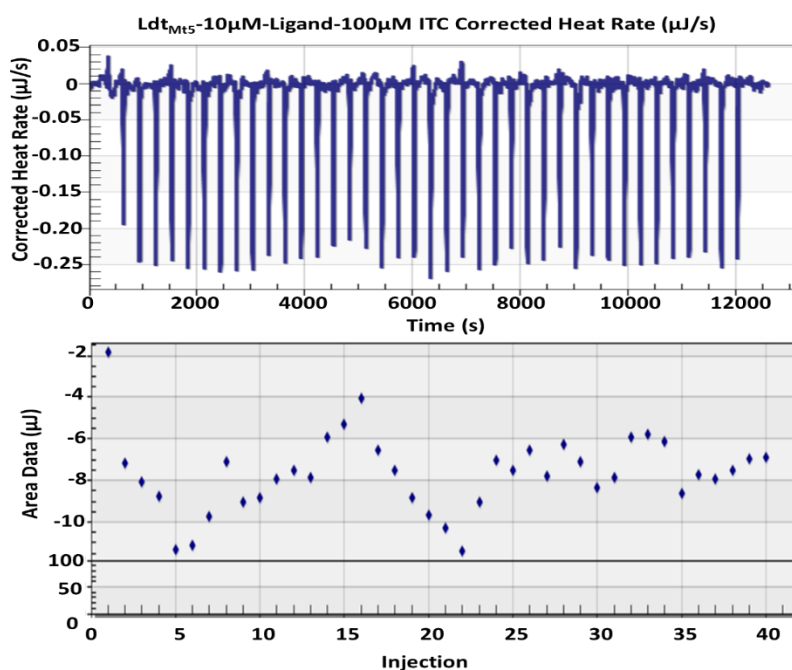

Figure 3. ITC of compound A binding to Ldt$_{Mt5}$. Upper panel shows titration of the Ldt$_{Mt5}$ with compound A. Lower panel is a plot of the total heat released as a function of total ligand concentration for the titration shown in the upper panel. No heat of binding is detected, only heat of dilution

4.3 Conclusion

According to the ITC performed in this study, results showed no binding of the lead compound which exhibited the highest affinity to Ldt$_{Mt5}$ through calculated free binding energies. It is important to highlight the extremely low solubility involved with the compound under study. The compound is a β-lactam, more specifically a monobactam and these compounds are well known for being highly insoluble. The same could have potentially played a negative role in the binding to the active site of Ldt$_{Mt5}$.

The findings revealed by the experimental study by Basta *et al*. by means of the same experimental technique in which a series of β-lactams including the carbapenems were evaluated, and measured the thermodynamics of binding to this protein was performed[11]. However, our experimental evaluation was also performed on a β-lactam but a monobactam, so it cannot be effectively compared to carbapenems. Also, a single β-lactam compound is insufficient statistically to draw up a concrete conclusion on.

References

[1] Walsh, G. (2010) Biopharmaceutical benchmarks 2010, *Nature biotechnology 28*, 917.
[2] Overton, T. W. (2014) Recombinant protein production in bacterial hosts, *Drug discovery today 19*, 590-601.
[3] Sezonov, G., Joseleau-Petit, D., and D'Ari, R. (2007) Escherichia coli physiology in Luria-Bertani broth, *Journal of bacteriology 189*, 8746-8749.
[4] Shiloach, J., and Fass, R. (2005) Growing E. coli to high cell density—a historical perspective on method development, *Biotechnology advances 23*, 345-357.
[5] Rosano, G. L., and Ceccarelli, E. A. (2014) Recombinant protein expression in Escherichia coli: advances and challenges, *Frontiers in microbiology 5*, 172.
[6] Schmitt, J., Hess, H., and Stunnenberg, H. G. (1993) Affinity purification of histidine-tagged proteins, *Molecular biology reports 18*, 223-230.
[7] Chowdhry, B. Z., and Harding, S. E. (2001) Protein-ligand interactions and their analysis, *Protein–ligand interactions: hydrodynamics and calorimetry: a practical approach. Oxford University Press, Oxford, UK*.
[8] Du, X., Li, Y., Xia, Y.L., Ai, S.M., Liang, J., Sang, P., Ji, X.L., and Liu, S.Q. (2016) Insights into protein–ligand interactions: Mechanisms, models, and methods, *International journal of molecular sciences 17*, 144.
[9] Leavitt, S., and Freire, E. (2001) Direct measurement of protein binding energetics by isothermal titration calorimetry, *Current opinion in structural biology 11*, 560-566.
[10] Laemmli, U. (1970) SDS-page Laemmli method, *Nature 227*, 680-685.
[11] Basta, L. A. B., Ghosh, A., Pan, Y., Jakoncic, J., Lloyd, E. P., Townsend, C. A., Lamichhane, G., and Bianchet, M. A. (2015) Loss of a functionally and structurally distinct ld-transpeptidase, LdtMt5, compromises cell wall integrity in mycobacterium tuberculosis, *Journal of Biological Chemistry 290*, 25670-25685.

Chapter 5

Conclusion and recommendations

The first part of the study (Chapter 2) sought to address the question of lack of known inhibitors for Ldt$_{Mt5}$. Throughout literature, no virtual screening study had been performed for L,D-transpeptidases, more importantly for the protein under study Ldt$_{Mt5}$. In humans, carbapenems are considered the last resort antibiotics against bacteria but unfortunately, they have extremely limited effect on Ldt$_{Mt5}$ thus prompting the search for potential inhibitors against the protein. L,D-transpeptidases are peptidoglycan polymerases which catalyse the formation of 3→3 peptidoglycan cross-links (80 %, unique to *M.tb*) and are essential in the biosynthesis of the cell wall through which antibiotic resistance is accomplished. Among the five *M.tb* Ldt paralogs, the most dominant and widely studied is Ldt$_{Mt2}$. Studies on antibacterial activity of carbapenems on Ldts revealed that Ldt$_{Mt5}$ remained active in the peptidoglycan cross-linking assay, thus inferring unique characteristics of the protein. It was also shown that *M.tb* lacking a functional copy of Ldt$_{Mt5}$ was vulnerable to denaturation. This typically necessitated the screening of compounds for potent leads against Ldt$_{Mt5}$.

Our virtual screening for prospective compounds against Ldt$_{Mt5}$ successfully identified many potential novel inhibitors which came from four different classes of antimicrobial compounds. It is important to note that β-lactams, more specifically carbapenems were among the successfully screened compounds with high binding affinity for the protein under study. The MD simulations also revealed favourable binding affinity of compounds from all classes, with the highest affinity being the β-lactam class. However, since it is known that certain β-lactams (carbapenems) inhibit Ldt$_{Mt2}$ but not effectively Ldt$_{Mt5}$, it is therefore plausible that the evaluation of the binding thermodynamics and mechanistic studies be performed from all four classes of antimicrobial compounds obtained from virtual screening against Ldt$_{Mt5}$. This is due to the lack of known experimental binding thermodynamics and inhibition mechanism for Ldt$_{Mt5}$. The β-lactams obtained in this study are novel and different from the ones evaluated in the other studies on Ldt$_{Mt5}$ as well as on any Ldt belonging to *M.tb* so it is worthwhile to investigate their effect on the protein. The current study has served as a reference point in which the identified compounds can be further analysed experimentally for bioactivity (*in vitro* and *in vivo*), thus assist in the validation of the model and also providing a better understanding of the protein's inhibition and binding mechanism. It also formed the basis of the second study (Chapter 3) on the mechanism of action of β-lactams on Ldt$_{Mt5}$.

In the current study (Chapter 2) we also performed a dual virtual screening approach in which two software programs were applied to the screening. This is an improvement on other virtual screening studies which screen chemical compound databases using a single program. The study revealed an important aspect on virtual screening that, in order to increase the chance of acquiring many leads, it is highly recommended that one performs the screening using two or more software with different search algorithms. Such an approach can enable the researcher to thoroughly explore the chemical search space and obtain a comprehensive screen in which many lead compounds are evaluated. Also, the general consensus among the different software programs on common potential leads can eliminate the need to perform MD simulations, thus saving time and computational resources.

Computational procedures have been employed to study this catalytic mechanism, which corroborates experimental observations for the mechanism of Ldt$_{Mt2}$. The first reported catalytic mechanism of L,D-transpeptidase of *M.tb* suggested a dual step process in which firstly, the Cys354-thiolate/His336-imidazolium pair formation initiated a four membered ring acylation step, followed by the nucleophilic attack of Cys354 on the carbonyl carbon of the substrate, thereby forming a covalent intermediate. The second step was characterised by an attack of the acyl-enzyme complex by the amine group (deacylation), resulting in the formation of the 3→3 peptide bond. A model for the acylation step of the β-lactam ring against Ldt$_{Mt2}$ was more recently investigated utilizing DFT calculations, [B3LYP/6-31 + G(d)]. The acylation mechanisms were studied as four-membered-ring (TS-4, TS-4-His and TS-4-water) and six-membered ring (TS-6-water) transition states. The thermochemical parameters for the proposed models were obtained and it was established that the activation barrier of TS-6-water model was considerably lower than the other models.

The same DFT approach utilized from the previously mentioned study was adopted in this study (Chapter 3) using the full protein (Ldt$_{Mt5}$) and the 6-membered ring transition states were obtained using constraints. We performed a two-stage minimization of the geometry which included a catalytic water molecule inserted in the active site. The complex from the MD run was partitioned into two layers and the ONIOM (QM/MM) approach was applied to investigate the mechanism of the reaction. The activation free energies of some virtually screened β-lactam compounds obtained from ONIOM (QM/MM) study gave insight on their reactivities. This describes the acylation mechanism involving the attack of the S-H group of cysteine active site residue of Ldt$_{Mt5}$. Our results showed that the $\Delta G^{\#}$ is comparable with obtained results for Ldt$_{Mt2}$ from other studies, indicative of the reactivity of the screened compounds.

The experimental section (Chapter 4) of the present study exhibited exceptionally good protein expression and purification as revealed by the affinity chromatogram and the SDS-PAGE. However, the binding analysis from the ITC exhibited limited binding affinity of the compound to the protein. At this point one cannot conclusively determine the cause of the lack of binding whether it is due to the protein binding-induced conformational changes or it is wholly due to poor solubility of the compound. Because of time constraints, limited financial and technical resources, we were unable to continue evaluating the binding dynamics. We therefore recommend that further fluorescent ligand binding assays can be performed to detect the binding of the ligand or a known substrate (nitrocefin) to the target. Thermal denaturation assays (TDA) can also be performed to monitor thermal denaturation process of proteins in the presence of the ligands. These assays may assist to determine the factors behind the observed lack of binding.

In the present study we used a single compound (a monobactam) which had the highest binding affinity to the protein under study to perform the binding thermodynamics assay, ITC due to the constraints mentioned earlier. A total of ten novel compounds from four different antimicrobial classes was obtained from our virtual screening of potential compounds against Ldt_{Mt5}. From the β-lactam class, five potential leads were obtained from the screen in which two were monobactams and three were carbapenems. Since certain carbapenems have previously been shown to be active against Ldt_{Mt2} but having a limited effect on Ldt_{Mt5}, we recommend that the binding thermodynamics assays be performed on these compounds for comparison with findings of previous studies. These carbapenems obtained from our virtual screening are novel, so evaluating their binding thermodynamics can bring about a conclusive understanding on carbapenems' effectiveness on the protein. Also, for an average statistical representation of the data, these three compounds would be ideal. We also suggest that a further binding thermodynamics analysis of the novel compounds from other classes to be performed to evaluate the effect of these compound on Ldt_{Mt5}. Furthermore, if any experimental observations suggest possible affinity to the protein, catalytic mechanistic studies can be undertaken.